

Increasing efficiency of particle separation in natural gas cyclones using passive and active enhancements

by

Walid Ibrahim Mazyan

B.Sc. Hons., American University of Sharjah, 2009

M.Sc., American University of Sharjah, 2013

A THESIS SUBMITTED IN PARTIAL FULFILLMENT OF
THE REQUIREMENTS FOR THE DEGREE OF
DOCTOR OF PHILOSOPHY

in

THE COLLEGE OF GRADUATE STUDIES

(Mechanical Engineering)

THE UNIVERSITY OF BRITISH COLUMBIA

(Okanagan)

May 2017

© Walid Ibrahim Mazyan, 2017

Committee Page

The undersigned certify that they have read, and recommend to the College of Graduate Studies for acceptance, a thesis entitled:

Increasing efficiency of particles separation in natural gas cyclones using passive and active enhancements

Submitted by Walid Mazyan in partial fulfillment of the requirements of

The degree of Doctor of Philosophy

Dr. Mina Hoorfar, School of Engineering, UBCO

Supervisor, Professor (please print name and faculty/school above the line)

Dr. Homayoun Najjaran, School of Engineering, UBCO

Supervisory committee member, Professor (please print name and faculty/school above the line)

Dr. Joshua Brinkerhoff, School of Engineering, UBCO

Supervisory committee member, Professor (please print name and faculty/school above the line)

Dr. Wilson Eberle, School of Engineering, UBCO

University Examiner, Professor (please print name and faculty/school above the line)

Dr. Alidad Amirfazli, School of Engineering, York University

External Examiner, Professor (please print name and faculty/school above the line)

May 2, 2017

(Date submitted to Grad Studies)

Abstract

Natural gas goes through several processes ranging from extraction, treatment, liquefaction and regasification. Among these processes, treatment, specifically the removal of solid particles, has a crucial role due to its impact on annual maintenance and efficiency of downstream equipment and processes. In essence, solid particles need to be removed at a high efficiency without increasing the pressure drop and hence power consumption in the system. Cyclone separators have been used to remove large solid particles through centrifugal forces. The main disadvantage of cyclones is their efficiency, especially for particles below 5 μm . Numerous studies have been conducted in improving the separation efficiency of cyclones by either spraying a mist of water or changing their geometry to increase the centrifugal forces. The main disadvantage of the majority of the geometrical modifications is the fact that they cause a significant increase in the pressure drop (at least by 15%). The mist approach, increasing the density of the particles and hence the efficiency, relies on water which adds additional cost.

This research focuses on the implementation of active and passive modifications to enhance the separation efficiency of cyclones without increasing the pressure drop. The active modifications include the addition of electrostatic and magnetic forces, effects of which are studied theoretically and experimentally. The passive method involves addition of a tangential collecting chamber at the conical section. The effect of such a modification is studied thoroughly based on experiments and CFD modeling. The theoretical and experimental investigation of the electrostatic and magnetic effects show an increase in the separation efficiency of 34% and 24% for 4- μm particles, respectively. The results of the CFD analysis and experimental study for the passive modification (i.e., the additional chamber) suggest an increase of maximum 26% for 4- μm particles. The CFD results conducted for a range of particles also suggest that such a geometrical

modification can increase the efficiency by 51% for 1- μm particles for which the increase in the pressure drop increase is only 8% (half of the minimum value reported before). These increases in the efficiency will make the cyclones a viable separator with minimum maintenance costs.

Preface

The research presented in this thesis is the original work of the author. The research was conducted under the supervision of Dr. Mina Hoorfar at the School of Engineering at UBC Okanagan and American University of Sharjah (AUS). Parts of this thesis have been published in peer reviewed scientific journals and conference proceedings, and my supervisor is the corresponding authors in all of the publications.

The results of this thesis were published in peer-reviewed journals and conference proceedings. The details of the author contribution are explained for each publication below:

a. Article published or submitted in refereed journals

- **W. Mazyan, A. Ahmadi, H. Ahmed, M. Hoorfar.** “Market and Technology Assessment of Natural Gas Processes – A Review”. *Journal of Natural Gas Science and Engineering*. Vol 30; pp. 487-514. 2016.
(Lead author: presenting the idea and conducting a thorough review of existing techniques, performing a market analysis, and writing paper)
- **W. Mazyan, A. Ahmadi, R. D. Jesus, H. Ahmed, M. Hoorfar.** “Use of Ferrous Powder for Increasing the Efficiency of Solid Particle Filtration in Natural Gas”. *Separation Science and Technology Journal*. Vol 51; pp. 2098-2104. 2016.
(Lead author: presenting the idea and building up the experimental setup, comparing the experimental results with conventional designs and writing paper)
- **W. Mazyan, A. Ahmadi, H. Ahmed, M. Hoorfar.** “Enhancement of solid particle separation efficiency in gas cyclones using electro-hydrodynamic method”. *Separation and Purification Technology Journal*. Vol 182; pp. 29-35. 2017.

(Lead author: presenting the idea and conducting a thorough review of existing technologies, performing a theoretical and experimental calculations, and writing paper)

- **W. Mazyan**, A. Ahmadi, H. Ahmed, M. Hoorfar. "Increasing the *COP* of a Refrigeration Cycle in Natural Gas Liquefaction Processes Using Refrigerant Blends". *International Journal of Refrigeration* (Submitted March 2, 2017)

(Lead author: presenting the idea and conducting a thorough review of existing techniques, performing theoretical calculation and software analysis on performance enhancement and writing paper)

- **W. Mazyan**, A. Ahmadi, J. Brinkerhoff, H. Ahmed, M. Hoorfar. "Computational Fluid Mechanics Investigation of Methods for Enhancing the Performance of Cyclone Separators in Gas Processes". *Physics of Fluids* (Submitted February 23, 2017)

(Lead author: presenting the idea and conducting a thorough review of existing techniques, performing theoretical calculation and software analysis on performance enhancement and writing paper)

- **W. Mazyan**, A. Ahmadi, H. Ahmed, M. Hoorfar. "Experimental Investigation of Using Tangential Chamber for Increasing the Efficiency of Solid Particle Filtration in Natural Gas Cyclones". *Journal of Aerosol Science*. (Submitted February 13, 2017)

(Lead author: presenting the idea and building up the experimental setup, comparing the experimental results with conventional designs and writing paper)

b. Other refereed contributions

- **W. Mazyan**, A. Ahmadi, H. Ahmed, M. Hoorfar (2016). A Technical Assessment of Natural Gas Liquefaction Processes. CSME. Kelowna. July 1, 2017.

(Lead author: presenting the idea and running the analysis, comparing the theoretical results with conventional designs and writing the manuscript)

- **W. Mazyan, A. Ahmadi, H. Ahmed, M. Hoorfar (2016).** A Market Assessment of Natural Gas Current and Future Demands. CSME. Kelowna. July 1, 2017.

(Lead author: presenting the idea and conducting a thorough review of existing techniques, performing a market analysis, and writing manuscript)

- **W. Mazyan, A. Ahmadi, M. Hoorfar (2016).** A Theoretical Model for the Evaluation of Solid-Gas Separation in Cyclone Separators. CSME. Kelowna. July 1, 2017.

(Lead author: presenting the idea and conducting a thorough review of existing technologies, performing a theoretical calculation, and writing manuscript)

- **W. Mazyan, A. Ahmadi, H. Ahmed, M. Hoorfar (2016).** Investigation of the Effects of Blended Propane-Ammonia and Propane-Carbon Dioxide Refrigerants on the COP of Refrigeration Cycles. PRTEC. Hawaii. March 1, 2016.

(Lead author: presenting the idea and running the analysis, comparing the theoretical results with conventional designs and writing the manuscript)

- **W. Mazyan, A. Ahmadi, H. Ahmed, M. Hoorfar (2016).** Experimental Investigation on the Enhancement of the Solid-Gas Separation Efficiency in Natural Gas Cyclones Using Magnetic Forces. 1st international scientific conference @ Southern Technical University. Basrah-Iraq. March 14, 2016.

(Lead author: presenting the idea and conducting a thorough review of existing technologies, performing the experimental calculations, and writing manuscript)

- **W. Mazyan, A. Ahmadi, H. Ahmed, M. Hoorfar (2015).** Investigation of Methods of Enhancing the Performance of Propane Pre-Cooling Refrigeration Cycles in Natural Gas Liquefaction Processes. ADIPEC. Abu Dhabi. November 7, 2015.

(Lead author: presenting the idea and conducting a thorough review of existing technologies, performing a theoretical analysis, and writing manuscript)

- **W. Mazyan, A. Ahmadi, M. Hoorfar** (2016). Evaluation of Solid-Gas Separation Efficiency in Natural Gas Cyclones. International Journal of Geological and Environmental Engineering Vol:3, No:8. WASET. Paris. August 1, 2016.

(Lead author: presenting the idea and conducting a thorough review of existing technologies, performing a theoretical analysis, and writing manuscript)

- **W. Mazyan, A. Ahmadi, M. Hoorfar** (2015). Enhancing the Solid-Gas Separation Efficiency in Natural Gas Cyclones Using Electro-Magneto-Hydrodynamic Forces. Accepted for IMECE. USA. November 13, 2015.

(Lead author: presenting the idea and conducting a thorough review of existing technologies, performing a theoretical calculation, and writing the paper)

Table of Contents

Committee Page.....	ii
Abstract.....	iii
Preface.....	v
List of Tables.....	xiii
List of Figures.....	xiv
Acknowledgements.....	xix
Dedication.....	xx
Chapter 1: Introduction *	1
1.1 Extraction	1
1.2 Preparation to transport	3
1.3 Natural gas liquefaction.....	5
1.4 Transportation.....	11
1.5 Regasification	12
1.6 Treatment.....	14
1.7 Motivation and objectives	28
1.8 Thesis organization.....	30
Chapter 2: Experimental setup *	32
2.1 Underlying principle.....	32
2.2 Dimensions	33
2.3 Fabrication.....	34

2.4	Addition of ferrous powder for magnetic forces	35
2.5	Addition of ferrous powder for electrostatic forces	40
2.6	Addition of a chamber	41
Chapter 3: Theoretical approach *		45
3.1	Background.....	45
3.2	Theoretical model for conventional cyclone separator	48
3.3	Theoretical model for electro-hydrodynamic effect.....	52
Chapter 4: Numerical approach		55
4.1	Background.....	56
4.2	Model.....	67
Chapter5: Active cyclone separator modification by adding electro-hydrodynamic forces – theoretical and experimental approaches *		73
5.1	Theoretical approach in conventional cyclone designs	73
5.2	Cyclones with additional electro-coat process under electrostatic attractions – theoretical and experimental approaches.....	74
5.3	Cyclones with additional ferrous-coat process under magnetic attractions – experimental approach.....	77
Chapter6:Passive modification by adding tangential collecting chambers *		82
6.1	Capturing efficiency	82
6.2	Pressure drop	94
6.3	Erosion rate.....	94

6.4	Experimental results	97
Chapter 7: Conclusions.....		102
7.1	Summary.....	102
7.2	Limitations.....	103
7.3	Contributions	103
7.4	Future work	104
References.....		107
Appendices.....		107
Appendix A: Performance of Refrigeration Cycle in Natural Gas Liquefaction Process *		125
A.1.	Introduction.....	125
A.2.	Material and methods.....	131
A.3.	Theory.....	132
A.4.	Results and discussion	135
A.5.	Cost analysis	142
A.6.	Emerging technologies	142
A.6.1.	Solar power	142
A.6.2.	Thermoacoustic.....	143
A.6.3.	Natural gas solidification	144
Appendix B: Current and future market *		147
B.1.	North America.....	148
B.2.	Central/South America.....	150

B.3. Europe and Eurasia	151
B.4. Middle East	151
B.5. Asia Pacific	152
B.6. Africa	154
B.7. Natural gas costs/prices.....	155
B.8. Major factors affecting NG prices	156
B.9. Cost of oil and gas production	156
Appendix C: Cost analysis	185
C.1. Electro-coating	185
C.2. Ferrous powder	186
C.3. Additional chamber.....	186

List of Tables

Table 1-1: The natural gas composition in a typical reservoir in USA	15
Table 2-1: Cyclone material cost	35
Table 2-2: Statistical values of the analyzed samples (for magnetic forces)	39
Table 2-3: Particles weights (for magnetic forces)	39
Table 2-4: Statistical values of the analyzed samples (for electrostatic forces)	41
Table 2-5: Particles weights (for electrostatic forces)	41
Table 2-6: Statistical values of the analyzed samples (for the tangential chamber)	43
Table 2-7: Data weights (for the tangential chamber)	44
Table 6-1: Pressure drop for i) the experimental results reported in [70] for conventional cyclone ran at the inlet velocity of 14 m/s, ii) the CFD modeling result for the conventional design at 14 m/s, iii) the CFD result with the addition of one tangential chamber at 14 m/s, and iv) the CFD result with the addition of one tangential chamber at 20 m/s	94
Table 7-1: Cost for the required for the addition of the electrostatic-based enhancement	186

List of Figures

Figure 1-1:Natural gas processing	2
Figure 1-2:A schematic of a step-wise drilling hole technique	4
Figure 1-3:Three steps of the recovery process: (a) primary, (b) secondary, and (c) enhanced	5
Figure 1-4:A schematic of a ConocoPhillips simple cascade refrigeration. WC is an abbreviation for water cooling.....	8
Figure 1-5:A flow diagram of a Linde process. HEX is an abbreviation for Heat Exchanger	9
Figure 1-6:A flow diagram of a DMR process	10
Figure 1-7: A schematic of an APCI process	11
Figure 1-8:Typical processes involved in natural gas treatment	16
Figure 1-9:Schematic of a cyclone separator.....	19
Figure 1-10:Several theoretical approaches (reproduced from [70] with permission from InTech).....	26
Figure 1-11:Effect of inlet velocity on separation efficiencies (reproduced from [70] with permission from InTech)	27
Figure 1-12:Effect of inlet velocity on pressure drop (reproduced from [70] with permission from InTech)	28
Figure 2-1:Experimental cyclone setup	33
Figure2-2:Experimental Setup.....	34
Figure 2-3:Schematic of centrifugal (FCent) with magnetic forces (Fferro) in a cyclone	36
Figure 2-4:(a) Microscopic image of an empty membrane, (b) microscopic image of captured dust particles on the membrane.....	38

Figure 2-5: Schematic of inlet solid-gas mixture (F_{Cent}) with the additional tangential collecting chamber.....	42
Figure 2-6: Experimental tangential chamber	43
Figure 3-1: Typical gas flow in cyclone separators.....	47
Figure 3-2: Typical velocity profile in cyclone separators.....	47
Figure 3-3: Control volume inside the cyclone path, where CV is the control volume, ds is the particle infinitesimal circumferential path, W is the averaged width of the controlled volume and V_{θ} is the inlet tangential velocity.	51
Figure 3-4: Schematic of inserting charged particles to coat solid particles	53
Figure 4-1: Mesh discretization for (a) 400,000, (b) 600,000 and (c) 800,000 mesh counts.....	58
Figure 4-2: Residuals for Simplec-Second Order_QUICK Scheme (steady followed by unsteady analysis) - total real time (0.01 s).....	61
Figure 4-3: Residuals for Simplec-second order_QUICK scheme - total time (0.071 s)	62
Figure 4-4: Residuals for steady analysis using second order - total unsteady time (0 s)	63
Figure 4-5: Residuals steady analysis followed by short period unsteady analysis using PRESTO scheme - total unsteady time (0.023 s)	64
Figure 4-6: Residuals for unsteady analysis without using small timescales - total unsteady time 500 s	65
Figure 4-7: Residuals for long unsteady analysis without using short timescales - total unsteady time (250 s without small timescale).....	66
Figure 4-8: obtained using different solution methods at low accurate residual convergence	67

Figure 4-9: CFD model boundary conditions	69
Figure 4-10: Residuals leading to converged results using long unsteady analysis followed by longer small timescales	70
Figure 4-11: Fluid Flow of (a) an immature flow, against (b) a mature flow	71
Figure 5-1: Comparison of the separation efficiency values obtained from the theoretical model and our experimental results [84], Ji et al. experimental results [71], and Leith and Licht theoretical modeling results [44].....	74
Figure 5-2: Electrostatic force compared to centrifugal force.....	75
Figure 5-3: Separation efficiency enhancement due to the electrostatic forces in the conventional cyclone setup. The symbols present the average values of three runs. The error bars were obtained at 95% confidence level.....	76
Figure 5-4: Count and percentage of the particle size distribution at the (a) inlet, (b) outlet of the conventional cyclone, and (c) outlet of the cyclone with the ferrous coating	78
Figure 5-5: Capture efficiency values obtained based on the conventional cyclone design, the conventional cyclone design of the Ji et al. [71], and the magnetic-based cyclone design proposed in this section. The symbols present the average values of three runs. The error bars were obtained at 95% confidence level.	80
Figure 6-1: Comparison between the experimental separation efficiency (Ji et al. [71]), CFD modeling conducted at 400,000 meshing elements, 600,000 meshing elements and 800,000 meshing elements for a conventional design.....	83
Figure 6-2: Errors obtained for different meshing grids.....	86
Figure 6-3: The comparison between the experimental results reported by Ji et al. [71], CFD results of a conventional design, CFD results for the proposed	

geometrical modification involving the addition of one tangential chamber, CFD results for the case of two chambers, CFD results for the case of three chambers	89
Figure 6-4: The turbulence eddy dissipation for the cases of adding one, two, or three tangential chambers	90
Figure 6-5: The fluid velocity contours for the cases of adding one, two, or three tangential chambers	91
Figure 6-6: The effect of the velocity at the inlet of the cyclone on the separation efficiency for the conventional design, and the design with one tangential chamber.....	93
Figure 6-7: Efficiency comparison between conventional cyclone design, conventional cyclone design with an elongated cone length, and the design with a tangential chamber.....	93
Figure 6-8: Locations of erosion in (a) conventional, and (b) the proposed design including one tangential chamber. The maximum erosion rates for (a) and (b) designs are 5.4×10^{-8} kg/m ² s and 2.5×10^{-8} kg/m ² s, respectively.	96
Figure 6-9: Velocity profile for (a) conventional, and (b) the design chamber added .	97
Figure 6-10: Count and percentage of the particle size distribution at the (a) inlet, (b) outlet of the conventional cyclone, and (c) outlet of the cyclone with the tangential chamber	100
Figure 6-11: Experimental capture efficiency values obtained using our conventional cyclone design and that of Ji et al. [71] as well as those after adding the tangential chamber (the proposed modification in this paper). The symbols present the average values of three runs. The error bars were obtained at 95% confidence level.	101

Figure 8-1: Particle size effect on the erosion rate (reproduced from [70] with permission from InTech)..... 106

Acknowledgements

I would like to thank my supervisor, Dr. Mina Hoorfar, for her immense support along this academic path. Her great enthusiasm to research has motivated me to push myself to my limits in order to experiment new research ideas. I would also like to thank my advisor Dr. Ali Ahmadi for all his support and availability to guide me through the theoretical and experimental work. My committee members have also played a sufficient role in shaping my research. Drs. Homayoun Najjaran, Hussain Ahmed and Joshua Brinkerhoff have been there at all times to assist me in any misunderstanding of my research topic.

Also, I thank the American University of Sharjah for collaborating with us on this research and allowing us to build our experimental setups at their labs under the supervision of Dr. Hussain Ahmed and under the observation of Mr. Ricardo De Jesus.

Moreover, at the beginning of this PhD path, Dr. Geoff Nesbitt has been an assist in providing information about the current and old natural gas technologies and their use in the market.

It is also difficult for me to give enough thanks to my dad, mom, lovely sisters and friends (especially Teela, Tibi, Ayman, Rasha, and Mathew) for all their support from the very first point of my PhD studies. They have been there to support me emotionally and were also there to give their opinions about new research ideas. Their immense love has assisted me in pushing forward to complete my studies smoothly.

Dedication

This thesis is dedicated to my parents Ibrahim Mazyan and Inas Kashkash. They are the life of my eyes. Without their support, I would have never been able to accomplish this great achievement. With Great Love!

Chapter 1: Introduction*

Natural Gas has become one of the most desired energy sources after the discovery of oil due to its efficient combustion and low carbon dioxide emission. For instance, to avoid the potential risks associated with the other energy sources such as nuclear energy, electrical power generation plants dependency on the natural gas is rapidly increasing [1]. To meet this increasing demand for the natural gas, there have been advances in the main natural gas processes. Natural gas goes through several processes before it is received by the consumer: at first, natural gas is extracted from reservoirs by means of drilling, pumping and extraction. So far, three methods have been used in the industry for extracting the natural gas. These methods (including water, chemical and steam injections) allow for natural gas extraction up to 60% of the reservoir's capacity. After extraction, the natural gas is transported to the treatment plant in which solid particles (fine sands), liquid particles (mercury, oil, and natural gas heavy liquids), and certain gases (CO₂ and H₂S) are removed. After treatment, the natural gas is compressed or liquefied through several technologies (such as refrigeration cycles using single or mixed refrigerants). Following the liquefaction/compression stage, the natural gas is transported to the receiving terminals through pipes or ships after which the liquefied/compressed gas is re-gasified again and sent to the consumers (end-users).

Figure 1-1 shows a schematic of the overall natural gas processes including drilling/extraction, treatment, preparation to transport, transportation to the desired destination. These processes are briefly explained in the following sections:

1.1 Extraction

Extracting oil and gas is relatively harder than simply drilling a hole. In essence, the hole must be supported by a cemented pipe [1]. In current wells, a stepwise-drilling method

shown in The liquefaction process, on the other hand, reduces the volume by 600 times which is three times more than the CNG process. See Appendix A for a detailed analysis of a liquefaction process. is used to maintain the pressure uniformity around the walls of the drilled hole.

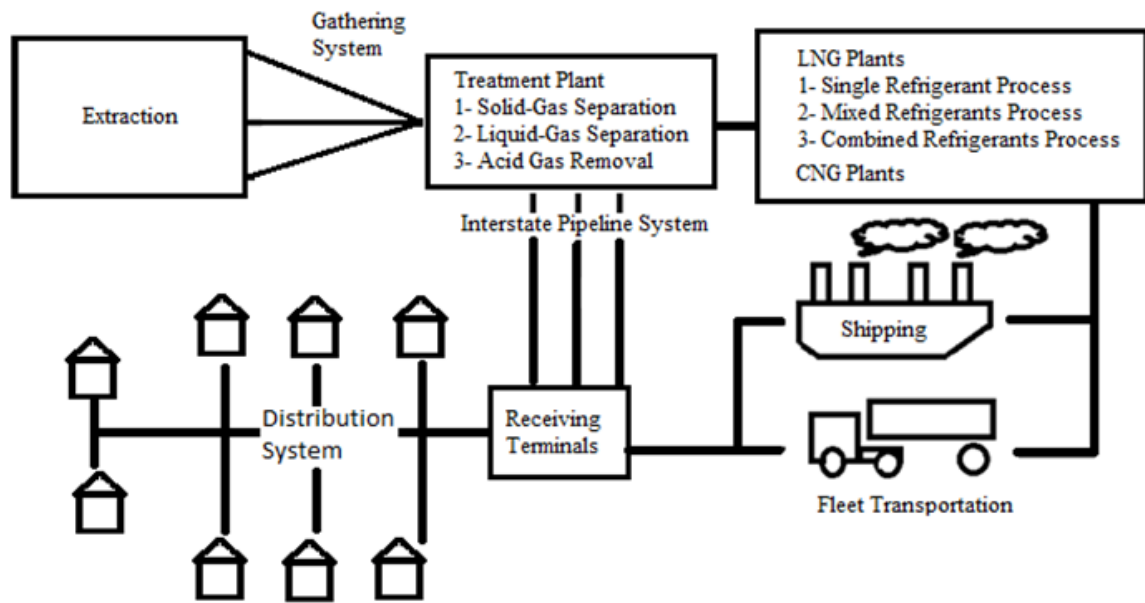


Figure 1-1:Natural gas processing

There are a number of factors which affect the efficiency of the oil and gas extraction from the well. These factors include the porosity of the rock and the viscosity of the oil and gas deposits [1].

In the early time of oil and gas extraction, the efficiency of the extraction methods was around 10% (only 10% of the reservoir's content was extracted due to its natural pressure). Recent technologies have enhanced the efficiency to 60% by implementing additional recovery steps including secondary and enhanced recovery (see Figure 1-3). The preliminary extraction method, referred to as primary, relies on the natural internal pressure of the well. After the underground pressure deteriorates, pumps are used for further extraction. This method is referred to as the secondary recovery method involving the

injection of water from the other side of the well to push oil and gas towards the drilled section [2] (see Figure 1-3 (b)). Water used for the drilling process is taken from two sources: i) underground water (wastewater) which is found in the geological formations [3], and ii) external sources such as nearby water sources. In essence, the water is injected back to the well to maintain the underground pressure. The secondary recovery step enhances the efficiency to 20% (20% of the reservoir's content is extracted at this step). To enhance the recovery process to 60%, the final step is applied using thermal recovery methods, gas injection techniques, and chemical flooding techniques (shown in Figure 1-3 (c)). The thermal recovery process is conducted through injection of the steam into the well. The heated steam reduces the viscosity of the reservoir's content which enhances the recovery process. The gas injection technique uses miscible or immiscible gases. The miscible gases dissolve the light gasses to lower the viscosity of the reservoir's content and increase the flow; whereas the immiscible gases increase the pressure in the "gas cap" (i.e., the segregated gas zone overlying the oil column) to drive additional reservoir's content to the well. The third stage of the recovery enhancement is conducted by injecting a mixture of dense water-soluble polymers with water into the well to push the reservoir's content to the well. In addition to conventional gas extraction techniques, more attention has been directed toward new technologies for shale gas extraction [1-3]. Hydraulic fracturing is an example requiring further enhancement to reduce its environmental impact during shale gas extraction [1-3]

1.2 Preparation to transport

For onshore extraction, the treated natural gas is liquefied prior to transport; whereas, for the offshore plants, the natural gas is either compressed or liquefied before transport, adding to the overall cost. There are two widely used methods for transporting natural gas from offshore to onshore or from onshore to onshore facilities [4]: i) compression to form

compressed natural gas (CNG), and ii) liquefaction of natural gas (LNG), respectively. In the former method, natural gas is compressed under the pressure of 230-250 bar, and can be used for transportation as well as vehicle direct fueling purposes [5]. Natural gas has to pass through several compression stages to reach the required pressure. A typical process for the compression is by three-stage natural gas compression. After each compression stage, the natural gas is intercooled to compensate for the increase in its temperature [6]. The liquefaction process, on the other hand, reduces the volume by 600 times which is three times more than the CNG process. See Appendix A for a detailed analysis of a liquefaction process.

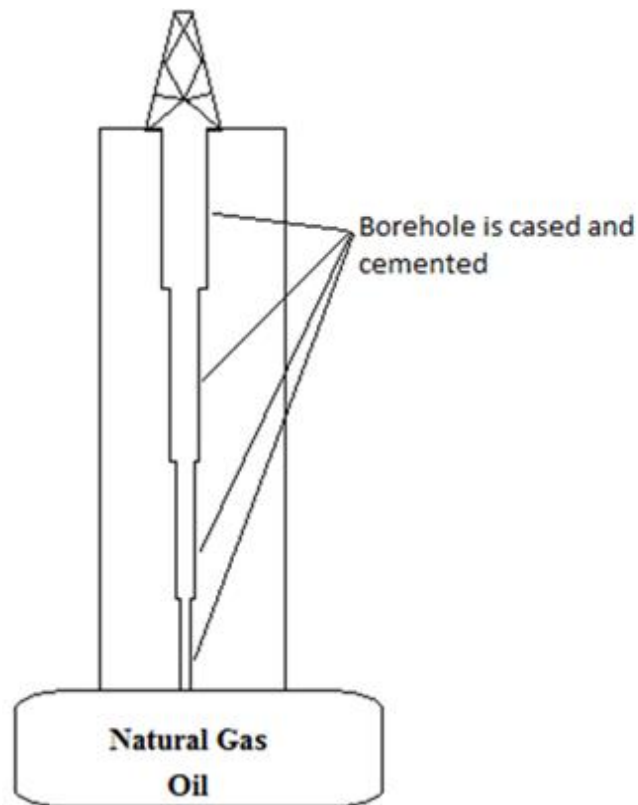


Figure 1-2:A schematic of a step-wise drilling hole technique

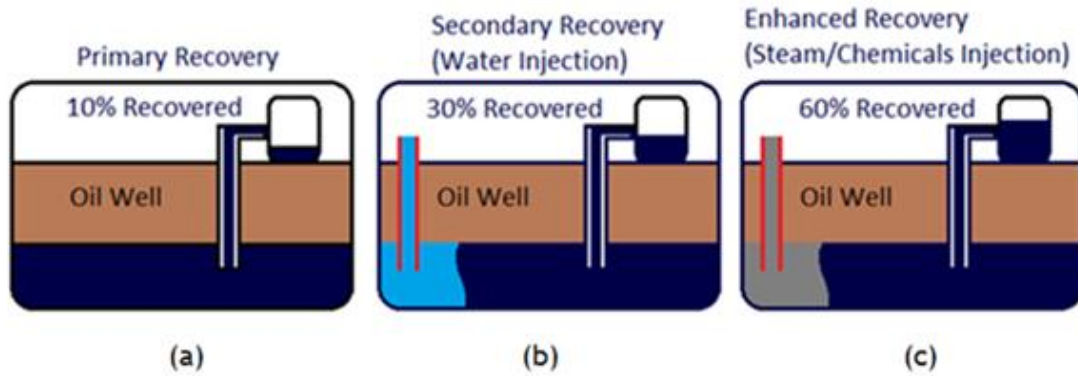


Figure 1-3: Three steps of the recovery process: (a) primary, (b) secondary, and (c) enhanced

There has recently been a growing interest in transporting natural gas by reducing its volume 200 times through compression. Due to enhancement in modern technologies, compressed natural gas will be an economical alternative form for natural gas transportation through ships for small distances [7]. During its transportation, CNG is maintained at around -30°C and 200 atm. This temperature range is higher compared to LNG (explained below), facilitating transportation with less insulation. On the other hand, thicker vessel walls are required to stand the high pressure.

1.3 Natural gas liquefaction

The most practical method to transport natural gas overseas is through liquefaction [8]. There are 71 major liquefaction plants globally [9] (see Appendix B). Among these plants, Qatar owns the largest liquefaction terminals and is considered to be the largest LNG exporter in the world with 77 mtpy (million tons per year) of natural gas produced. The existing LNG plants are not going to be enough to satisfy the ever increasing natural gas demands in future. Therefore, governments and major companies have proposed future plans to expand LNG production. Exxon Mobil and BHP Billiton are planning to construct

the world's largest floating LNG processing (FLNG) and export plant [10] called Scarborough Field. This plant is planned to export LNG from the northwestern shore of Australia. The plant will be 500 m long, increasing Australia's current LNG production by nearly 30% (6-7 mtpy). This production amount is predicted to be enough to fuel Japan's LNG needs for a month which is considered to be the largest importer of the natural gas [10]. As a result, Australia is considered to replace the largest LNG exporter (i.e., Qatar) by 2020. Australian's government has invested \$190 billion for the upcoming LNG plant projects. However, the cost inflation of the country remains an issue which needs to be resolved before proceeding with their production plan. In addition to the cost inflation, there are LNG plants located in North American and East Africa with competitive cost which might limit the growth of the Australia's future plans.

Several liquefaction processes have been introduced using refrigeration cycles. There are three main categories for liquefying the natural gas which are based on the type of the refrigerants used in the cooling process. These categories include i) pure refrigerant cycles (single refrigerant), ii) mixed refrigerant (MR) cycles, and iii) combined pure with mixed refrigerant cycles (combined refrigerant types). For pure refrigerant cycles, ConocoPhillips cascade process is the most famous process used in the LNG plants with a 90% relative efficiency (the efficiency of the plant normalized based on the highest efficiency obtained from the refrigeration cycles available in the market). For the mixed refrigerant cycles, Dual Mixed Refrigerant (DMR) and Linde processes with a 100% relative efficiency are used. For the combined refrigerant cycles, APCI (C3MR) with a 100% relative efficiency process is used.

Depending on the size of the plant and the owner's requirements, different plant designs need to be taken into consideration. There are three types of plants in the fields: i) large LNG production plants (above 1 mtpy), ii) medium LNG production plants (0.5 - 1 mtpy),

and iii) small LNG production plants (0.03 - 0.5 mtpy). For selecting the appropriate liquefaction process, the designer needs to pay attention to the overall cost and overall efficiency of the plant. For example, for large LNG production plants, mixed refrigerants (MR) with propane as the first stage refrigerant have shown the highest efficiency in the LNG production [11] although it is more expensive (see Appendix A). MRs, which are more complicated in their design, are more efficient since their cooling curves matches well with that of the natural gas. In small plants, on the other hand, MR adds to the capital cost of the plant which makes them less desirable. In addition to the increase in the capital cost, MRs are less desired in offshore plants for safety and limited spaces available for storage.

Single Refrigerant Process – the ConocoPhillips shares 5% of the total LNG production plants. It has been used in the industry for the past 30 years [12]. A schematic of the Conoco Phillips Cascade Process is shown in Figure 1-4. In this three-stage process, the first stage consists of cooling the natural gas to -35°C using propane as the refrigerant. Propane is used in the first stage because it is available in large quantities and considered to be one of the cheapest refrigerants. While the propane is cooling the natural gas, it also cools down the ethylene and methane used in the cascade process. The second stage uses the ethylene refrigerant, which is considered to be a good refrigerant to condense methane and be condensed by propane at pressures above the atmospheric pressure. At this stage, the natural gas is cooled down to -95°C at which it starts to liquefy. However, the liquefied natural gas needs to be sub-cooled further to compensate for the 5% gas excess when LNG is flashed in a later stage. Thus, LNG is sent to the third stage where it is sub-cooled further down to -155°C and then passed through a valve which reduces its temperature further to -160°C . Methane is used at this final sub-cooling stage for its availability, low cost, and ability to sub-cool LNG to -155°C .

Mixed Refrigerants (MR) Process – Linde process, also known as the mixed fluid cascade process, is a liquefaction process where the natural gas is cooled using mixed refrigerants in a stepwise process. A schematic of the Linde process is shown in Figure 1-5. The working fluid consists of methane, ethane, propane and nitrogen [12]. The natural gas is cooled in three stages in which the first stage uses “Plate and Frame Heat Exchangers” (PHE); whereas the second and third stages use “Spiral Wound Heat Exchangers” (SWHE). Although it is less efficient, PHE is desirable in the first stage due to its low cost.

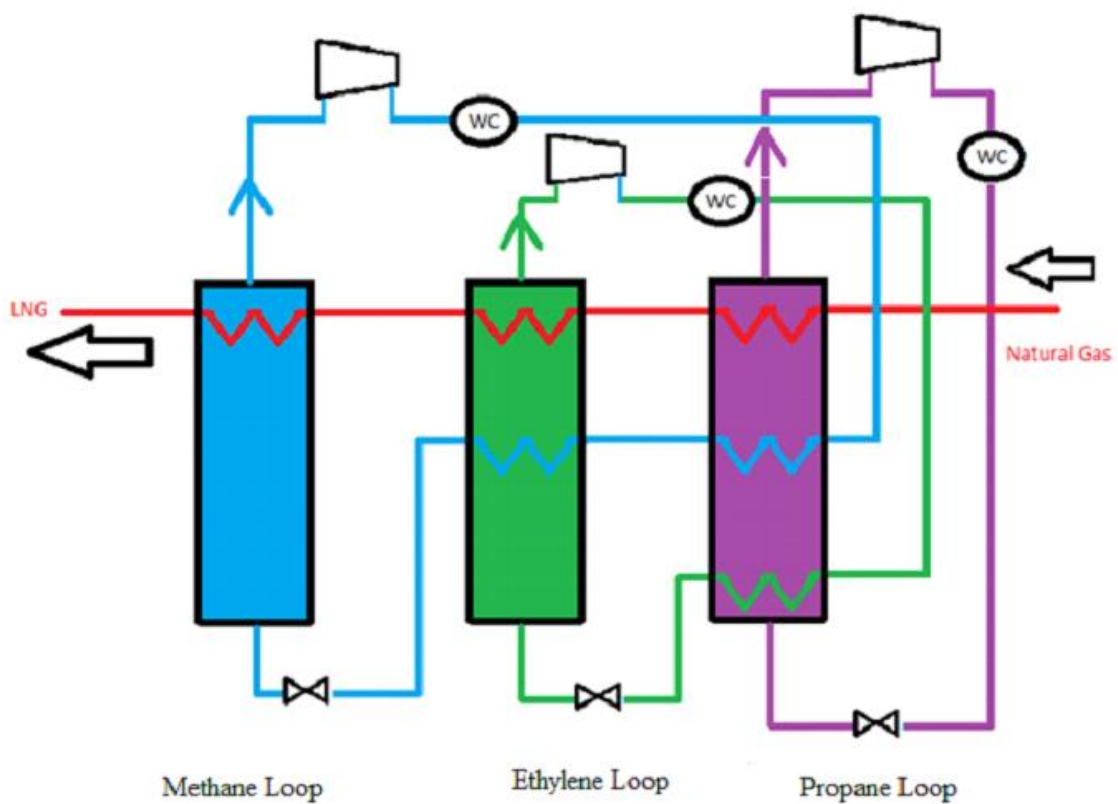


Figure 1-4: A schematic of a ConocoPhillips simple cascade refrigeration. WC is an abbreviation for water cooling

Another process that uses the mixed refrigerants is the Dual Mixed Refrigerant (DMR) process. Similar to the Linde process, the natural gas is cooled down using mixed refrigerants; however, the cooling process occurs in two liquefaction cycles each of which using mixed refrigerants. Figure 1-6 shows a flow diagram of a typical DMR process. DMR

cycles require large size and large number of equipment. These two factors made DMR feasible mainly for onshore operations. On the other hand, offshore services requiring small and compact liquefaction cycles use single mixed refrigerant (SMR) cycles (these cycles were developed as simple and power efficient cycles for offshore plants with a capacity of 2.5 million tonnes per annum (MTPA) [13]).

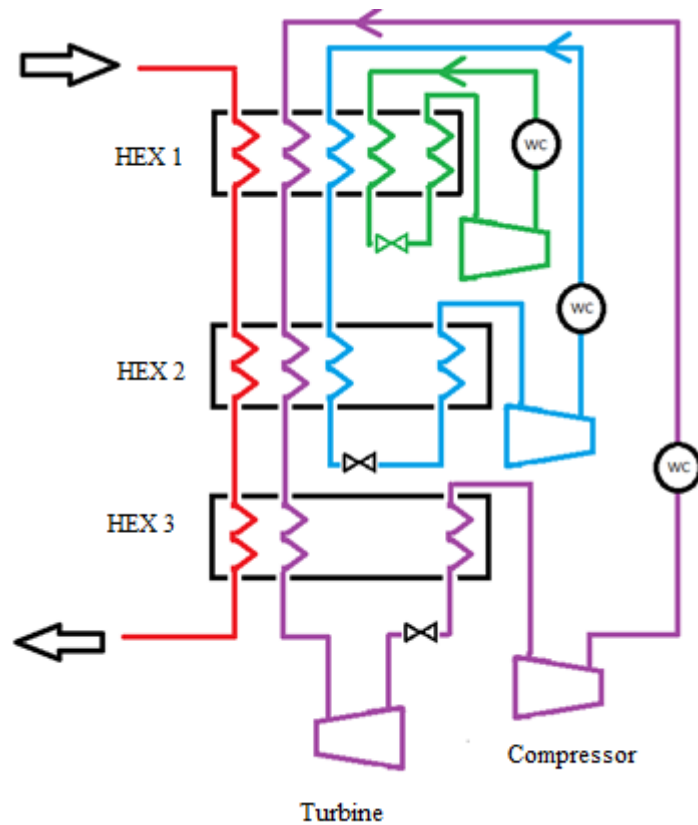


Figure 1-5:A flow diagram of a Linde process. HEX is an abbreviation for Heat Exchanger

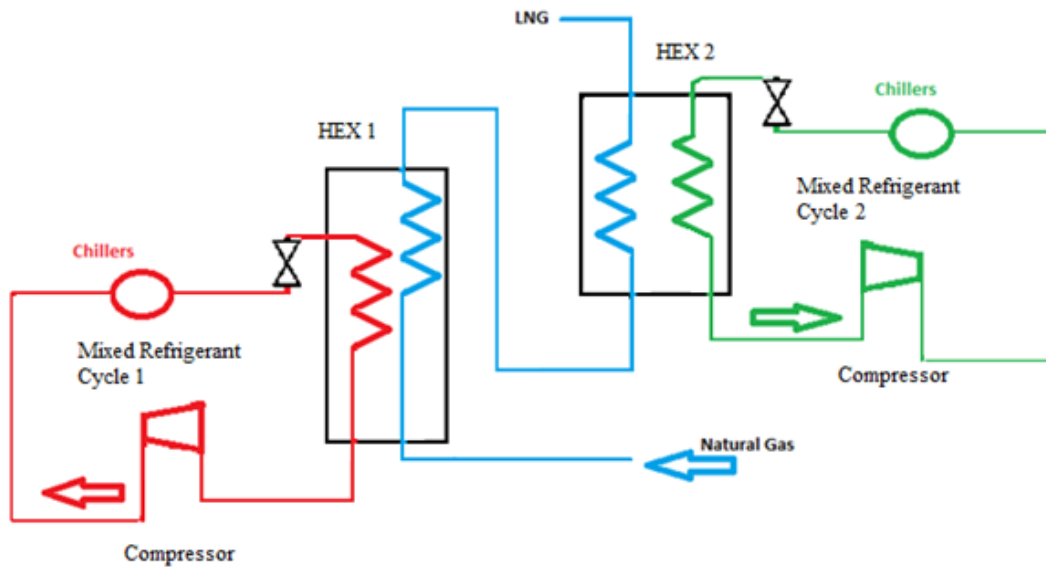


Figure 1-6: A flow diagram of a DMR process

Combined Refrigerant Process – the APCI is used in 88% of the world’s LNG plants. A typical APCI cycle is shown in Figure 1-7 [12]. It consists of three stages for cooling down the treated natural gas. The first stage is by cooling the natural gas to 1.7 °C using chilled propane. This stage takes place after cooling down the natural gas from 38 °C to 15.5 °C using air and water coolers. The second stage in the APCI process takes place by feeding the precooled natural gas to a two-staged heat exchanger tower. The first stage of the heat exchanger tower uses cold heavy propane and butane mixed refrigerants to cool the precooled natural gas down to -50 °C. The second stage of the heat exchanger (i.e., the 3rd stage in APCI) sprays a mixture of light gases (such as methane, ethane and nitrogen) over the natural gas. The valves are used to cool down further the natural gas to -160 °C. In some plants, an additional working fluid is added to the above cooling cycle. The most common additional refrigerant is nitrogen which enhances the efficiency of the liquefaction process. Such a cycle is referred to as the AP-X cycle.

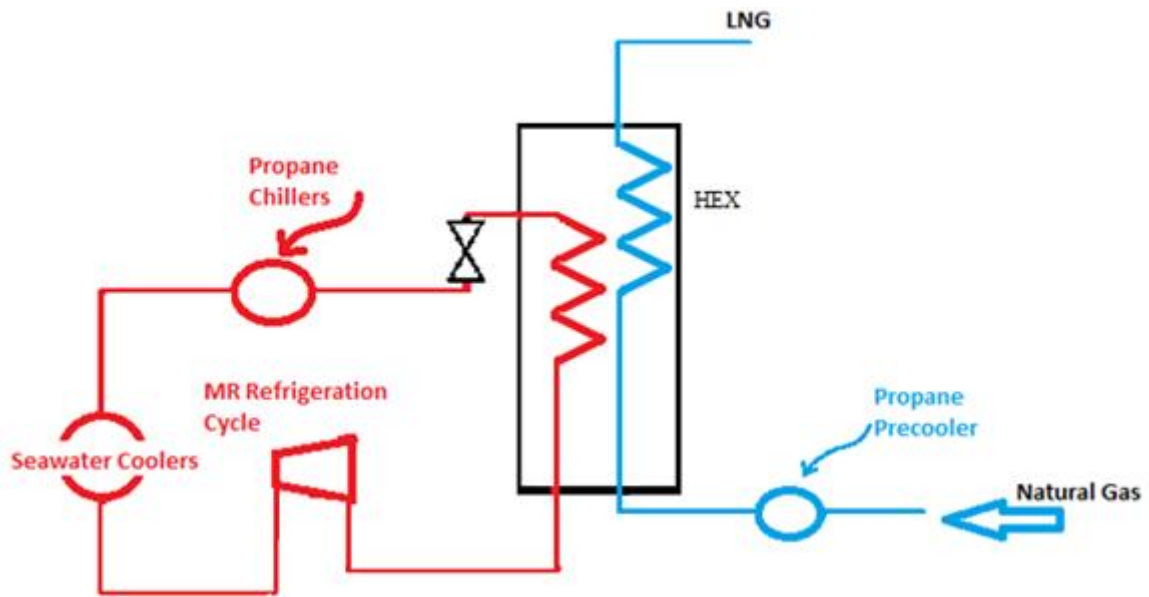


Figure 1-7: A schematic of an APCI process

1.4 Transportation

Transportation happens between different steps of natural gas extraction, treatment and distribution. The first transportation mode, which is through pipelines, happens from the reservoir to the treatment plant. This system is called the “gathering system”. The second transportation mode occurs after treatment where the natural gas will be either transferred to the receiving terminals or to the LNG/CNG plants. For the latter, ships or trucks are used to transfer LNG or CNG to overseas or in-land receiving terminals, respectively. The mode of transportation from the treatment plant to the receiving terminal occurs through pipelines which is called the “interstate system”. After reaching the receiving terminal, CNG or LNG (which will be re-gasified and transferred to gas) will be distributed to its destination through pipelines called the “distribution system” [14, 15, 16].

Compressed natural gas transportation – CNG transportation over the seas is practical and economical for the stranded gas fields which produce small amounts of natural gas [17]. Natural gas goes under pressures of 230-250 bars for this type of transportation. A number of parameters need to be considered in the design of the ship (transporting CNG) including

its weight, stability and capacity against the water conditions. For CNG transportation, the ship length is generally divided into five main parts: the extreme aft, the engine room, the cargo zone (where CNG is stored in multiple pressure vessels), the house for the submerged turret loading (STL), if applicable, and the fore end. On the ground, CNG is transported to receiving terminals or to CNG stations by fleet transportation.

Liquefied natural gas transportation – LNG transportation over the seas is practical and economical for stranded gas fields which produce large amounts of natural gas. Similar to CNG, LNG is shipped overseas by LNG cargo ships which usually contain four to five spherical vessels with heat insulations to preserve the low temperature of LNG. To achieve the proper insulation (steels such as fully killed, fine-grain, carbon-manganese steel, sometimes alloyed with 0.5% nickel) is used [18]. An insulation layer is applied on this metal layers to protect it against vapor and hence water ingress which can reduce the insulation efficiency. One method of insulation involves the use of a foil skin which acts as a vapor barrier. On the ground, LNG is also transported to receiving terminals by fleet transportation equipped with an insulation layer of similar types.

1.5 Regasification

Liquefied natural gas (LNG) providers export LNG to 73 plants across the globe. Asia-Pacific region is considered to be the largest LNG importer. This region alone has 30 LNG regasification plants to produce the energy they require, with the largest storage LNG regasification plant in Thailand named Rayong [9]. This plant alone has a capacity of importing 5 mtpy. Also, there are 22 regasification plants planned for near future [9].

The combustion properties of the natural gas and its low CO₂ emission have made it a very desirable source of energy. Transporting the natural gas across the seas in its liquefied form allows shipping the maximum amount of natural gas in a contained volume. To liquefy the natural gas, the natural gas needs to be cooled down to -160 °C which requires an immense

cooling energy. Sun et al. [19] suggested that the energy spent on liquefying the natural gas could be recovered when the natural gas is re-gasified. In essence, it is important to recover the "cryogenic" or "cold" energy from LNG. For recovering the "cold energy" for producing power, it is suggested to attach a Rankine cycle to the regasification plant [19]. Rankine cycle is mostly used in the recovery of the LNG's cold energy. To recover most of the waste heat generated from the cryogenic energy, various researchers have studied the effect of different working fluids in the single-stage Rankine cycle. Heng Sun et al. [20] suggested the working fluid in the simple Rankine cycle as a mixture of methane, ethane, and propane. In this cycle, the cold energy from the natural gas is utilized to run the simple Rankine cycle and a partial energy output is obtained. In the Rankine cycle, the condenser's cooling medium source comes from two separate locations: 1) from the conventional coolers (such as air or water coolers), and 2) from the cold energy associated with the liquefied natural gas. This process has added to the cost savings coming from the cooling medium. Szargut and Szczygiel [21] suggested ethane hydrocarbon to be used as a working fluid in the Rankine cycle (producing an efficiency of 40% assuming a 29% liquefaction exergy efficiency). Their studies showed exergy efficiencies between 29.58% and 49.68% from the LNG re-gasification based on different Rankine cycle schemes. Wang et al. [22] suggested the ammonia-water mixture be used as a working fluid in the Rankine cycle. They obtained an exergy efficiency between 19-27%. Another working fluid that can be used is Freon: Hisazumi et al. [23] have used a mixture of refrigerants of R134 and R23 as working fluids. They showed that 400 kWh could be produced per ton of vaporized LNG. Liu and Guo [24] proposed a mixture of CF_4 and propane as the working fluid. This mixture provided a 66.3% improvement in the power generation compared to the case where C_3H_8 was solely used. In another study, CO_2 has been used as the working fluid of the Rankine cycle [25]. Although this is attractive for reducing overall greenhouse effect and is a

simpler cycle, the efficiency of these cycles is around 47% which is relatively lower than the Rankine Cycles operating using organic working fluids.

Another widely used cycle in the LNG cold recovery is the Brayton cycle. Kaneko et al. [26] presented two types of Brayton cycles at 1500 °C which improves the efficiency of the cycle by 60%. However, this type of cycle has its own limitations due to the high temperature requirements. The Brayton cycle utilizes a part of the natural gas extracted as the running fuel in the combustion chamber. In the internal combustion, the power is generated which is then fed to multistage compressors to run an external generator. In between the compressors, the cooling heat exchangers utilize the cold energy associated with the LNG in the pipeline in order to obtain a higher efficiency compression. Lu and Wang [27] showed that the use of nitrogen Brayton cycle in conjunction with the ammonia-water Rankine cycle can create exergy efficiencies between 25% and 36% depending on the inlet and outlet turbine pressures. They presented optimization of the complicated cycle using hot fumes (generated by the Rankine cycle) as the working fluid in the Brayton cycle. They have realized that the use of an expander in the open LNG cycle contributes to the majority of the increase in the performance. Dong et al. [28] studied the LNG cold recovery cycle using a Stirling cycle in which nitrogen in the compressor was cooled down using the LNG cold energy with an exergy efficiency of 24.26%. Stirling cycles can also be used with different working fluids besides nitrogen, in which the decision of which working fluid to be used depends on the designer of the plant. Regardless of the choice of the working fluid, the cold energy from the LNG and warm energy from the surrounding are the driving forces of the Stirling Engine.

1.6 Treatment

Depending on the reservoir's source, the raw natural gas has certain compositions. Table 1-1 shows the composition of natural gas from a typical reservoir in USA.

Table 1-1: The natural gas composition in a typical reservoir in USA

Component	Specification
CO ₂	<2 mol%
H ₂ O	<120 ppm
H ₂ S	<4 ppm
Hydrocarbons (C ₃₊)	950-1050 Btu/scf (35387.5-39112.5 kJ/m ³)
Inert Gases	<4 mol%

Natural gas is generally composed of methane (CH₄), other light hydrocarbons (C₂H₆-C₅H₁₂), heavy hydrocarbons, water, carbon dioxide (CO₂), hydrogen sulfide (H₂S), helium and nitrogen [29]. To meet the pipeline specifications and regulatory standards required during transportation, natural gas has to be sweetened (treated). Figure 1-8 shows a typical natural gas treatment process plant where the feed gas extracted from the reservoir is sent to an inlet processing unit through which gas, liquid gas, water and mixed solid particles are separated from each other [30]. The liquid portion of the raw natural gas which contains heavier hydrocarbons (such as ethane and propane) will be used as refrigerants in the cooling process. The gas portion of the raw natural gas is first transferred to the acid gas removal unit (referred to the gas sweetening unit) to remove CO₂ and H₂S due to their corrosive properties. After this step, the sweetened gas is transferred to the dehydration and mercury removal unit to prevent solidification of water during cooling process and reaction of mercury with aluminum heat exchangers, respectively. After this step, the gas is prepared for transport.

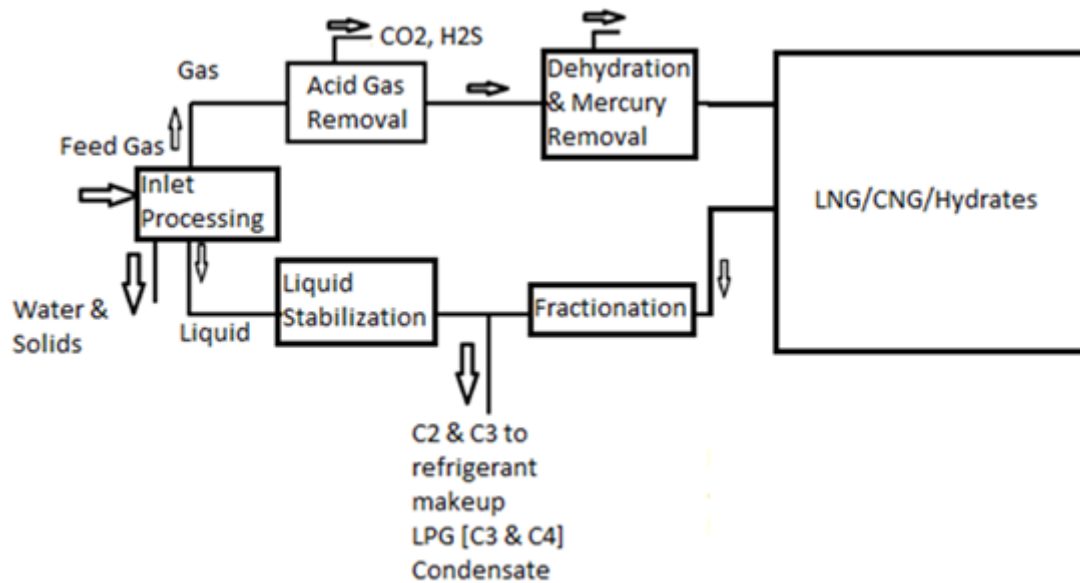


Figure 1-8: Typical processes involved in natural gas treatment

Acid gas removal – Several sweetening processes are being implemented in the natural gas acid removal industry. Among these methods, chemical solvent absorption techniques (amine treatment) are the most widely-used method in current natural gas sweetening industries. Amine absorption techniques use chemicals ranging from MEA (Monoethanolamine), DEA (Diethanolamine), and TEA (Triethanolamine) [31]. These methods have been used for numerous plants as they are relatively independent of the CO₂ and H₂S pressure and reduce the amount of acid gas to ppm (particles per million) levels. However, these methods consume high energy for the regeneration of the solvents. In addition to this high-energy requirement, the chemical solvent absorbents are dissolved in water, and hence, natural gas becomes saturated with water after mixed with these solvents [31]. Therefore, innovative technologies for gas sweetening (separation of H₂S and CO₂ from the main gas) have been implemented using polymeric membranes for their ease of manufacturing [32, 33]. Polymeric membranes are non-porous, and are either made of glass or rubber. The latter is selected based on the gas solubility and the former is selected based on the gas diffusion in the dense membrane matrix. Total separation of the gases depends

on the molecular size of the gas in addition to the chemical interaction between the polymer and the gases. These membranes are mostly common when reservoir's quality deteriorates and H₂S and CO₂ contents increase [32]. Also, membranes have better efficiency in capturing acid gases allowing for low ppm traces. However, a major disadvantage of polymeric membranes is the pressure drop occurring across the membrane. This pressure drop requires higher energy input from the upstream compressors.

One of the major projects in which the polymeric membranes are used is the \$120-million USD project in South East Asia run by the Cynara-Natco group [34]. Polymeric membranes which were first marketed in the 1980's for CO₂ removal [35, 36] can also be used for the heavy hydrocarbons removal [36], dehydration [36], and nitrogen separation [36]. For CO₂ and H₂S removal, there are three types of polymeric membranes commercially available: cellulose acetate, polyimides and perfluoropolymers. These polymers are used due to their mechanical strength, thermal and chemical resistance, and long lifetime.

Liquid removal – Water particles that are re-fed to the well to maintain the well's pressure are separated from the natural gas using different filtration techniques including filter separators, cartridge filters, coalescing filters, and cyclone filters. Filter separators, used to remove fine liquid mists, are usually located in the upstream where the primary filtration is required. Cartridge filters consisting of cellulose membranes, steel screens or phenolic resins are used to filter the particles as small as 0.5 μm [39]. Coalescing filters used for separation particles as small as 0.01 μm are designed to cause a sudden change in the direction of gas/liquid flow; these filters located downstream near the process equipment are used to remove glycol, fine oil droplets and other liquid contaminants [40]. Cyclone filters are another type of filtration techniques operating based on centrifugal forces to separate liquid particles as small as 8 μm from the gas [39].

Natural gas may contain traces of vapor which needs to be removed before liquefaction. In essence, vapor traces frozen during the liquefying process are harmful for the compressors and pumps used in the liquefied natural gas (LNG) plants. Vapor also reduces the efficiency of the storage of liquefied natural gas as it reduces the stored amount of LNG. Typically, glycols are used to absorb the water found in the wet gas. The wet glycol, referred to as “rich glycol”, is then thermally dried and re-fed to absorb more water from the feed gas. Different types of glycols used include tri-ethylene glycol (TEG), di-ethylene glycol (DEG), ethylene glycol (MEG) and tetra-ethylene glycol (TREG). TEG is the most common type used in the natural gas industry.

Solid removal – There are many technologies available for the filtration of solid particles. Current solid-gas filtration technologies include i) cyclone scrubbers (5 μm filtration capability), ii) vertical gas separator with vane (8 μm filtration capability), iii) in-line vane (8 μm filtration capability), iv) vertical separator with wire mesh (8 μm filtration capability), and v) filter separators with vane (3 μm filtration capability) [41]. On the other hand, there are three main types of solid-gas filtration processes including i) dry gas filters (1-3 μm filtration capability), ii) filter separators with vanes (0.5-3 μm filtration capability), and iii) cyclone scrubbers (5-8 μm filtration capability). The efficiency of these solid-gas separators generally depends on the particle size, the spatial distribution of particles, and their working principle [41]. The dry gas filters use filtering media with very small pores which capture solid particles [41]. Filter separators with vanes use angled plates to reduce the momentum of the solid particles as they impact these plates [41]. The cyclone scrubber uses the centrifugal force to push the particles towards the wall, and ultimately separate them from the gas.

Cyclone scrubbers are one of the most widely-used separators as they can handle high temperature and corrosive liquids, and offer low capital cost and ease of operation (due to

no moving parts). A typical design of the cyclone separators is shown in Figure 1-9. As the dusty gas enters the chamber tangentially, the particles go through a helical path and experience centrifugal forces. Since the solid particles are denser than the gas particles, they are pushed towards the cyclone walls by the centrifugal force, and are collected at the bottom of the cyclone. The filtered natural gas is then collected at the gas outlet vent located at the top of the cyclone.

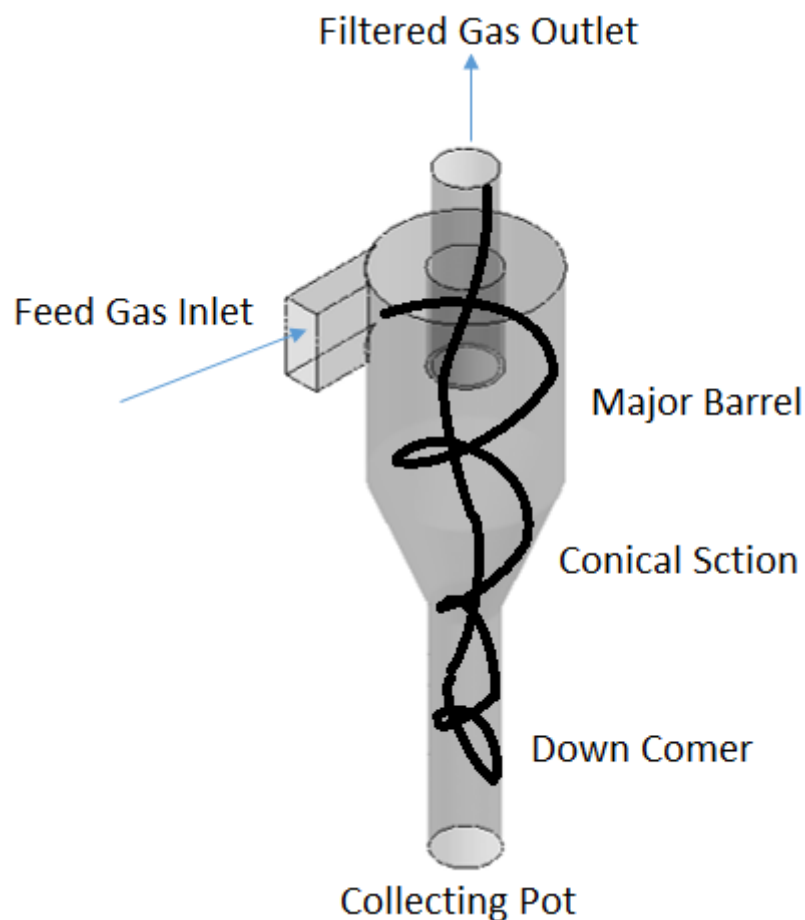


Figure 1-9: Schematic of a cyclone separator

Since the introduction of cyclones, modeling the particle separation efficiency has been researched [42]. For example, Zhao [43] developed a time-of-flight model to predict the particle separation efficiency, and compared the model efficiency with experimental work [43] and other numerical models presented by Leith and Licht [44] and Barth [45]. The time of flight model estimates the separation efficiency of solid particles based on the time

they spend in the cyclone. The model was in agreement with the experimental results with a maximum error of 10%. In another study, Qian and Zhang [46] added the effect of the straight tube and dustbin in the separation efficiency. The straight tube effect was included in their model by modifying the particle residence time so that the entire cyclone geometry is used. Their findings indicated a maximum error of 7% compared to the experimental data reported by Hoffmann et al. [47] and Qian et al. [48].

The main drawback of the cyclone filters is their low efficiency in solid particle removal. Based on the current designs of cyclones, the efficiency of solid removal increases at higher inlet velocities. However, a higher velocity causes a greater pressure drop (due to the increased turbulence), and hence, an increase in the operating cost. Most of the industrial cyclones use a certain optimum velocity (of 18.3 m/s) for the highest efficiency. The pressure drop is directly related to inlet velocity [42]. The direct relation shows that increasing the inlet velocity would increase the pressure drop due to turbulence. As for high Reynolds (Re) numbers, turbulence will be large inside the cyclone resulting an increase in the pressure drop. However, the main reason for the increase in the pressure drop is due to the increased in the friction loss occurring at the bottom of the cyclone where there is a sudden change in the flow direction. In recent years, many researchers have focused on increasing the efficiency of cyclones while maintaining the pressure drop and reducing the operating cost [42]. These studies have focused on alternative designs to enhance the cyclone performance. For instance, to further reduce the pressure drop, Xiong et al. [42] proposed the use of vortex finders at the inlet of the cyclone; the vortex finders, which are plates/cavities with straight or helical profiles, were able to reduce the overall pressure drop by generating a vortex. Compared to cyclone separators possessing a basic vortex finder, the helical design reduced the pressure drop by 73% and improved the overall separation efficiency by 9%. As a result, an efficiency of 99% was obtained for removal of particles

bigger than 10 μm , and 40% was obtained for removal of 2- μm particles. Xiong et al. [49] also compared the efficiency of a single cyclone with that of a multi-cyclone setup. Their multi-cyclone system consisted of 15 single cyclone separators positioned in parallel with the same inlet. Their findings indicated that the collection efficiency of the multi-cyclone separator is 2 to 10% less than that obtained from the single cyclone separator. This efficiency reduction is suggested to be due to the non-uniform distribution of the intake flow at each of the cyclones, resulting in different separation performance [49].

In recent years, wet cyclone scrubbers, which are based on spraying mist to the particulate gas, have been proposed to increase the centrifugal force acting on the solid particles. For instance, Yang and Yoshida [50] investigated the injection of pure mist (water at varying rates from 0 to 2.4 l/hr) within particulate natural gas and the subsequent effects on the separation efficiency. The flowrate provided in their work is based on the volumetric flowrate. Their results showed a maximum of 20% improvement in the particle capture efficiency at the 0.042 mist to gas flowrate ratio. Despite the general success of the wet cyclone scrubbers in enhancing the separation efficiency, they have limitations due to the additional centrifugal force provided by these systems. In essence, the additional centrifugal force requires an increase in the size of the mist, which will ultimately add to the operating cost of the cyclone.

The use of electro-hydrodynamic and magnetic forces to increase the efficiency of the cyclones has also been proposed. Yoshida et al. [51] studied the effect of the conical length on separating negatively charged silica particles from water in electro-hydro cyclones. In this particular study, sodium hydroxide was added to the water-silica mixture to increase the pH of the mixture, and thus increase the negative charge on the silica particles. Their findings indicated that the 50% cut-size (i.e., the particle size for which the separation efficiency of the cyclone is at 50%) decreased as the electrical potential increased. Despite

the potential of their design, it cannot be applied to pure gas applications. In another study, Svoboda et al. [52] investigated the effects of applying a radial magnetic field to control the density difference of the ferro-coated silicon particles between the overflow and underflow of the dense medium cyclone. Since the particles at the inlet have different ferrous-silicon compositions, a reduction in the density difference between the overflow and underflow is required to reduce the wide range of densities available inside the cyclone. Their study showed that by increasing the magnetic flux density from 0 to 70 G, the density difference between the overflow and underflow outlets reduced from 0.45 g/cm³ to 0.25 g/cm³ at a ferro-silicon feed of 2.35 g/cm³. This design is only applicable when the silica particles are ‘naturally’ mixed with the ferrous particles.

Park et al. [53] investigated numerically the separation efficiency using cyclones in series. In their study, one cyclone separator is divided into three sections. Each section is composed of a different diameter decreasing from the top cyclone to the bottom. This setup allows for larger particles with higher inertial forces to be separated without interfering with the smaller ones which are separated at a later stage. Their results showed that the first cyclone segregates particles in the range of 4.5 – 11.0 μm, whilst the second setup traps the particles in the size of 3.4 – 7.9 μm, and the third cyclone collects the particles in the range of 1.8 – 4.3 μm. This design provides an overlap in terms of the particle size between the three stages, so if a certain particle size is missed in the earlier stage it will be trapped in the following stages. However, the series configuration of the cyclones increases the pressure drop across the setup as compared to one cyclone. Kim et al. [54] implemented helical guiding vanes inside the cyclone to study experimentally their effect on the separation efficiency. Their design with 6 revolutions of helical vanes at the inlet flow rate of 15 l/min led to a 27% enhancement in the separation efficiency of 4-μm particles. Despite the general enhancement in the efficiency, the design provides a complexity in the

manufacturing process of the cyclone. In addition, only a certain size of the particles follows the same helical path as provided by the fixed design proposed by Kim et al. [54]. For the sizes outside this range, the particles impact the vanes. Brar et al. [55] increased the conical length of the cyclone and numerically studied the effect on the separation efficiency. This approach increased the separation efficiency by 9.5% for 3- μm particles by increasing the major cyclone cylinder length by 5.5 times of the cyclone diameter. Moreover, the proposed increase in the conical length reduced the pressure drop by 34% as compared to the conventional design. They also showed that by a further increase in the conical length (6.5 times of the cyclone diameter) the separation efficiency increases by 11% while the pressure drop reduces from 34% to 29%. This is due to the fact that a longer conical section means a larger angle between the main barrel and the conical section walls, which makes the flow transition of the gas smoother before it redirects towards the exit. Xiang et al. [56] also investigated experimentally the effect of the dimension of the conical section on the separation efficiency. At the inlet flow rate of 30 l/min, their experimental results showed that reducing the cone bottom opening from 19.4 mm to 11.6 mm enhances the 4- μm particle separation efficiency from 70% to 86%. By increasing the inlet flow rate to 40 l/min, the efficiency for the same size of the particles was further increased to 92%. Similar to previous geometrical modifications, this reduction in the cone diameter increases the pressure drop through the cyclone separator by 15%. In another study, Chuah et al. [57] studied numerically the effect of the conical dimensions on the cyclone performance. By reducing the bottom conical diameter from 19.4 mm to 11.6 mm, they achieved a 40% increase in the efficiency for 1.5- μm particles. Despite this enhancement in the separation efficiency, the main disadvantage of this method is the pressure drop increase by 42%. Another important part affecting the separation efficiency in the cyclone separators is the length of the down comer (which has also been referred to as the vertical tube in literature

[57]). Bryant et al. [58], Zhu and Lee [59] and Mothes [60] emphasized that the down comer controls the natural vortex length of the flow and particle capture. Qian et al. [61] studied the enhancement of the cyclone separation efficiency by investigating numerically the influence of the prolonged vertical tube attached to the bottom of the conical section at the dust outlet. Their study showed that an increase of 0.5 m in the length of the vertical tube increases the separation efficiency by a maximum value of 15% for 3- μm particles. Another example is the CFD analysis conducted by Bogodage and Leung [62] on the effect of the down comer height on the efficiency. Their results showed that increasing the down comer height by 381 mm increases the separation efficiency by 20% for particles smaller than 3 μm . A similar study conducted by Gil et al. [63] showed the effect of the increase in the down comer height (without the use of the hopper) enhancing the separation efficiency to 87% for particles smaller than 5 μm .

Another innovative cyclone design was developed by Lim et al. [65], in which they introduced a double inlet cyclone by splitting the cyclone's inlet using a thin plate. Using this approach, they were able to increase the separation efficiency by 15% as compared to the conventional cyclones with one inlet. However, the reduced inlet area increases the pressure drop by 20% compared to the conventional cyclone designs. Moreover, this design requires an additional infrastructure (e.g., the mass flow controller and diffusion dryer) to provide the clean gas at one of the inlets. In a similar study, Kim and Lee [65] studied the enhancement of the cyclone separation efficiency by investigating the influence of the exit tube size. Their study showed that increasing the exit tube size from 0.8 cm to 1.0 cm decreases the collection efficiency from 80% to 45% for 4- μm particles. Although the increase in the exit tube size reduced the collection efficiency and vice versa, the increase in the exit tube diameter reduced the pressure drop by at least 33%. In another study, Misiulia et al. [66] carried out an experimental analysis to evaluate the effect of the cyclone

inlet angle on the separation efficiency. Their results showed a reduction in the pressure drop coefficient from 460 to 150 as the inlet angle increases from 7 to 15 deg. However, increasing the inlet angle reduces the collection efficiency by 32%. Lim et al. [67] investigated the effect of vortex finders on the enhancement of the cyclone separation efficiency. Their results showed an increase in the collection efficiency (14% for 2- μm particles) as the vortex finder diameter decreased. However, the decrease in the vortex finder diameter would increase the pressure drop. In another study, Jung et al. [68] proposed the addition of a granular packed bed at the clean gas outlet for enhancing the separation efficiency of smaller particles. In their study, they used two sizes of granules (2 mm and 4 mm sizes). In essence, the large contact area between the granules and the solid particles escaping with the clean gas enhances the capture efficiency of fine particles; while larger particles are still separated by the conventional cyclone in their setup. At the inlet flow rate of 10 l/min, their experimental results showed that the efficiency increases for 4- μm particles (from 5%) to 58% and 92% using 4 mm and 2 mm granules, respectively. Despite this large enhancement in the capture efficiency, the main disadvantage of this method is the fact that the void spaces in the granules are filled with the captured particles over time, requiring a periodic replacement.

Many researchers have tried developing a theoretical model which can mimic the cyclone separation efficiency. Figure 1-10 shows the different curves achieved by different groups. For example, Leith and Licht [69], who introduced the temperature factor in their separation model have over-estimated separation results for particles smaller than 2 μm ; whereas they have underestimated separation results for particles larger than 2 μm . Similarly, the model proposed by Clift et al. [70] underestimated the efficiency for all particle sizes as compared to the simulated results. Among different theoretical models, the best model for describing the separation efficiency is the one developed by Mothes and

Loffler. Even their model does not fit the simulated results perfectly. The different profiles in Figure 1-10 are all obtained based on different analytical approaches proposed by different groups [69, 70].

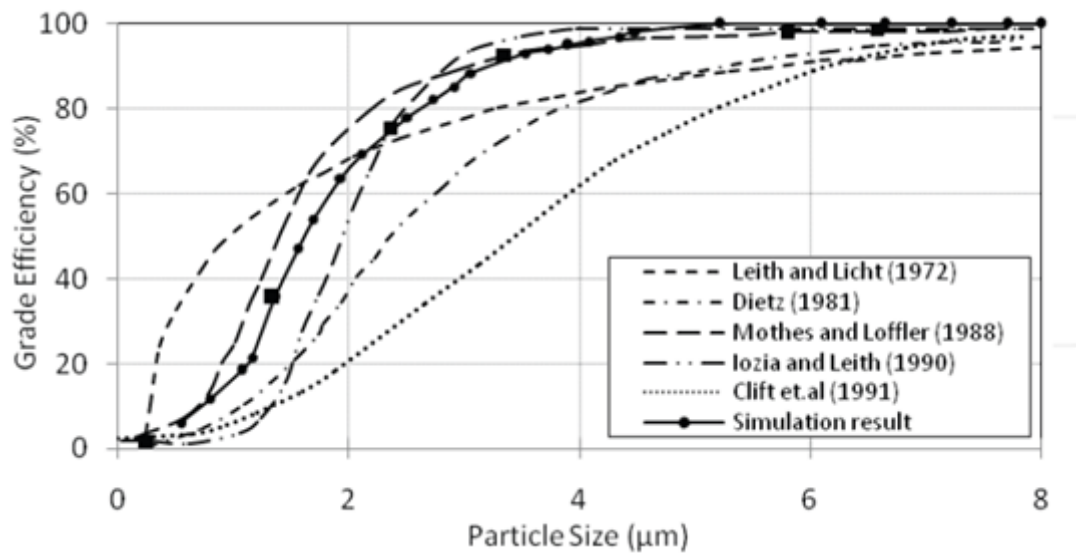


Figure 1-10: Several theoretical approaches (reproduced from [70] with permission from InTech)

Researchers have pointed out some of the variables which potentially affect the separation efficiency. For example, Ji et al. [71] studied the effect of inlet velocity on the separation efficiency. They reached a conclusion that increasing the inlet velocity enhances the separation efficiency (see Figure 1-11). Similarly, Wang et al. [72] studied the effect of the inlet velocity on the pressure drop inside the cyclone separator. Their curves show that increasing the inlet velocity increases the pressure drop exponentially (see Figure 1-12).

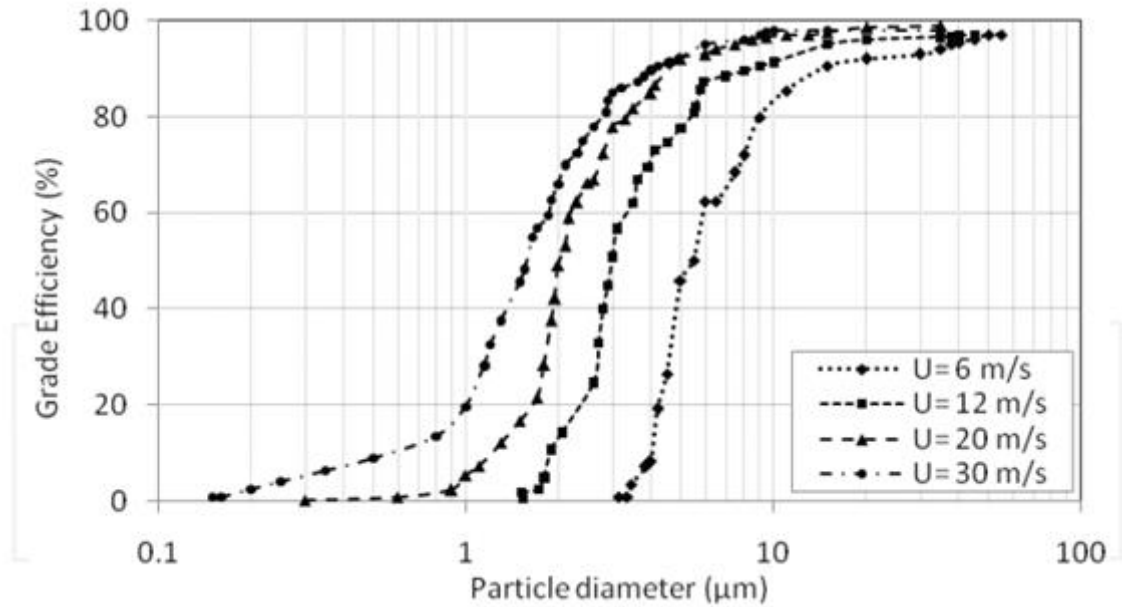


Figure 1-11: Effect of inlet velocity on separation efficiencies (reproduced from [70] with permission from InTech)

Although the above innovative modification enhances the solid-gas separation in cyclone scrubbers, they cannot be implemented in existing cyclones in operations. In essence, reducing the overall capital cost while enhancing the separation efficiency at low pressure drops would be cost effective. Therefore, alternative methods aiming at further increase in the efficiency of existing cyclone separators must be explored.

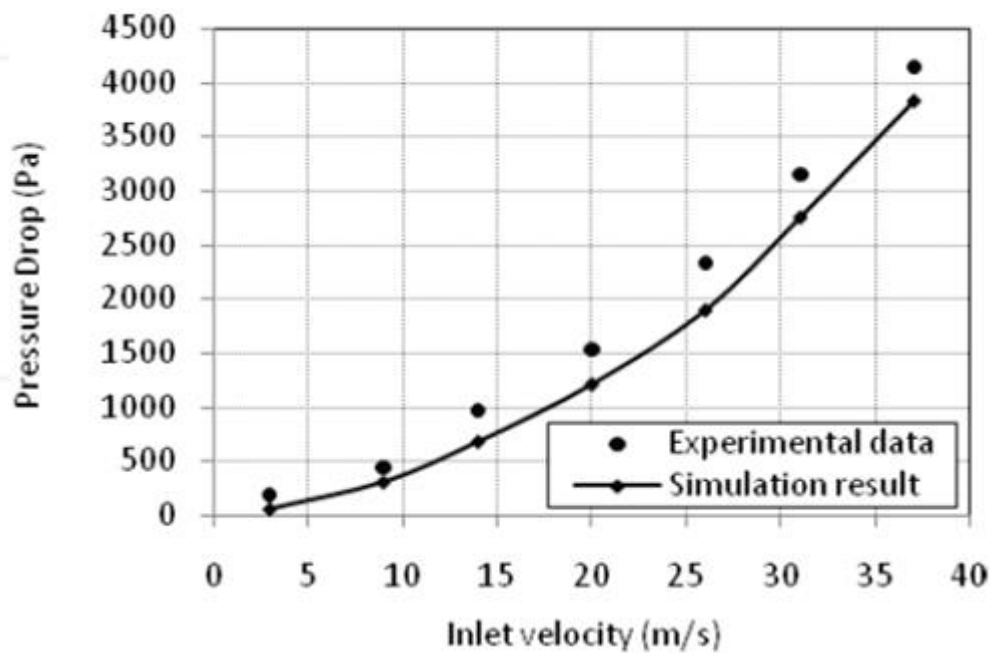


Figure 1-12:Effect of inlet velocity on pressure drop (reproduced from [70] with permission from InTech)

1.7 Motivation and objectives

The continuous enhancement of the efficiency of cyclone separators is crucial for natural gas industry. Many plants are heading towards cyclone separators as they require less maintenance and they are simple in design. Cyclone separators also have a cost advantage over other filters such as cartridge and coalescers. However, to replace the cartridge and coalescer filters, the efficiency of the cyclone separators must be improved especially for small size particles.

The aim of this study is to increase the capturing efficiency of fine particles using passive and active modifications that can be implemented in the current operating systems (as opposed to many other enhancements reviewed in the previous section). These modifications are based on: i) magnetic force attraction with the use of the ferrous powder coating process, ii) electrostatic force attraction using the charged coating process, and iii)

the addition of a tangential capturing chamber at the conical section in addition to the existing bottom collection chamber. The reasons behind each of these additions are explained below:

Magnetics – In several natural gas extraction locations (such as Rocky Mountains) the gas stream contains ferrous in addition to nonferrous solid particles. Permanent magnets can be used to remove the ferrous powder. Nonferrous powder can also be attracted by magnetic forces if coated with ferrous powder. This requires the spray of adhesive ferrous powder to the non-ferrous powder. The magnetic attraction between the permanent magnet and the ferrous powder increases the centrifugal forces applied on the particles and hence increases the separation efficiency. (see Figure 2-3 shows a schematic of the procedure and Appendix C for cost analysis).

Electrocoating – similar to magnetic-based attractions, the second method for the enhancement of separation efficiency proposed here is the use of electrostatic forces. In this approach, the solid particles are coated with a charged powder. The charged coated particles can then be attracted to an oppositely charged surface inside the cyclone. This approach also increases the centrifugal forces applied on the particle (Refer to Appendix C for cost analysis).

Additional collection chambers – Similar to the other modifications, the addition of a collection chamber is proposed to maximize the centrifugal forces acting on the particles at the conical section. The increased centrifugal forces are generated to enhance the particles capture due to the increased centrifugal forces occurring as the result of the reduction of the rotational radius of the particles. Small particles in traditional cyclone separators would impact the walls of the conical section, bounce back, and then get carried away with the gas flow [51]. The additional collection chamber, on the other hand, will

collect these particles before they get the chance to gain their momentum with the flow (Refer to Appendix C for cost analysis).

1.8 Thesis organization

This thesis is comprised of 8 chapters which are organized as follows:

Chapter 1: A review of natural gas processes has been presented. The focus of this research is on the treatment processes involving the separation of solid particles from the gas stream. The advantages and the shortcomings of current technologies were discussed. The objectives of the present thesis were presented.

Chapter 2: The experimental setup is presented. Afterwards, the fabrication methods for different components of the cyclone separator and its materials used for the experiments are explained.

Chapter 3: The current theoretical approaches used for modeling conventional cyclones, and the details of the modified theoretical approach presented here are explained.

Chapter 4: The numerical model developed for understanding particle behavior in the cyclones is presented.

Chapter 5: Active modifications to the cyclone separation process are discussed. This chapter explains the theoretical and experimental approaches studied for the cyclone separator enhancement. This includes the theoretical and experimental results of the conventional cyclone, cyclone with electrostatic forces and the experimental results of cyclone with magnetic forces.

Chapter 6: Passive modifications to the cyclone separation process are discussed. This chapter explains the numerical and experimental approaches studied for the cyclone

separator enhancement. This chapter discusses the addition of a tangential chamber and its effect on separation efficiency enhancement.

Chapter 7: This chapter presents the costs associated with each of the modifications presented here.

Chapter 8: Finally, the summary and a list of contributions, and the suggestions for future studies are presented.

Chapter 2: Experimental setup*

This chapter presents the experimental setups developed to study the enhancements proposed here for increasing the efficiency of cyclone separators. The first setup was developed for addition of ferrous powder to study the effect of magnetic and electrostatic attractions. The second setup was developed to study the addition of a tangential chamber at the conical section. In these setups, the separation efficiency is evaluated by dividing the outlet particle count by the inlet particle count. Both counts were evaluated based on a sample taken from the outlet and inlet particles as described in this chapter.

2.1 Underlying principle

The experimental setup of the cyclone separator under study is shown in Figure 2-1. The fan attached at the inlet of the cyclone blows the air-sand mixture into the cyclone inlet at a tangential velocity of 14 m/s. The inlet velocity is determined from the volumetric flowrate and the inlet area (with the radius of 17.4 cm). The solid-gas mixture entering the inlet chamber tangentially follows a helical path inside the cyclone and experiences centrifugal forces. Since the solid particles are denser than the gas, they are pushed towards the cyclone walls by the centrifugal force, impacting the walls and falling at the bottom of the cyclone due to their momentum loss. The filtered gas changes its direction and flows to the open path at the clean gas exit located at the top of the cyclone cylinder. However, finer particles gain their momentum quicker than larger ones after their impact to the cyclone walls. These particles are able to cope with the sudden change of the gas stream and escape with the clean gas. This causes vibration and erosion of the downstream equipment. Therefore, in the cyclone design, it is very important to enhance the removal of fine particles (smaller than 10 μm). This can be achieved by increasing the radial forces.

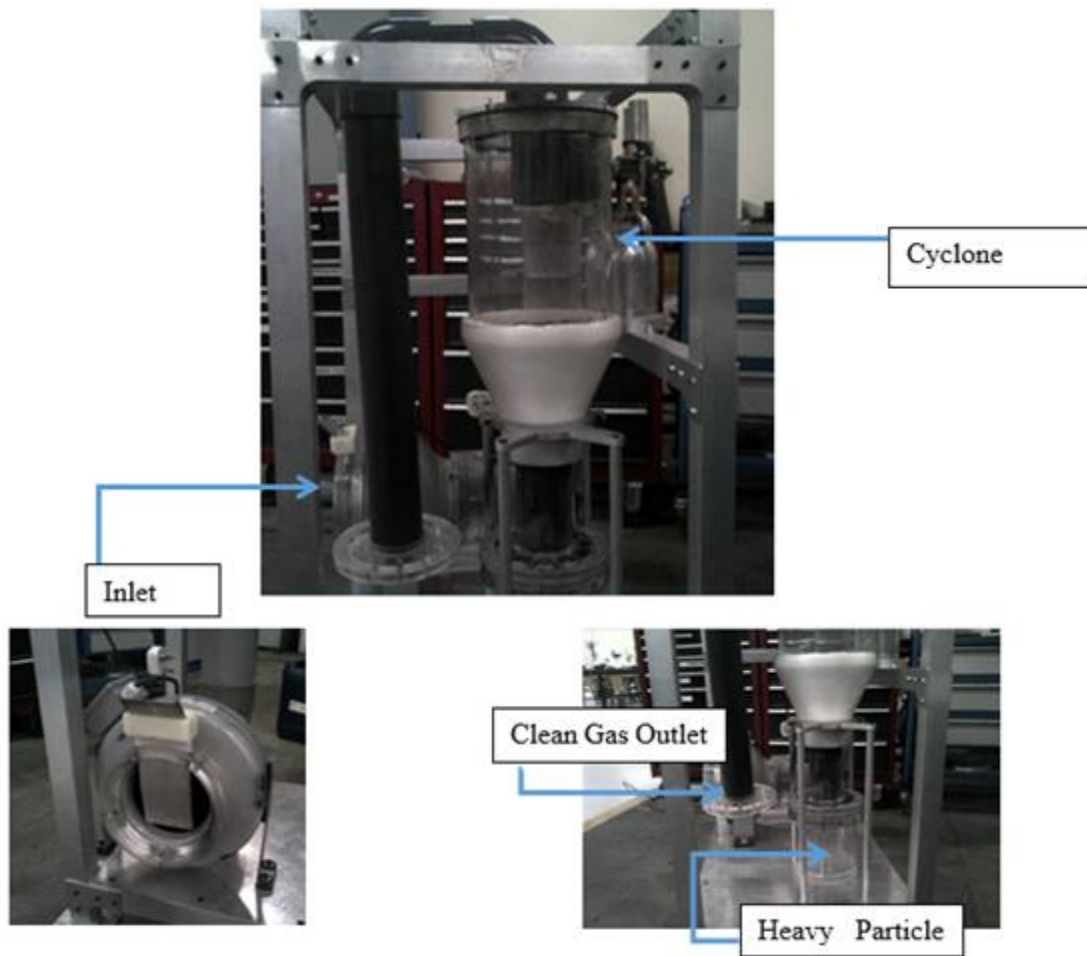


Figure 2-1:Experimental cyclone setup

2.2 Dimensions

Dimensions of the cyclone are shown in Figure 2-2. In this study, a cyclone with a radius of 190 mm is analyzed. These dimensions are based on Stairmand's design [55]. The inlet velocity of the gas-dust mixture is set to be 14 m/s, where the analysis of the sample particles was modeled at the average width of the inlet (40 mm). To verify the results, the separation efficiency is determined for a conventional cyclone and compared to the experimental values presented by Ji et al. [71].

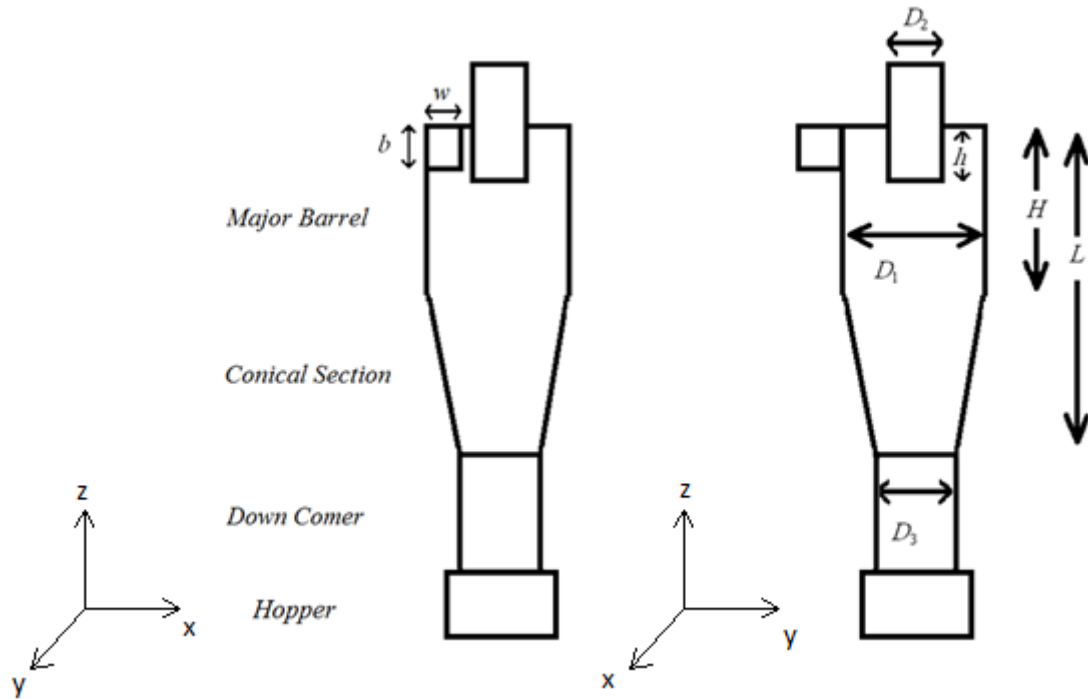


Figure 2-2: Experimental Setup Dimensions (Side and Front Views). Inlet Velocity ($V_0=14$ m/s), $H = 240$ mm, $h = 115$ mm, $L = 390$ mm, $D_1 = 190$ mm, $D_2 = 65$ mm, $D_3 = 70$ mm, b (height of the inlet chamber) = 90 mm and w (width of the inlet chamber) = 40 mm.

2.3 Fabrication

The cyclone apparatus was fabricated using several types of material. The first one was used in fabrication of the major barrel, minor barrel, down comer, hopper, inlet and outlet chambers. For these sections, transparent material is used to visualize the sand particles movement inside the cyclone. Therefore, a Nylon bar was used and machined to build the upper parts (mentioned above). The inlet, however, was built from 4 Nylon plates attached together to form a rectangular inlet. The helical section of the cyclone was made of Teflon using the CNC machine. Teflon was selected for this part as there was a difficulty finding a readymade Nylon helical section according to the cyclone's dimensions. The outer pipes connected to the cyclone (e.g., the pipe connecting the inlet to the inlet fan and the pipe

connecting the outlet to the hopper) were made from PVC pipes. Finally, the fan with a 4800 m³/hr volume flowrate was installed to provide the gas inlet at a speed of 14 m/s. In the experimental study, the flow is considered to be uniform and with a constant rate. This is assumed based on the fan's manufacturer specification regarding the volumetric flowrate input from the fan. In reality, the fan would have a none-uniform flow input with a fluctuated inlet velocity. To overcome this fluctuation, the experiments were run three times to ensure the reproducibility of the results and reduce the role of uncertainties due to the assumption made about the flowrate of the fan. The entire setup was attached inside a rolling cage for ease of movement. The cost of different parts is listed in Table 2-1.

Table 2-1: Cyclone material cost

Part	Description	Cost
1	PVC external pipes	42 USD
2	Nylon bar (250 Dia)	300 USD
3	Aluminum pipe	55 USD
4	Fan (6"x6")	110 USD
5	Elbows	20 USD
6	Whatman filters	110 USD

2.4 Addition of ferrous powder for magnetic forces

To increase the radial forces acting on the particles, particles are coated with ferrous powder which consists of nano iron particles (100 nm in size) found in laser printer toners (i.e., MICR Toner for HP Laser Jet or Jet Black Powder Toner). In the proposed system, solid particles are mixed with the ferrous powder prior to their inlet to the cyclone. An additional radial magnetic field is created inside the cyclone by placing a neodymium disc magnet (D9mm × T1.5mm grade N35) at the clean gas outlet. In the presence of a radial

magnetic field, the ferrous powder-coated sand particles experience an additional magnetic force, and therefore, are captured inside the cyclone setup.

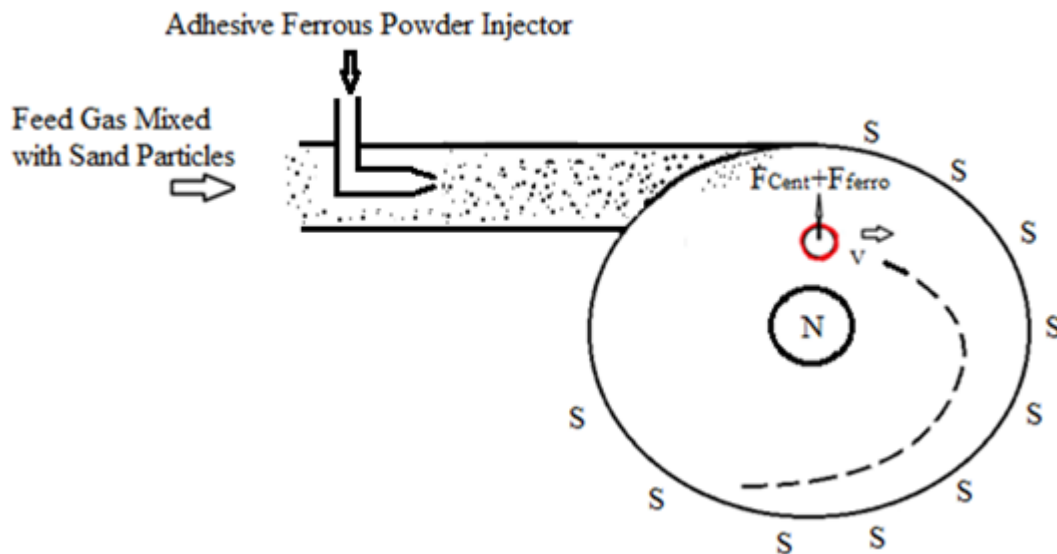


Figure 2-3: Schematic of centrifugal (F_{Cent}) with magnetic forces (F_{ferro}) in a cyclone. The coating process is performed using an inlet tangential ferrous powder sprayer (see Figure 2-3). The sand particles enter the inlet chamber, where they intersect with the ferrous powder sprayer used for the coating process. In the injection process, a part of the clean gas stream is extracted and used for the ferrous powder injection by means of a small gas compressor. The sprayer creates a cloud of the ferrous powder to ensure all sand particles are coated. The ferrous powder is injected using a coaxial parallel flow. The velocity of the injected particles was close to zero and was ensured to not alter the overall velocity of the fluid flow entering the cyclone separator.

The escaped solid particles are collected on a membrane (Whatman membranes, GE Healthcare) at the outlet stream and analyzed under the Qualitest Digital Microscope (Hardness Tester). The MH_VK_E software package is used for determining the particle dimension. Figure 2-4 shows the membrane surface under the microscope before (a) and after (b) collecting the particles on the membrane, respectively. To assure that there is a close correlation between the samples taken from the outlet and inlet, the mean, standard

deviation of each of the samples taken and their corresponding errors are presented in Table 2-2. The small error in the mean and standard deviation between both samples indicate a close correlation between them.

The sampled particles at the inlet and outlet are chosen to achieve a 10% variation in the mean value of the inlet and outlet samples. The size distribution within the sampled particles is used to estimate the volume (and consequently the mass using sand density of 1780 kg/m³ [73]) of the sampled particles. On the other hand, the overall mass of the particles deposited on the filters (at the inlet and outlet) was measured after 2 min. Therefore, the size distribution obtained from the analyzed sample investigated under the microscope is multiplied by a scaling factor to obtain the real size distribution of the inlet and outlet particles. Scaling up of the size distribution is conducted by dividing the weight of the real sample by the weight of the sample characterized under the microscope (i.e., weight of 100 particles) as

$$SF = \frac{W_{WS}}{W_{AS}}, \quad (2-1)$$

where SF is the scaling factor, and w_{WS} and w_{AS} are the weights of the whole sample and analyzed sample, respectively. Table 2-3 represents the weight of the analyzed sample, the weight of the real sample and the scaling factor calculated using Equation (2-1). The scaling factor decreases after the addition of ferrous powder to the inlet sand stream. This reduction is an indication of the solid-gas separation efficiency enhancement.

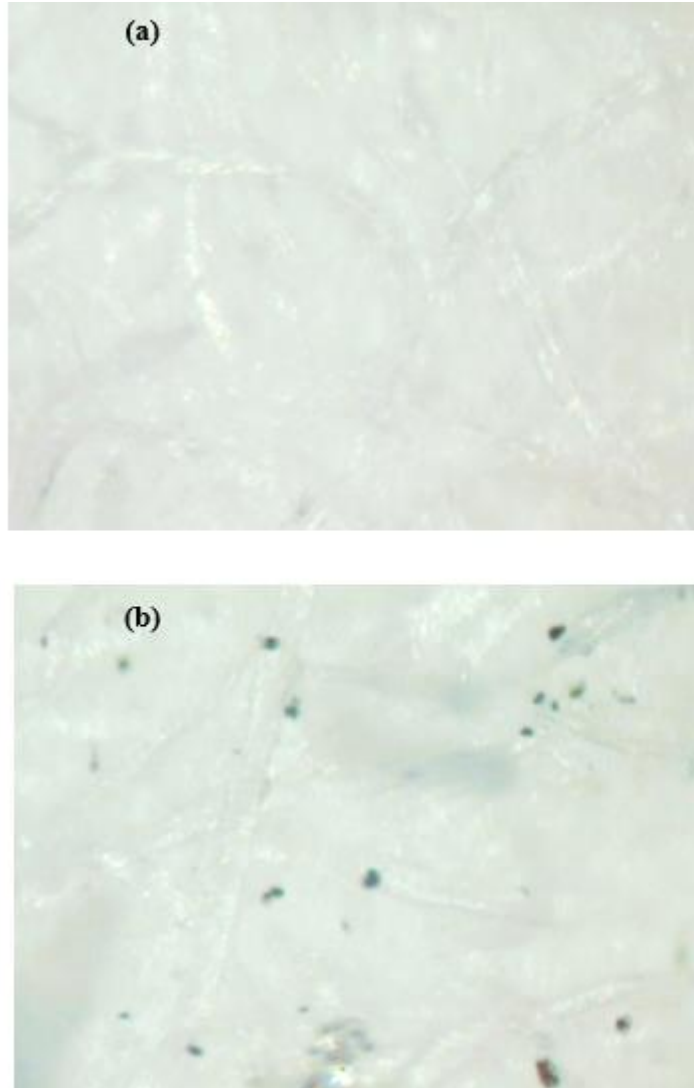


Figure 2-4:(a) Microscopic image of an empty membrane, (b) microscopic image of captured dust particles on the membrane

To evaluate the enhancement in the solid-gas separation in the proposed approach, the size distribution of the collected dust particles at the outlet and inlet are compared. For each particle size, the count of the outlet particles (dry and ferrous-coated) is compared against the inlet dust particles. The separation efficiency is calculated as

$$\varepsilon_{SP} = \left[1 - \frac{n_{Outlet}}{n_{Inlet}} \right], \quad (2-2)$$

where n represents the scaled number of particles.

Table 2-2:Statistical values of the analyzed samples (for magnetic forces)

Sample Category	Sample Number	Mean (μm)	Mean Error (%)	Standard Deviation (μm)	Standard Deviation Error (%)
Inlet Samples	Sample 1: 100 Particles	27.5	5.33	37.4	6.92
	Sample 2: 100 Particles	26.1		40.2	
Outlet Sample (Conventional Separation)	Sample 1: 50 Particles	7.35	3.07	2.11	1.78
	Sample 2: 50 Particles	7.13		2.15	
Outlet Sample (Ferrous Coating Separation)	Sample 1: 50 Particles	6.86	1.37	2.02	7.07
	Sample 2: 50 Particles	6.95		1.89	

Table 2-3:Particles weights (for magnetic forces)

Description	W_{AS} (kg)	W_{WS} (kg)	SF
Inlet	4.98×10^{-8}	1.80×10^{-2}	3.61×10^5
Outlet (Conventional)	4.63×10^{-11}	2.80×10^{-6}	6.04×10^4
Outlet (Ferrous Coated)	3.87×10^{-11}	5.00×10^{-7}	1.29×10^4

2.5 Addition of ferrous powder for electrostatic forces

To increase the radial forces acting on the particles, the particles are coated with ferrous powder similar to the previous section. The solid particles in this study are mixed with the ferrous powder through Redline E-coating gun. The gun provides an electric charge of 30kV-50kV to the ferrous-coated solid particles through its nozzle. Thus, the solid particles are mixed with the ferrous powder and becomes charged prior to their inlet to the cyclone. The charged particles are attracted to the inlet walls of the cyclone that are grounded. On the other hand, the escaping solid particles are collected on a membrane (i.e., Whatman membranes, GE Healthcare) at the outlet stream of the cyclone, and then are analyzed under the Qualitest Digital Microscope (Hardness Tester). In essence, the particle distribution on the sampled outlet are analyzed using a zoomed image produced by the MH_VK_E software. Similar to Section 2.4, the mean, standard deviation of each of the samples taken and their corresponding errors are presented in Table 2-4. The small error in the mean and standard deviation between both samples indicate a close correlation between them.

The sampled particles at the inlet and outlet are chosen to achieve a 10% variation in the mean value of the inlet and outlet samples. The size distribution within the sampled particles is used to estimate the volume (and consequently the mass using sand density of 1780 kg/m^3 [73]) of the sampled particles. On the other hand, the overall mass of the particles deposited on the filters (at the inlet and outlet) was measured after 2 min. The same procedure used in the previous section has been followed to obtain the weight of the real sample and the scaling factor calculated using Equation (2-1). These results are summarized in Table 2-5. The scaling factor decreases after the addition of ferrous powder to the inlet sand stream. This reduction is an indication of the solid-gas separation efficiency enhancement.

Table 2-4: Statistical values of the analyzed samples (for electrostatic forces)

Sample Category	Sample Number	Mean (μm)	Mean Error (%)	Standard Deviation (μm)	Standard Deviation Error (%)
Inlet Samples	Sample 1: 100 Particles	27.5	5.33	37.4	6.92
	Sample 2: 100 Particles	26.1		40.2	
Outlet Sample (Conventional Separation)	Sample 1: 50 Particles	7.34	2.99	2.10	1.86
	Sample 2: 50 Particles	7.12		2.14	
Outlet Sample (Electro-static process)	Sample 1: 50 Particles	9.22	1.30	3.12	1.92
	Sample 2: 50 Particles	9.34		3.06	

Table 2-5: Particles weights (for electrostatic forces)

Description	W_{AS} (kg)	W_{WS} (kg)	SF
Inlet	4.98×10^{-8}	1.80×10^{-2}	3.61×10^5
Outlet (Conventional)	4.63×10^{-11}	2.80×10^{-6}	6.04×10^4
Outlet (Ferrous Coated)	7.95×10^{-11}	7.00×10^{-7}	8.802×10^3

2.6 Addition of a chamber

The proposed additional chamber is introduced to create an additional collecting pot for all particles. In this method, solid particles in the gas stream reach the conical section by which

their rotational velocity increases. Hence, the particles from all sizes experience larger centrifugal forces which pushes them towards the conical section walls faster.

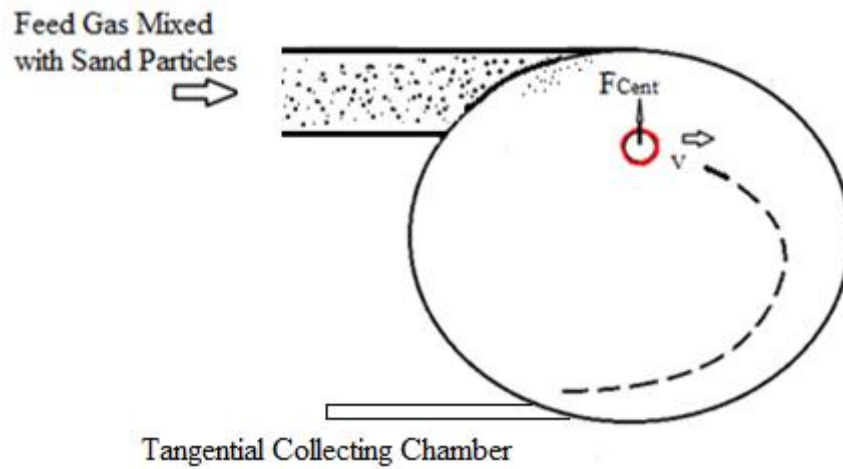


Figure 2-5: Schematic of inlet solid-gas mixture (F_{Cent}) with the additional tangential collecting chamber

Figure 2-5 shows the experimental set up of the proposed cyclone model under study with the additional tangential chamber. The tangential chamber is placed in the middle (future) of the conical section. Since the centrifugal forces on the particles are inversely proportional to their rotational radius, the centrifugal forces applied on the particles would increase due to the reduced rotational radius of the conical section. Thus, there are higher chances of smaller particles to reach the outer walls of the cyclone.

To assure that there is a close correlation between the samples taken from the outlet and inlet, the mean and standard deviation of each of the samples and their corresponding errors are presented in Table 2-6. The small error in the mean and standard deviation between both samples indicate a close correlation between them.

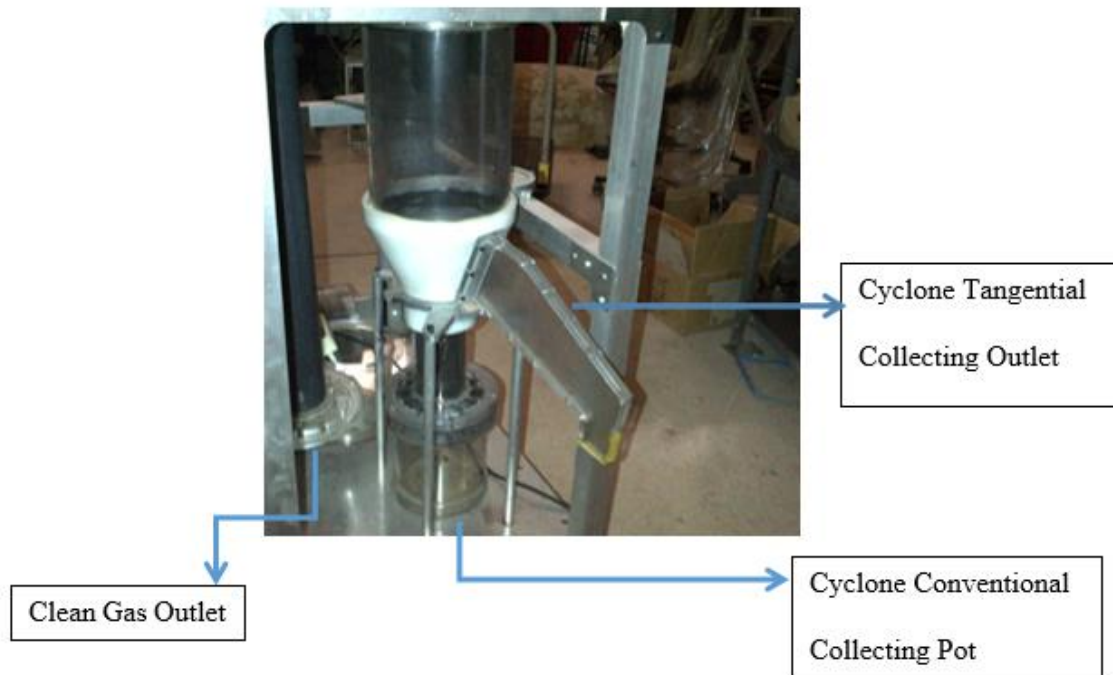


Figure 2-6: Experimental tangential chamber

Table 2-6: Statistical values of the analyzed samples (for the tangential chamber)

Sample Category	Sample Number	Mean (μm)	Mean Error (%)	Standard Deviation (μm)	Standard Deviation Error (%)
Inlet Samples	Sample 1: 100 Particles	27.5	5.33	37.4	6.92
	Sample 2: 100 Particles	26.1		40.2	
Outlet Sample (Conventional Separation)	Sample 1: 50 Particles	7.35	3.07	2.11	1.78
	Sample 2: 50 Particles	7.13		2.15	
Outlet Sample (Chamber)	Sample 1: 50 Particles	7.7	2.8	2.1	9.8
	Sample 2: 50 Particles	7.9		1.9	

The sampled particles at the inlet and outlet are chosen to achieve a 10% variation in the mean value of the inlet and outlet samples. The size distribution within the sampled particles is used to estimate the volume (and consequently the mass using sand density of

1780 kg/m³ [73]) of the sampled particles. Similar to the previous experimental procedure mentioned in the ferrous coated particles, the overall mass of the particles deposited on the filters (at the outlet and outlet) was measured after 2 min. Therefore, the size distribution obtained from the analyzed sample investigated under the microscope is multiplied by a scaling factor to obtain the real size distribution of the inlet and outlet particles. Scaling up of the size distribution is conducted by dividing the weight of the real sample by the weight of the sample characterized under the microscope (i.e., weight of 100 particles). Table 2-7 represents the weight of the analyzed sample, the weight of the real sample and the scaling factor calculated using Equation (2-1). The scaling factor decreases after the addition of the tangential chamber to the conical section. This reduction is an indication of the solid-gas separation efficiency enhancement.

Table 2-7: Data weights (for the tangential chamber)

Description	W_{As} (kg)	W_{ws} (kg)	SF
Inlet	4.98×10^{-8}	1.80×10^{-2}	3.61×10^5
Outlet (Conventional)	4.63×10^{-11}	2.80×10^{-6}	6.04×10^4
Outlet (Chamber design)	5.21×10^{-11}	1.40×10^{-6}	2.68×10^4

Chapter 3: Theoretical approach*

This chapter discusses theoretical models developed here to understand the effect of the active modifications presented in this thesis. First, the theoretical approach developed for evaluating the conventional cyclone separation efficiency is presented. The same theoretical approach is applied to the electrostatic attractions between the solid particles and walls of the cyclone.

3.1 Background

Due to the two-phase (solid-gas) swirl flow, it is difficult to develop an analytical model which can take into account all the phenomena occurring in terms of the flow inside a cyclone separator [74]. In essence, to analyse the solid-gas flow inside the cyclone separator, two sets of analyses should take place. The first set involves the fluid flow equations inside the cyclone separator using Navier Stoke's equations. However, solving the fluid flow inside the cyclone separator using the Navier Stoke's equation can only be done numerically. The second set involves the evaluation of the solid particles motion inside the separator using Newton's second law. The interaction between the particles and the surrounding fluid is not identical within all particles size ranges [42]. One reason for this discrepancy is due to the fact that the geometry and drag forces of each of the particles is not the same. Another complexity, which arises during the comparison of different analytical models developed for the cyclone's separation efficiency, is related to the shear stress of the fluid near the cyclone's walls. The shear stress reduces the flow velocity near the walls, creates turbulence, and hence, reduces the particles velocities near the walls. As particle's velocities reduce in theory, their momentum should reduce and hence, it should take them longer to reach the outer walls of the cyclone.

The difference between the velocity of the particles and that of the flow can create another complexity in the theoretical analysis of the separation efficiency in cyclones. In fluids, the velocity of the molecules is not equal at all points due to the eddy currents; therefore, the solid particle might at some points be carried away with the flow at the fluid velocity, and at another location, particles might fall in the eddies and have a reduced velocity. Finally, cyclone separators are designed to cause a sudden change in the flow direction at the end of its conical section. This sudden change, in addition to particles impacting the walls, is responsible for further separation of the solid particles from the flow. Hence, at the bottom of the cyclone, the fluid flow becomes very turbulent (see red highlight in Figure 3-1). In addition, turbulence is created at the location where the fluid coming from the inlet meets the fluid escaping at the top middle exit; thus, it is very difficult to include this turbulence in an analytical form [72]. Figure 3-2 shows the boundary, where the inlet and exiting flow meet, and the flow sudden change at the bottom. The highest velocities occur between the middle and the walls (shown in red). Near the walls, low velocity profiles appear, representing the higher shear stress between the fluid and walls. Finally, the velocities in the middle show the counter flow of the clean fluid which is escaping from the cyclone.

Last but not least, there are different geometries for cyclone separators in the literature [74]. Developing a model which fits all geometries is challenging. This challenge is due to the fact that the traveling distance of each of the particles inside the cyclone will be different in different geometries. As a result, the separation time and separation efficiency will alter in each design [74].

Despite all these complexities, analytical models provide a qualitative measure of the effect of enhancements applied to the same cyclone geometry. This chapter presents the analytical model developed to evaluate the separation efficiency of a conventional cyclone and that with the addition of the electro-hydrodynamic forces.

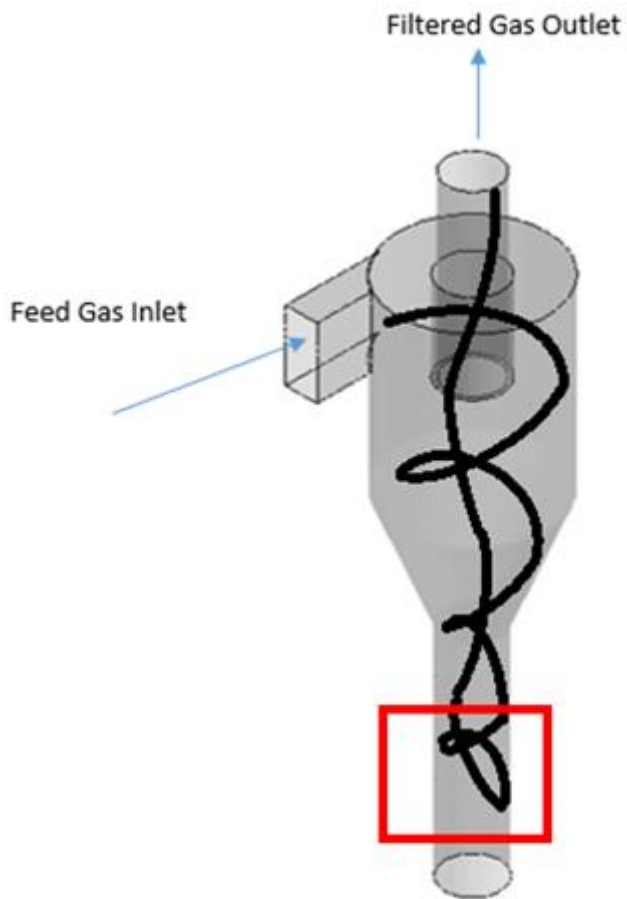


Figure 3-1: Typical gas flow in cyclone separators

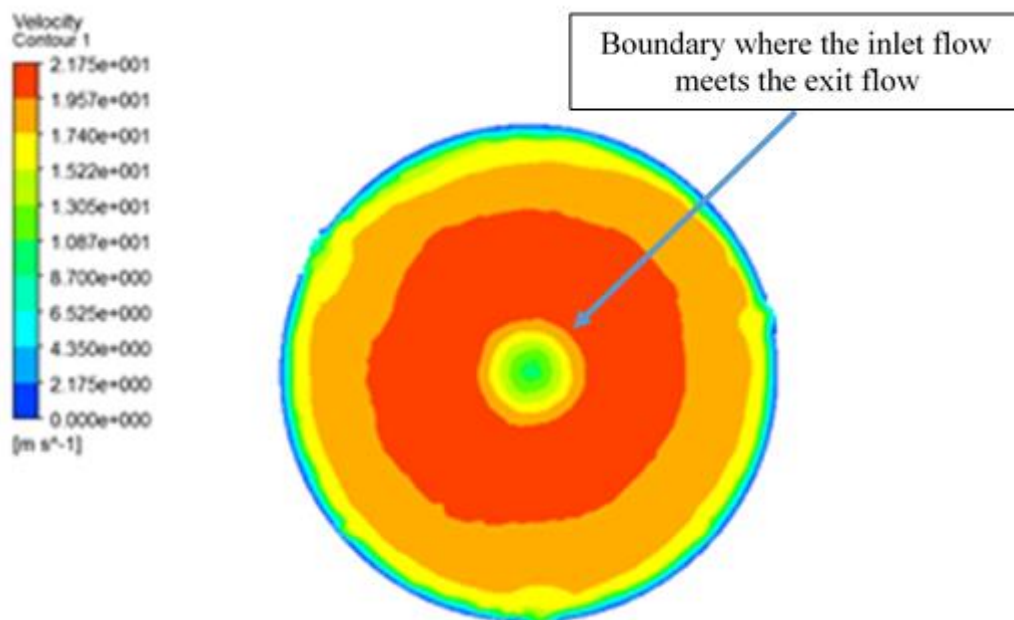


Figure 3-2: Typical velocity profile in cyclone separators

3.2 Theoretical model for conventional cyclone separator

A solid particle motion path inside a cyclone can be simplified as a spiral motion based on the forces in the gravity direction (vertical) and the direction perpendicular to gravity (horizontal). In the absence of any external forces, the main radial components of the horizontal forces are the inertial centrifugal and hydrodynamic drag forces, whereas the particle weight is the only vertical force. To inspect the importance of the gravitational force, Froude number (Fr) can be calculated as

$$Fr = \frac{V_{\theta}^2}{gR}, \quad (3-1)$$

where V_{θ} is the inlet tangential velocity, g is the gravitational acceleration, and R is the average radius of the cyclone. Since the Froude number for the cyclone under study is approximately 500 (which means the centrifugal forces are 500 times larger than the gravitational forces), the effects of the gravitational forces are ignored in this study.

Moreover, the following assumptions have been made:

- the particles are spherical;
- the radial velocity is constant;
- the particle tangential velocity equals to the gas velocity;
- turbulence effects are ignored; and
- the traveling distance (S) of the solid particle is the same as that of the gas.

The equation for particle motion in the horizontal plane is [74]

$$F_{\text{cent}} - F_{\text{drag}} = m \frac{dV_r}{dt}, \quad (3-2)$$

where F_{cent} is the centrifugal force, F_{drag} is the drag force, m is the particle mass, and V_r is the particle radial velocity. It can be assumed that the particles follow the gas streamlines

in the tangential direction, and hence, the tangential acceleration and slip velocity are zero. However, as the solid particle reaches its terminal radial velocity, the radial component of the gas acceleration is zero, and the particle radial velocity is the radial slip velocity.

A particle's Reynold number is evaluated as

$$\text{Re} = \frac{\rho_{gas} V_{\theta} D_{particle}}{\mu} \quad (3-3)$$

where ρ_{gas} is the gas density (1.2 kg/m³), V_{θ} is the particle's tangential velocity (14 m/s), $D_{particle}$ is the particle diameter (10 μm is the largest particle size studied in this paper), and μ is the gas viscosity (1.8 $\times 10^{-5}$ kg/m.s). The Reynolds number is evaluated to be $0.93 < 1$; therefore, the Stokes drag equation is applicable for the particle size ranges (i.e., 1 μm to 10 μm) studied here.

As a result, the drag force can be written as [74]

$$F_{\text{drag}} = 6\mu\pi r V_r, \quad (3-4)$$

where μ is the air viscosity, r is the particle's radius, and V_r is the radial velocity. On the other hand, the centrifugal force is expressed as [74]

$$F_{\text{cent}} = m \frac{V_{\theta}^2}{R}, \quad (3-5)$$

where V_{θ} is the tangential velocity, and R is the radial distance of the particle from the center.

The particle capturing efficiency is calculated as [74]

$$\varepsilon_{\text{SP}} = 1 - \frac{m_{\text{out}}}{m_{\text{in}}}, \quad (3-6)$$

where m_{out} is the mass of the outlet sand particles and m_{in} is the mass of the inlet sand particles. The conservation of the dust particles' mass entering and exiting a specified control volume allows for the evaluation of the particle collection efficiency. A control

volume having a dust mass inlet of m and outlet of $(m-dm)$ is shown in Figure 3-3. During the filtration process, the filtered particles hit the curved section and fall into the collecting pot below the cyclone cylinder. A mass flow inlet can be expressed as [74]

$$\dot{m}_{in} = w \times b \times V_{\theta} \times C, \quad (3-7)$$

where C is the dust concentration (in kg/m^3), w is the width of the control volume, and b is the height of the control volume. The same approach can be followed to estimate the dust particles attached (i.e., filtered particles) to the wall of the cyclone [74] as

$$d\dot{m} = -V_r \times b \times ds \times C = -C \times b \times V_r \times V_{\theta} dt, \quad (3-8)$$

where ds is the partial tangential length traveled by the particle.

Therefore, the mass ratio between the filtered and the inlet particles can be calculated by combining equations (3-7) and (3-8), resulting in the following equation [74]:

$$\frac{d\dot{m}}{\dot{m}} = \frac{-V_r dt}{w}. \quad (3-9)$$

Assuming the radial velocity to be constant, the radial acceleration will be equal to zero.

Therefore, equation (3-2) simplifies to:

$$F_{cent} = F_{Drag}. \quad (3-10)$$

By substituting equations (3-4) and (3-5) in equation (3-10), the relationship between the tangential and radial velocities is derived as

$$V_r = \frac{mV_{\theta}^2}{6\mu\pi R} \quad (3-11)$$

and equation (3-9) becomes

$$\frac{d\dot{m}}{\dot{m}} = -\frac{mV_{\theta}^2}{6\mu\pi R} \frac{dt}{w}, \quad (3-12)$$

where μ is the air viscosity, r is the particle radius, and R is the average radial path. The generic acceleration (a) equation can be written as [74]

$$dt = \frac{dV_\theta}{a}, \quad (3-13)$$

and therefore, using the chain rule, equation (3-9) can be written as

$$\frac{d\dot{m}}{\dot{m}} = -\frac{m_p V_\theta}{6\mu\pi R w} \frac{1}{V_\theta} \frac{dV_\theta}{a} = -\frac{m_p V_\theta}{6\mu\pi R w} ds. \quad (3-14)$$

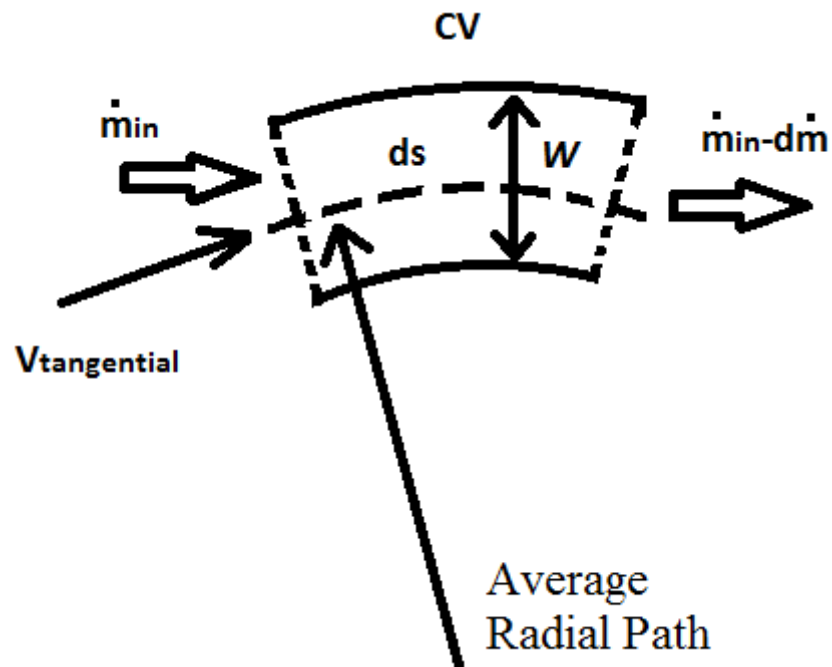


Figure 3-3: Control volume inside the cyclone path, where CV is the control volume, ds is the particle infinitesimal circumferential path, W is the averaged width of the controlled volume and V_θ is the inlet tangential velocity.

To solve for the ratio of the mass flowrates, Equation (3-14) is integrated as

$$\ln \dot{m}_{out} - \ln \dot{m}_{in} = -\frac{m_p V_\theta}{6\mu\pi R w} S. \quad (3-15)$$

The equivalent particle path, S , can be determined by multiplying the cyclone perimeter by the equivalent number of particle turns inside the cycle (given by Lapple and expressed as [75])

$$S = 2\pi R N_{eq}, \quad (3-16)$$

where

$$N_{eq} = \frac{1}{b} \left(H + \frac{L-H}{2} \right). \quad (3-17)$$

Equation (3-17) represents the overall length of the helical path that the particle travels inside the cyclone separator. Therefore, equation (3-6) can be written as

$$\varepsilon_{SP} = 1 - \frac{m_{out}}{m_{in}} = 1 - \exp \left\{ - \frac{m_p V_\theta}{6\mu\pi R} \frac{1}{w} S \right\} \quad (3-18)$$

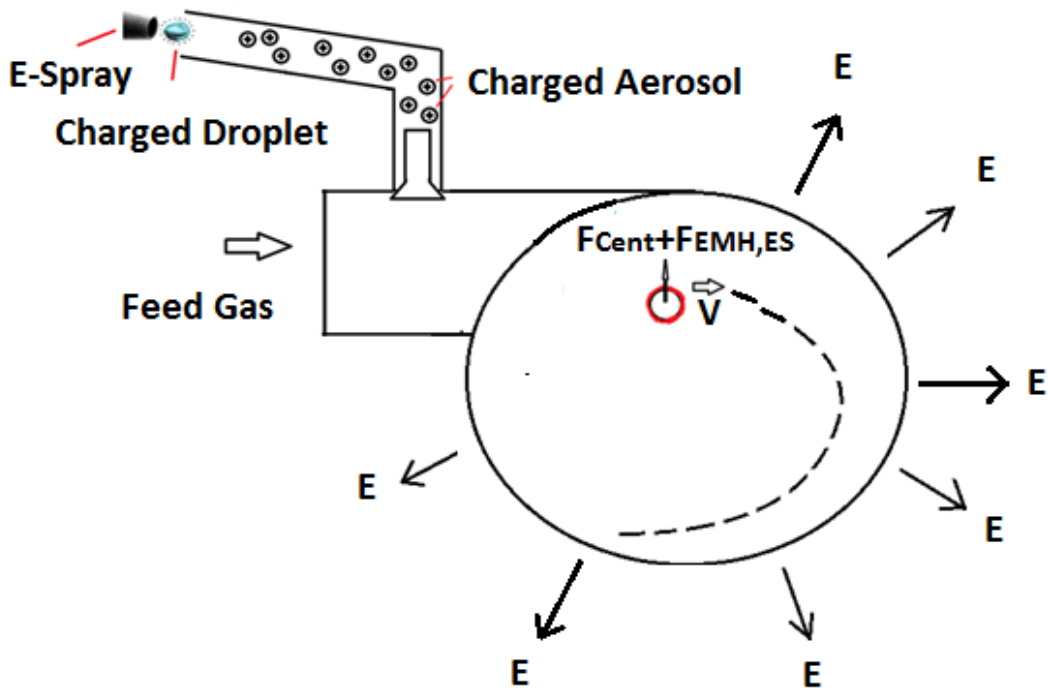
where w is the inlet width.

3.3 Theoretical model for electro-hydrodynamic effect

One of the enhancements proposed in this thesis is the addition of the electro-hydrodynamic (EH) forces introduced by creating an electromagnetic field acting on the particles which are coated by electro-coat. In this method, solid particles in the natural gas are electro-sprayed by a charged fluid in an insulated chamber. Electro-spray process consists of a nozzle in which voltage of 30-50 kV is applied across its orifice while the coating liquid passes through the nozzle. The liquid coat gets charged and evaporates to fine aerosols [76-77]. The electro-coating liquid is a viscous fluid, and hence, attaches to the dust particles. These charged particles move in a spiral path as they enter the cyclone. Therefore, in the presence of a radial electric field, the charged particles experience an additional force in the direction of the centrifugal force (radial). To extend the analytical model including the

electro-hydrodynamic effect, the following two assumptions were considered in addition to those mentioned in the previous section:

- the electro-coat covers completely the dust particles prior their entrance to the electric charge;
- the static charge does not reduce with time;



(i) Figure 3-4: Schematic of inserting charged particles to coat solid particles

Adding the EH forces changes the balance of the radial forces, and hence, Equation (3-2) becomes

$$F_{EH} + F_{cent} - F_{drag} = m \frac{dV_r}{dt} = 0, \quad (3-19)$$

where F_{EH} is the EH force. When the EH force is caused by the interaction of the charged particles with an electric field, the resulting electrostatic force, $F_{EMH,ES}$, can be estimated as [78]

$$F_{\text{EH,ES}} = qE, \quad (3-20)$$

where E is the magnitude of the electric field. It should be noted that the effect of the electrophoretic force is ignored as methane gas consists of covalent bonds, and there are no free ions to cause a double layer around the charged particles. Due to the additional electrostatic forces, the separation efficiency is altered by ways of the following

$$\varepsilon_{\text{SP}} = 1 - \frac{m_{\text{out}}}{m_{\text{in}}} = 1 - \exp\left\{-\frac{\left[\frac{qER}{V_{\theta}} + m_p V_{\theta}\right]}{6\mu\pi R} \frac{1}{w} S\right\}. \quad (3-21)$$

Chapter 4: Numerical approach

This chapter presents a numerical model developed for estimating the separation efficiency inside the conventional cyclone separator. Later on, this model will be used to study the effect of passive modification (i.e., geometrical modification) proposed here on the separation efficiency. More specifically, the numerical model will be used to show the effect of the addition of a tangential collecting chamber at the cyclone separator's conical section to further collect particles. For this purpose, the model needs to be first introduced and validated. This chapter presents the basics of the model including the mesh sizes and solver schemes.

Fluid flow inside cyclone separators with the injection of solid particles is considered as one of the most complicated fluid dynamics problems. To start with, the software simulator solves for the fluid pressure and velocities based on fluid flow equations such as Navier Stokes equations [79]. Afterwards, the solver solves for the solid particles velocities and momentum using the kinematics equations of motion [79]. The one-way coupling utilizes the forces coming from the pressure difference around the solid particles and applies them on the solid particles. On the other hand, the particles rotation and movement would not affect the fluid flow. The reason for using this method is that particle sizes are in the micrometer size. Small sized particles would not have a major effect on the fluid flow [79]. After identifying the solvers, mesh independency has to be evaluated. In other words, the results of the model must not alter with the change in the number of the meshing elements [80]. This approach can be achieved by running the analysis and study the output results using multiple meshing elements count. Following the mesh independency analysis, the solution of the proper results may be obtained using different options provided inside Fluent-ANSYS. The solutions of the separation efficiencies vary between the different solving schemes used.

4.1 Background

Spatial grid – During the Computational Fluid Dynamics (CFD) analysis, the solver approximates the medium in the form of a continuous solution space using discrete elements [81-83]. A hybrid mesh type is used: it consists of unstructured tetrahedral cells in the far-field and clustered triangular prisms near the walls (inflation layers). Near the boundary layer of the cyclone walls, the inflation-layer growth rate is set to 1.2 with 5 layers. The cell size has a minimum value of 0.09 mm and a maximum size of 5.7 mm. The size of each element determines the number of mesh cells for which the solver calculate the flow pressure and velocity. If the mesh cells are too large, the error in the pressure and velocity in the cell will be large. Reducing the cell dimension will provide more accurate results but will increase the computational time. Therefore, it is essential that the results obtained from the solver to be consistent regardless of the size and number of the meshed cells (mesh independent results). In this study, the meshing elements number was increased until the separation efficiency curves have consistent results with different mesh grids: the mesh count was varied from 400,000 to 800,000 elements with an interval of 200,000 elements. Figure 4-1 shows three samples of different mesh intensities. Figure 4-1 (a), (b), and (c) show the cyclone with 400,000, 600,000, and 800,000 mesh elements. The concentration of the mesh elements is vital in determining accurate results. Chapter 6 discusses the correlation between the mesh number and the separation efficiency results.

Solver Scheme – The basic principle for solving the fluid mechanics behavior is the Navier Stokes equations shown in Equation (4-1).

$$\left. \begin{aligned} \rho \frac{du}{dt} &= \rho F_x + \frac{\partial p_{xx}}{\partial x} + \frac{\partial p_{yx}}{\partial y} + \frac{\partial p_{zx}}{\partial z} \\ \rho \frac{dv}{dt} &= \rho F_y + \frac{\partial p_{xy}}{\partial x} + \frac{\partial p_{yy}}{\partial y} + \frac{\partial p_{zy}}{\partial z} \\ \rho \frac{dw}{dt} &= \rho F_z + \frac{\partial p_{xz}}{\partial x} + \frac{\partial p_{yz}}{\partial y} + \frac{\partial p_{zz}}{\partial z} \end{aligned} \right\} \quad (4-1)$$

The above equations can be rewritten as below:

$$\rho \frac{Du}{Dt} = -\frac{\partial P}{\partial x} + \rho g_x + \mu \left[\frac{\partial}{\partial x} \left(\frac{\partial u}{\partial x} + \frac{\partial v}{\partial y} + \frac{\partial w}{\partial z} \right) + \frac{\partial^2 u}{\partial x^2} + \frac{\partial^2 u}{\partial y^2} + \frac{\partial^2 u}{\partial z^2} \right] \quad (4-2)$$

where ρ is density, u , v and w are the linear velocities in x , y and z directions; g is the body force acting on each cell fluid.

The viscous term represents the shear forces in the fluid flow; the gravitational term represents the gravitational forces of fluid particles; the pressure gradient term represents the pressure difference between both sides of the fluid particle; and the velocity gradient represents the acceleration terms of the fluid particle.

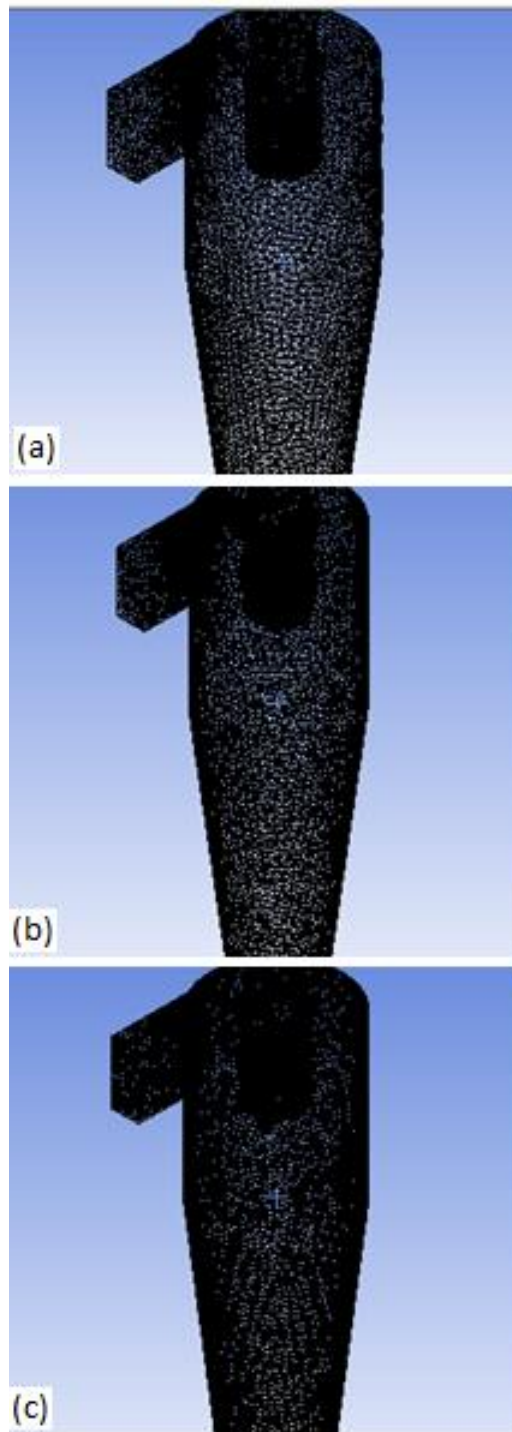


Figure 4-1: Mesh discretization for (a) 400,000, (b) 600,000 and (c) 800,000 mesh counts

There are different schemes that have been used for the discretization of the Navier Stokes equations to evaluate the pressure values, velocity values, and turbulence at each mesh element. For example, for the pressure interpolation, there are the i) second-order [80], ii) QUICK [80], and iii) PRESTO [80] schemes. For the pressure-velocity coupling, there are i) SIMPLE and ii) SIMPLEC schemes [80]. The Steady second-order scheme gives more accurate results compared to the first order scheme. The second-order scheme is also recommended for compressible flows. The Quadratic Upstream Interpolation for Convective Kinematics (QUICK), is a higher order differencing scheme as it interpolates the values of a node using three point upstream weighted quadratic interpolation. PRESTO that is a pressure interpolation scheme is recommended for flow with high swirls. In cyclone separators, this type of schemes would be applicable and provide better accuracies as compared to others. The steady analysis was performed by setting a steady flow numerical simulations in the ANSYS software. On the other hand, the unsteady analysis refers to flow simulations which consider flow changes with time (i.e. unsteady flow). Both types of simulations were run for a short period of time (i.e. up to 1,800 simulations) and for a long period of time (i.e. up to 12,000 simulations).

Each one of the solver models (schemes) has its own set of numerical calculations, accuracy and computational running time. For example, the Second order scheme has better results when convergence is achieved. On the other hand, it has less accurate results than PRESTO scheme. The reason is that PRESTO solves for the pressure and velocity values at the middle of the mesh cell. However, the second order solves for the velocities and pressure values at the corners of each cell and extrapolate the values to the center of the cell [80]. This is a main reason why PRESTO scheme is more accurate than the second or third orders.

One of the main problems in running a 3-D rotational fluid flow in cyclone separators is the need for running the analysis for a long time in order for the flow to reach the bottom of the cyclone before it exits (especially that the exit is located just next to the inlet). On the other hand, the solution of the residuals does not converge if small timescales are not implemented. The best method to reach a converged solution occurs when the user runs the analysis first using large timescale (0.1s) to allow the flow to reach the bottom of the cyclone (total between 7-10 s). Then, this should be followed by smaller timescales until the residuals converge gradually. The converged residuals do not necessarily lead to accurate CFD results. Another aspect that is important in obtaining accurate results is related to the simulation type as explained before. For example, Figure 4-2 to Figure 4-4 show the non-convergence of the residuals regardless of the simulation type selected. Mainly, non-convergence is due to the selection of larger timescales only. Moreover, in Figure 4-5, the residuals do converge with a large error between two consecutive values. This is mainly due to the convergence which does not occur gradually. The software tries to reach convergence at a faster pace with the improper evaluation of mesh cells at the selected timescale. Similarly, Figure 4-6 and Figure 4-7 show non-convergence in the solution due to smaller timescales absence.

Figure 4-8 shows the values of the separation efficiency obtained using different solution methods at low accurate residual convergence. The results highly depend on the convergence of the residuals and the amount of time given to run the analysis. Although the curves obtained from small timescales are closer to the experimental data (presented by Ji et al. [71]), discrepancies may be up to 20% for small particle sizes. Therefore, to reduce the difference between the experimental and numerical results, the timescale should be reduced gradually after a long run using larger timescales (0.1 s) until the residuals converge with a small error.

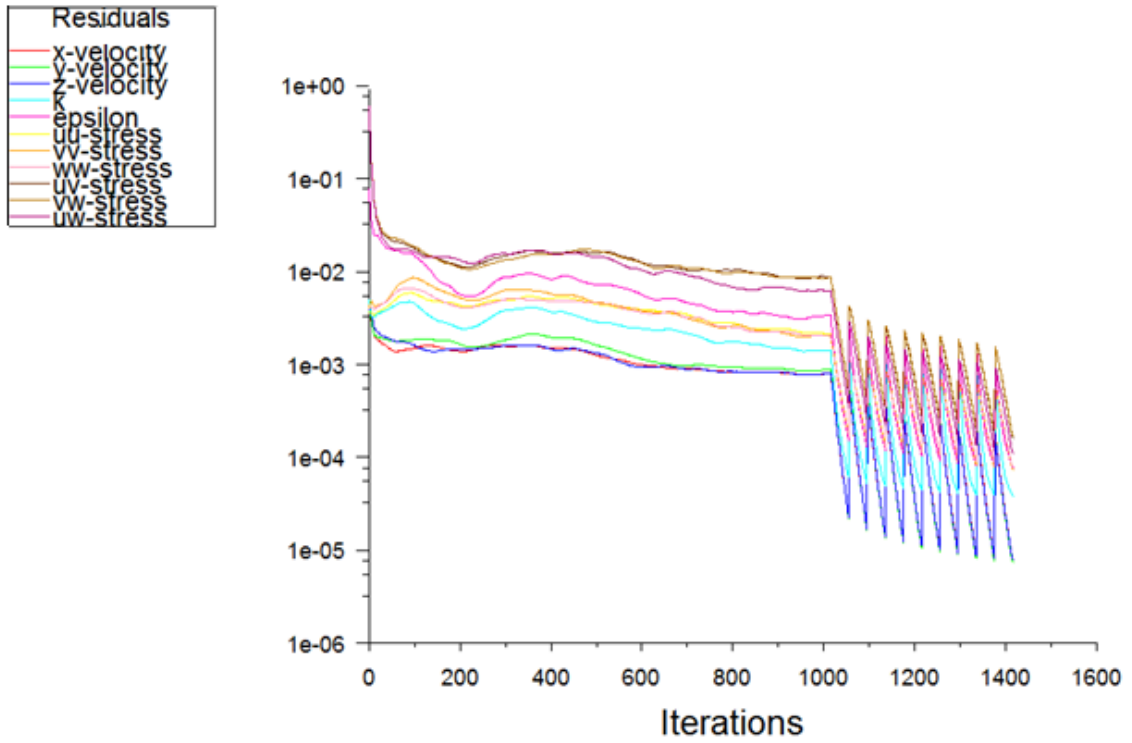


Figure 4-2:Residuals for Simplec-Second Order_QUICK Scheme (steady followed by unsteady analysis) - total real time (0.01 s). Where the velocity represents the velocity in the x, y and z directions, k represents the flow kinetics, epsilon represents the dissipation rate and stress represents the shear forces in the uu, ww, vv, uv, vw and uw directions

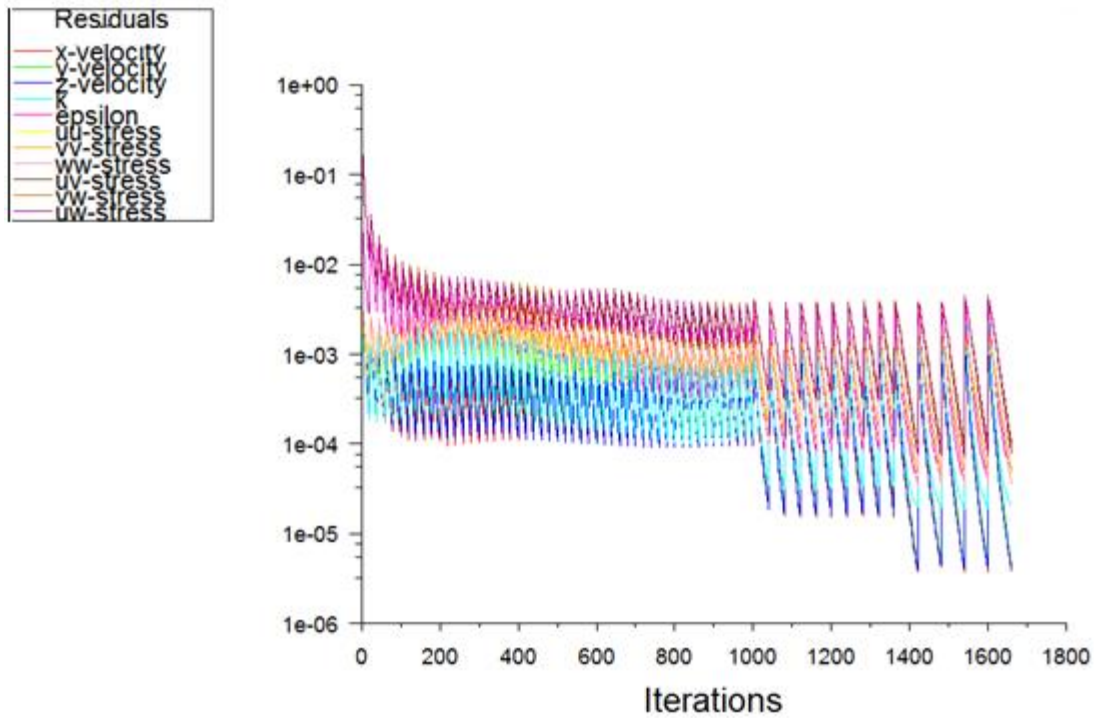


Figure 4-3:Residuals for Simplec-second order_QUICK scheme - total time (0.071 s).

Where the velocity represents the velocity in the x, y and z directions, k represents the flow kinetics, epsilon represents the dissipation rate and stress represents the shear forces in the uu, ww, vv, uv, vw and uw directions

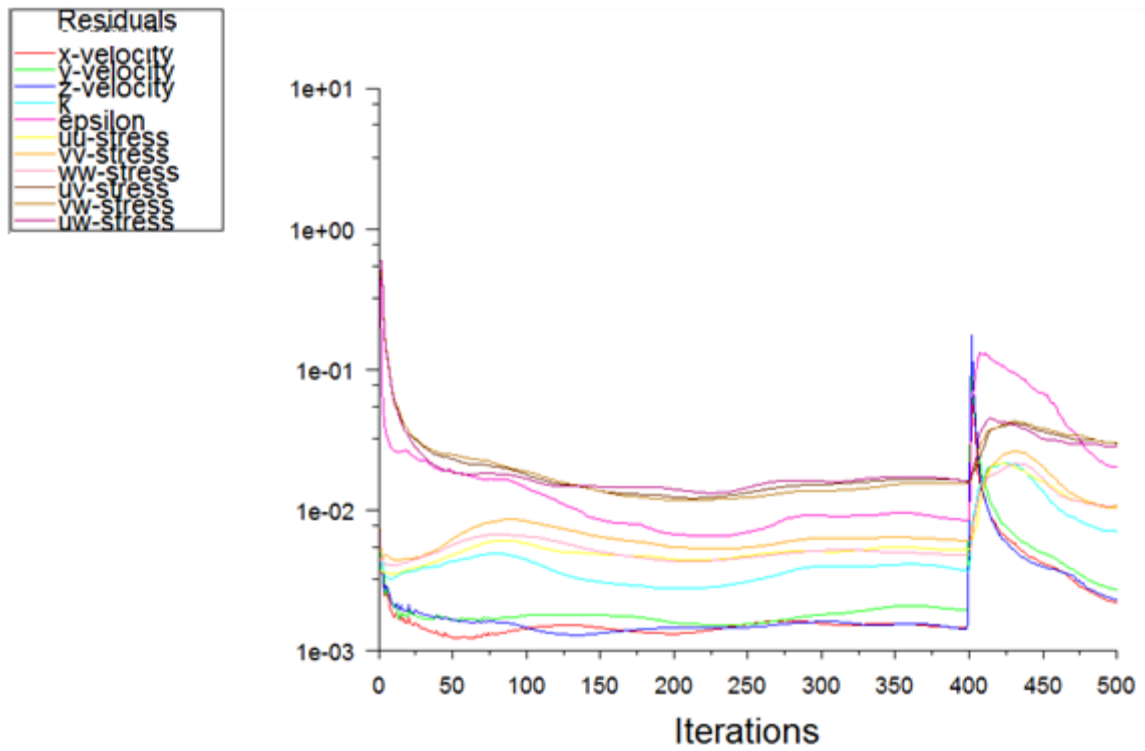


Figure 4-4:Residuals for steady analysis using second order - total unsteady time (0 s).

Where the velocity represents the velocity in the x, y and z directions, k represents the flow kinetics, epsilon represents the dissipation rate and stress represents the shear forces in the uu, ww, vv, uv, vw and uw directions

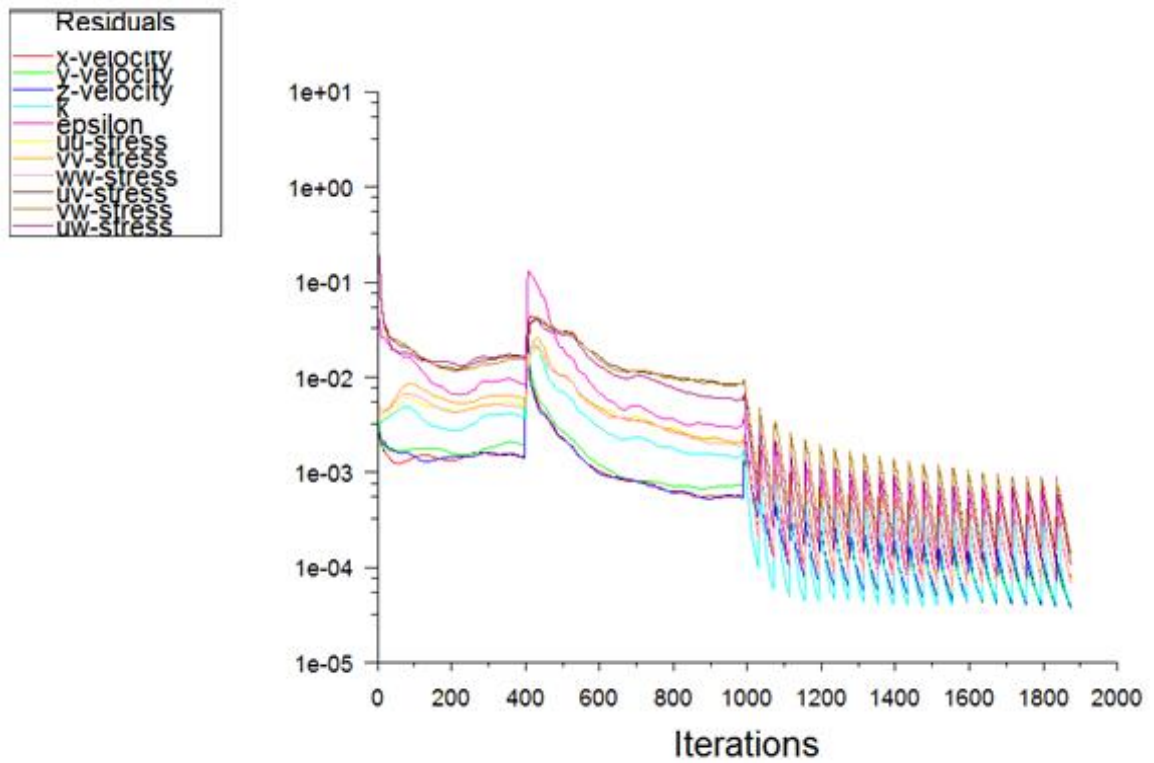


Figure 4-5:Residuals steady analysis followed by short period unsteady analysis using PRESTO scheme - total unsteady time (0.023 s). Where the velocity represents the velocity in the x, y and z directions, k represents the flow kinetics, epsilon represents the dissipation rate and stress represents the shear forces in the uu, ww, vv, uw, vw and uw directions

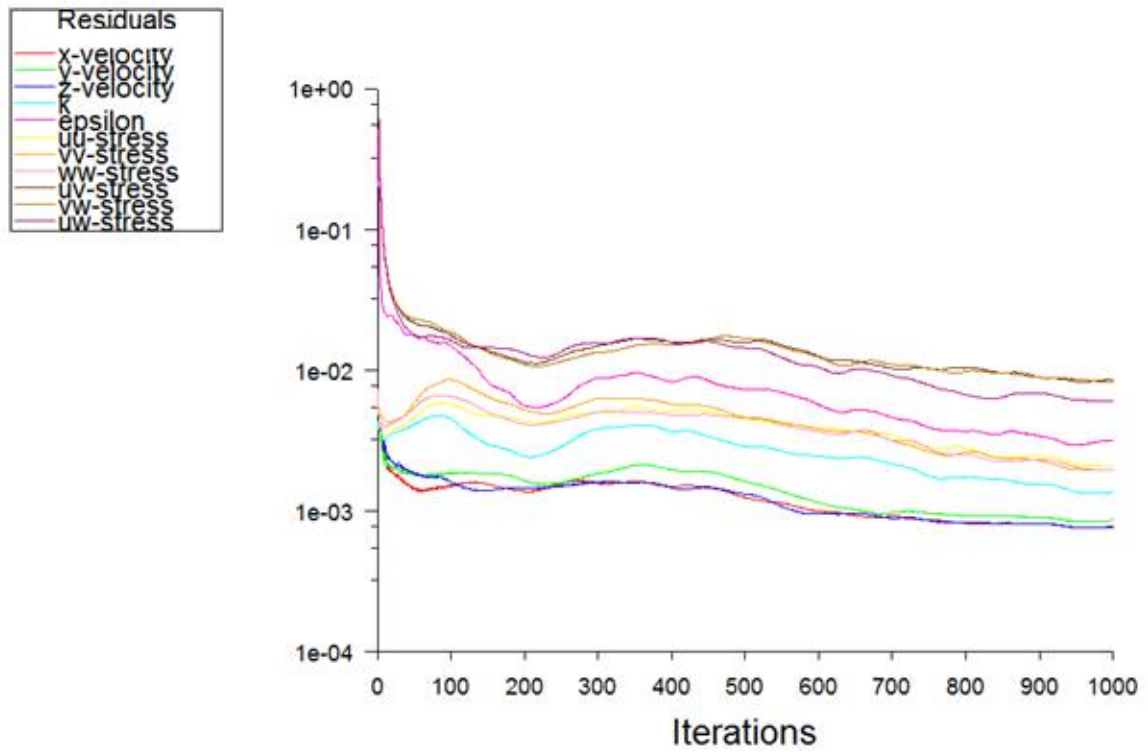


Figure 4-6:Residuals for unsteady analysis without using small timescales - total unsteady time 500 s. Where the velocity represents the velocity in the x, y and z directions, k represents the flow kinetics, epsilon represents the dissipation rate and stress represents the shear forces in the uu, ww, vv, uv, vw and uw directions

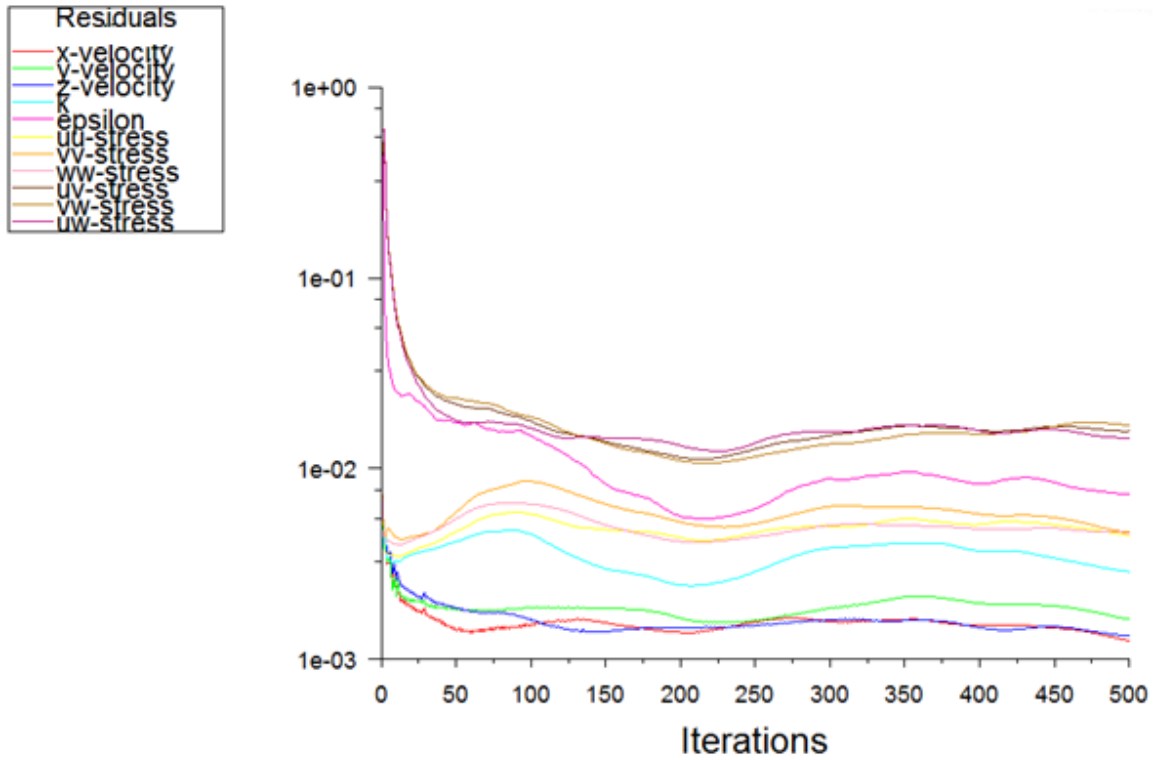


Figure 4-7:Residuals for long unsteady analysis without using short timescales - total unsteady time (250 s without small timescale). Where the velocity represents the velocity in the x, y and z directions, k represents the flow kinetics, epsilon represents the dissipation rate and stress represents the shear forces in the uu, ww, vv, uw, vw and uw directions

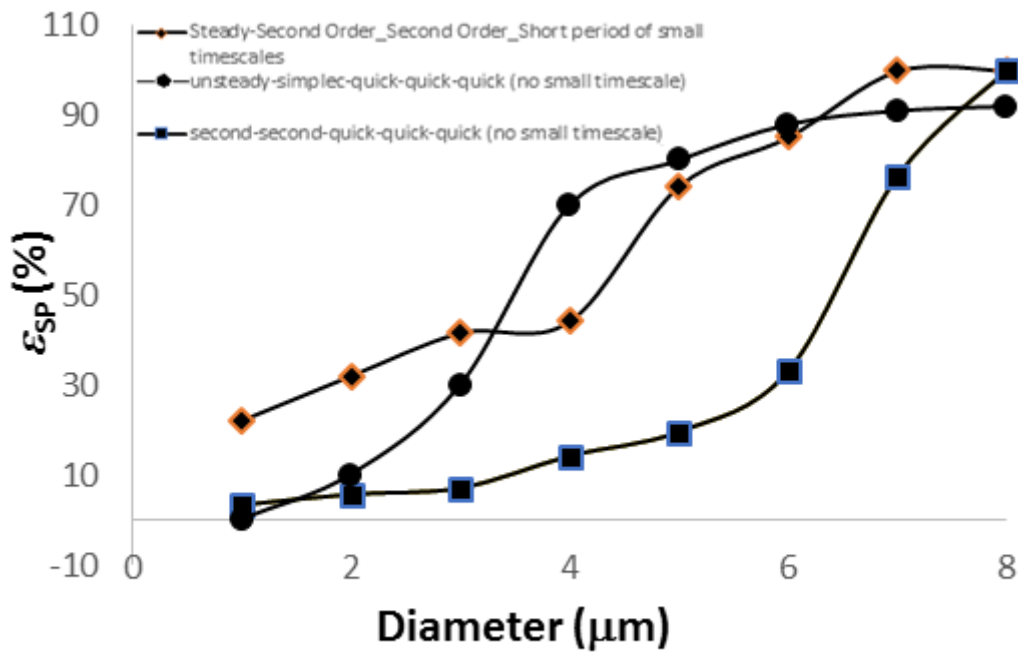


Figure 4-8: Obtained efficiencies using different solution methods at low accurate residual convergence

4.2 Model

This study relies on the ANSYS Fluent software package with the particle injection scheme. For the cyclone investigated, the Reynolds Stress Model (RSTM) (i.e., the most complicated of the Reynolds-Averaged Navier Stokes (RANS) models [79]) is used. For the cyclone investigated, the Reynolds Stress Model (RSTM) (i.e., the most complicated of the Reynolds-Averaged Navier Stokes (RANS) models [79]) is used. The advantage of using this model is that it accurately accounts for anisotropy of the turbulence, which is the case of the turbulent flow inside the cyclone due to the influence of flow swirl [79]. The advantage of using this model is that it accurately accounts for anisotropy of the turbulence, which is the case of the turbulent flow inside the cyclone due to the influence of flow swirl [79]. The analysis was discretized using the finite volume method with transient simulation having a varying time step from 0.1 to 10^{-4} sec. The scheme used in the analysis is QUICK

scheme. As for the spatial discretization, the PRESTO method [80] was used for the pressure solution in an incompressible flow regime. This method evaluates the pressure of each meshing element at its center rather than interpolating the center pressure from the corner values, resulting in smaller errors. The boundary conditions (as shown in Figure 4-9) include the inlet velocity of 14 m/s as an initial condition, an outlet pressure of 0 Pa, stationary walls, and a collecting chamber (similar to the stationary wall but capturing the particles). The pressure-velocity coupling used in this study consists of SIMPLEC scheme [80], which is more accurate than SIMPLE scheme [80]. The injection scheme using the discrete phase model was used to inject particles ranging from 1-6 μm (with a particle density of 1500 kg/m^3). The discrete phase model in Fluent couples the particle motion to the fluid motion by applying kinematic equations on the particle subjected to flow and pressure forces from the surrounding fluid. The convergence assessment for the residual evaluations is set to 10^{-4} to ensure a small error between the consequent iterations. The total flow time required to reach a 10^{-4} residual errors range between 8 s to 12 s for 11,000 iterations (i.e., the total time steps for each iteration range will add up to the flow time). This range depends on the mesh element counts and the shape of the cyclone (e.g., conventional against the one with the chamber added (see Chapter 6)). As for the particles, the tracking parameter was set to 10^7 steps, which is sufficient for all particles to reach a steady state condition. The flow time step varies from 0.1 to 10^{-4} sec.

As shown in Figure 4-10, the residuals have a larger error between each run when a short analysis to run for 0.07 s is used with a smaller time interval (0.1 s, 0.01 s and 0.001 s). Figure 4-10 shows the residuals convergence while allowing a long interval for the CFD analysis. The user allowed the unsteady analysis to run for 7.2 s (using the intervals of 0.1 s, 0.01 s and 0.001 s). Unsteady flow approach converges better in the unsteady analysis due to more accurate pressure evaluations. Since pressure values around the particles

changes over time due to eddies, the unsteady simulation evaluates the small eddy variations in the flow. Therefore, residuals for the pressure, velocity and momentum would converge faster.

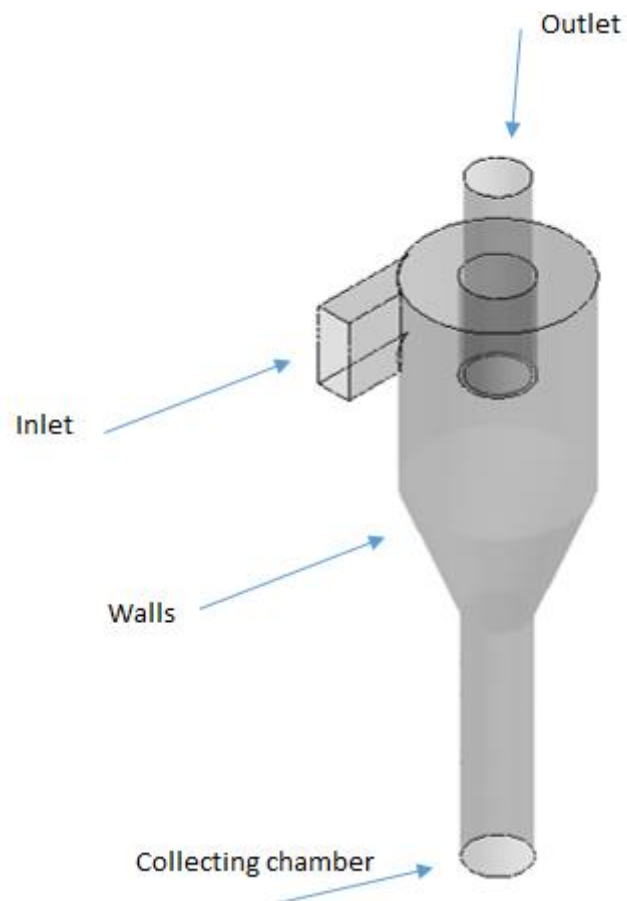


Figure 4-9: CFD model boundary conditions

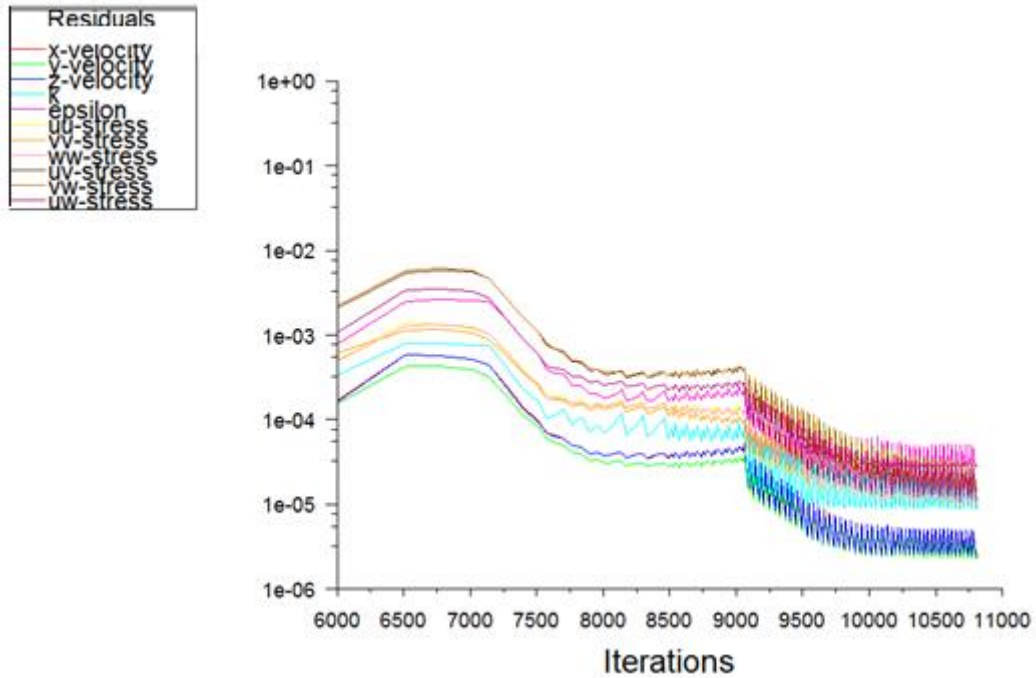


Figure 4-10: Residuals leading to converged results using long unsteady analysis followed by longer small timescales. Where the velocity represents the velocity in the x, y and z directions, k represents the flow kinetics, epsilon represents the dissipation rate and stress represents the shear forces in the uu, ww, vv, uv, vw and uw directions

Figure 4-11 shows the difference between the analysis conducted using a shorter time versus a longer time. It is obvious from Figure 4-11 (a) that the flow will not reach its mature state using a short timescale. If the flow is not filling the whole cyclone, the results will not be correct. The user should give enough time for the flow to reach down the cyclone and then find its way out from the top side of the cyclone.

To study mesh independency, the mesh elements ranging from 400,000 to 800,000 were tested based on the separation efficiency (see Chapter 6). Relatively, the actual computational time varied between 3 consecutive days (e.g., for 400,000 mesh elements) to 10 consecutive days (e.g., for 800,000 mesh elements) using one processor.

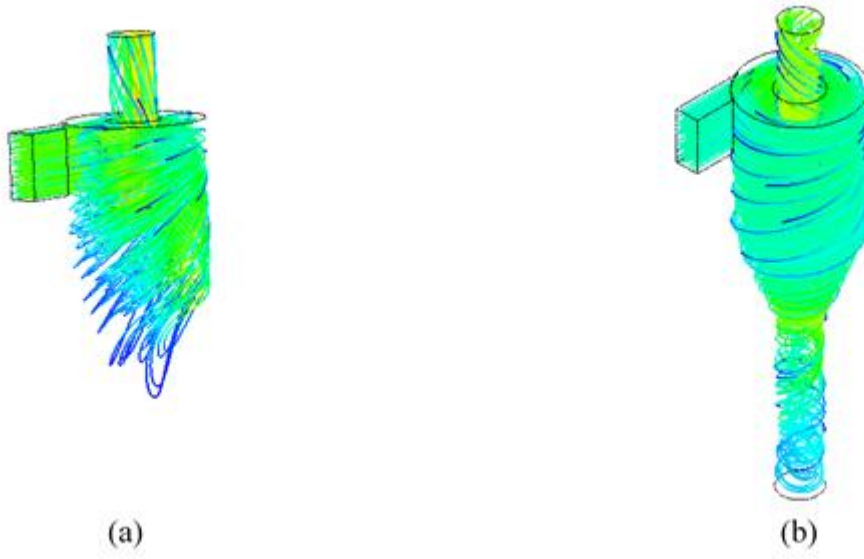


Figure 4-11: Fluid Flow of (a) an immature flow, against (b) a mature flow

Chapter 5: Active cyclone separator modification by adding electrohydrodynamic forces – theoretical and experimental approaches*

The effect of the particle diameter and the proposed method on the separation ratio efficiency (ε_{sp}) is investigated here for the conventional cyclone design, in which the centrifugal, drag forces and the electrostatic forces are the only forces acting on the particles. As indicated by previous studies [70-72], conventional cyclones have higher efficiency for larger particles. Larger particles experience larger centrifugal force, and hence, are expected to reach the outer walls faster.

5.1 Theoretical approach in conventional cyclone designs

To verify the modeling results explained in chapter 3, the calculated separation efficiency values from the proposed model are shown in Figure 5-1 and are compared with i) the measured values from our experimental setup (for the conventional cyclone separator) [84], ii) Leith and Licht [44] analytical modeling results, and iii) the experimental results reported by Ji et al. [71]. As it can be seen in Figure 5-1, the experimental and modeling results for the conventional cyclones are generally in good agreement, and the observed difference is mainly due to i) ignoring the turbulence effects (Turbulence tend to decrease the separation efficiency), ii) use of Stokes approximation for the drag force evaluation, and iii) the assumption of the spherical shape of the solid particles in the analytical model developed here. Additionally, the observed difference between our analytical model and Leith and Licht model can be due to different assumptions taken by Leith and Licht (such as the assumption of including the effect of gas temperature inside the cyclone).

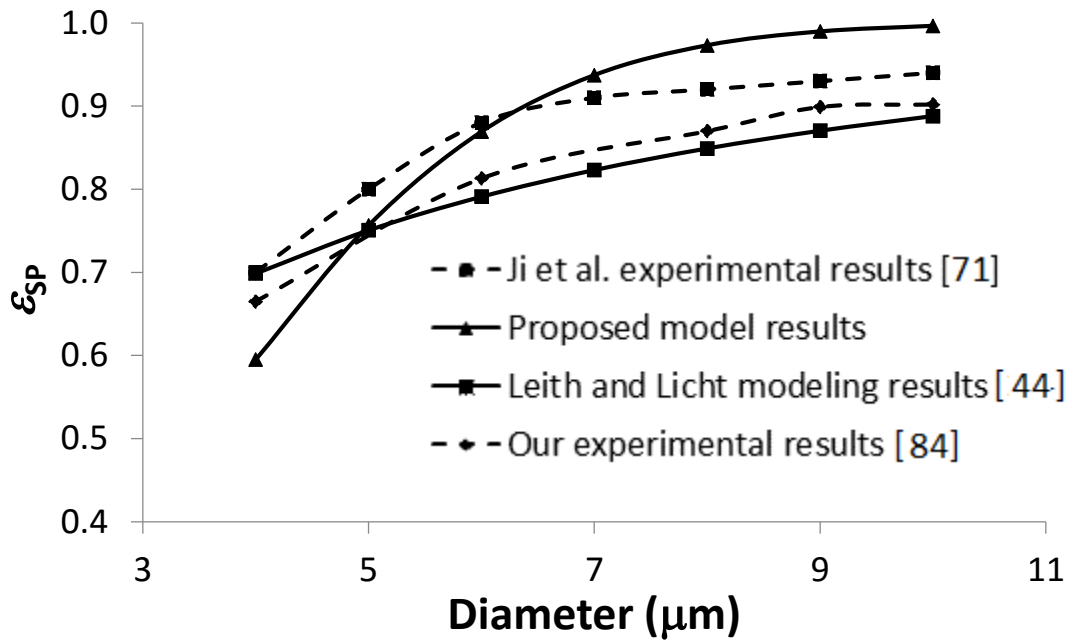


Figure 5-1: Comparison of the separation efficiency values obtained from the theoretical model and our experimental results [84], Ji et al. experimental results [71], and Leith and Licht theoretical modeling results [44]

5.2 Cyclones with additional electro-coat process under electrostatic attractions – theoretical and experimental approaches

When a radial electric field is created in the cyclone, the charged particles experience an electrostatic force towards the wall. This additional electrostatic force decreases the separation time, and hence, enhances the efficiency. The magnitude of this electrostatic force versus the particle diameter is shown in Figure 5-2 for the electric field of $E=0.05$ N/C. The increase in the overall force applied to the particle in the radial direction is expected to accelerate the separation process and increase the separation efficiency. As it can be seen in Figure 5-2 the electrostatic force increases at a faster rate compared to that of the centrifugal force. As a result, the capture efficiency of the dust particles increases, as seen in Figure 5-3. Although the electrostatic force is higher for larger particles, the resulting acceleration is lower because of the larger mass and the drag force, as it can be

seen from Equation (3-19); therefore, the ‘enhancement’ in the separation efficiency as the result of the additional electrostatic force decreases as the size of the particles increases.

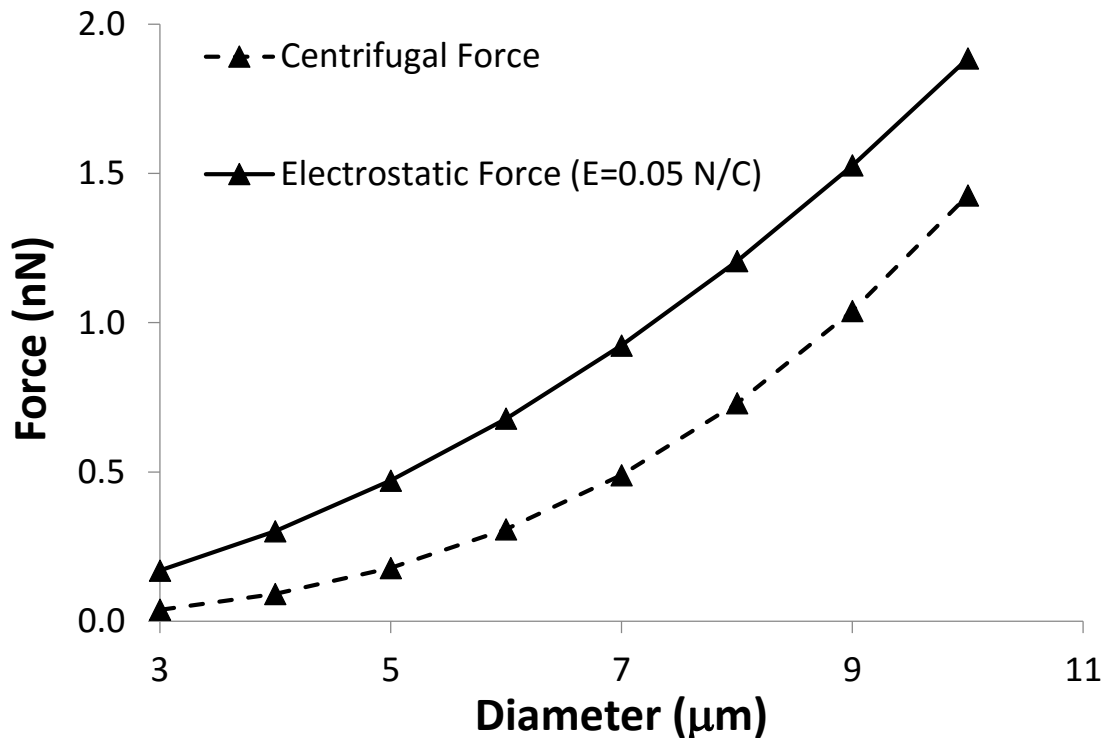


Figure 5-2: Electrostatic force compared to centrifugal force.

The experimental results obtained using the electrostatic charge approach show a promising enhancement in the solid particles separation. As seen in Figure 5-3, the maximum error between the theoretical and experimental electrostatic charge efficiencies is 4% at 4 μm. However, the trend in the experimental e-coating results does not follow the exact trend observed in the results of the proposed e-coating analytical model. Predominantly, this could be due to the fact that charged particles lose their charge within 1 to 2 minutes. Therefore, there is a higher tendency for larger particles to become loose and escape with the gas flow after losing their charge partially (this can be seen in the e-coating experimental efficiency values for larger particles). The electro-coating process has another effect: it increases the humidity inside the cyclone. It has been previously shown [50] that an increase in humidity leads to particle aggregation (especially for small

particles) and therefore an increased separation efficiency [50] (as it can be seen in the experimental results obtained for smaller particles).

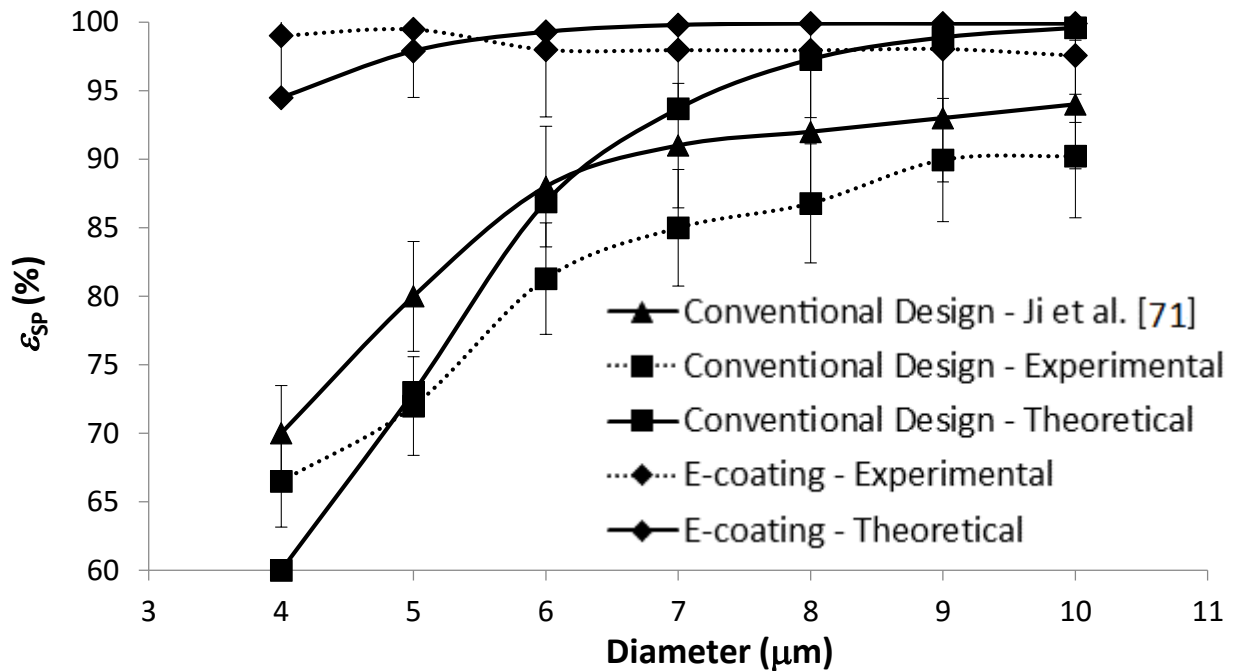


Figure 5-3: Separation efficiency enhancement due to the electrostatic forces in the conventional cyclone setup. The symbols present the average values of three runs. The error bars were obtained at a 95% confidence level.

Overall, the addition of the electrostatic force increases the overall cyclone separation efficiency for a wide range of particle sizes compared to the conventional method. This complimentary method, in particular, offers higher efficiencies for smaller particles, which are the sizes limiting the efficiency of the conventional cyclones. Therefore, the implementation of this separation mechanism in current cyclone designs could provide a powerful tool for separation of the smaller particles with a high efficiency. This design can play an influential role in non-flammable separation industries, such as nitrogen-solid and air-solid separation processes.

5.3 Cyclones with additional ferrous-coat process under magnetic attractions – experimental approach

This section investigates experimentally the feasibility of using magnetic forces to enhance the efficiency of the overall solid-gas separation in cyclone separators used in gas treatment. More specifically, the use of adhesive ferrous powder to further increase the lateral forces on the solid particles is investigated. The size distribution of the escaping solid particles with clean gas is compared between the conventional cyclone design and the proposed technique. It is shown that these additional forces are added to the centrifugal force, enhancing the separation efficiency in conventional cyclones, particularly for smaller particles.

The separation efficiency, ε_{sp} , is used as a way to evaluate the performance of the proposed approach. The larger the value of ε_{sp} , the larger the enhancement in cyclone capturing. An inlet sample is taken from the desert sand located in the United Arab Emirates. The size distribution of the inlet sample is presented in Figure 5-4 (a) with error bars representing a 95% level of confidence. It can be noted that this particle sample has a size range starting from 4 μm – 150 μm with a peak at 9 μm .

The effect of the centrifugal force on solid-gas separation is investigated here for conventional cyclone design. As larger particles experience larger centrifugal forces, they are expected to reach the outer walls and be filtered. However, fine particles (smaller than 20 μm) escaping with the gas stream are observed under the microscope. The characterization of the dry dust particles from the outlet of the conventional cyclone is presented in Figure 5-4 (b) with error bars representing a 95% level of confidence. Similar to the inlet pattern, the minimum size collected at the outlet is 4 μm . Experimental evaluations for the conventional cyclone separator indicate a maximum count of 19% of

the total particles at 7 μm particle size. In addition, all particles larger than 20 μm are separated from the gas stream when they went through the cyclone process.

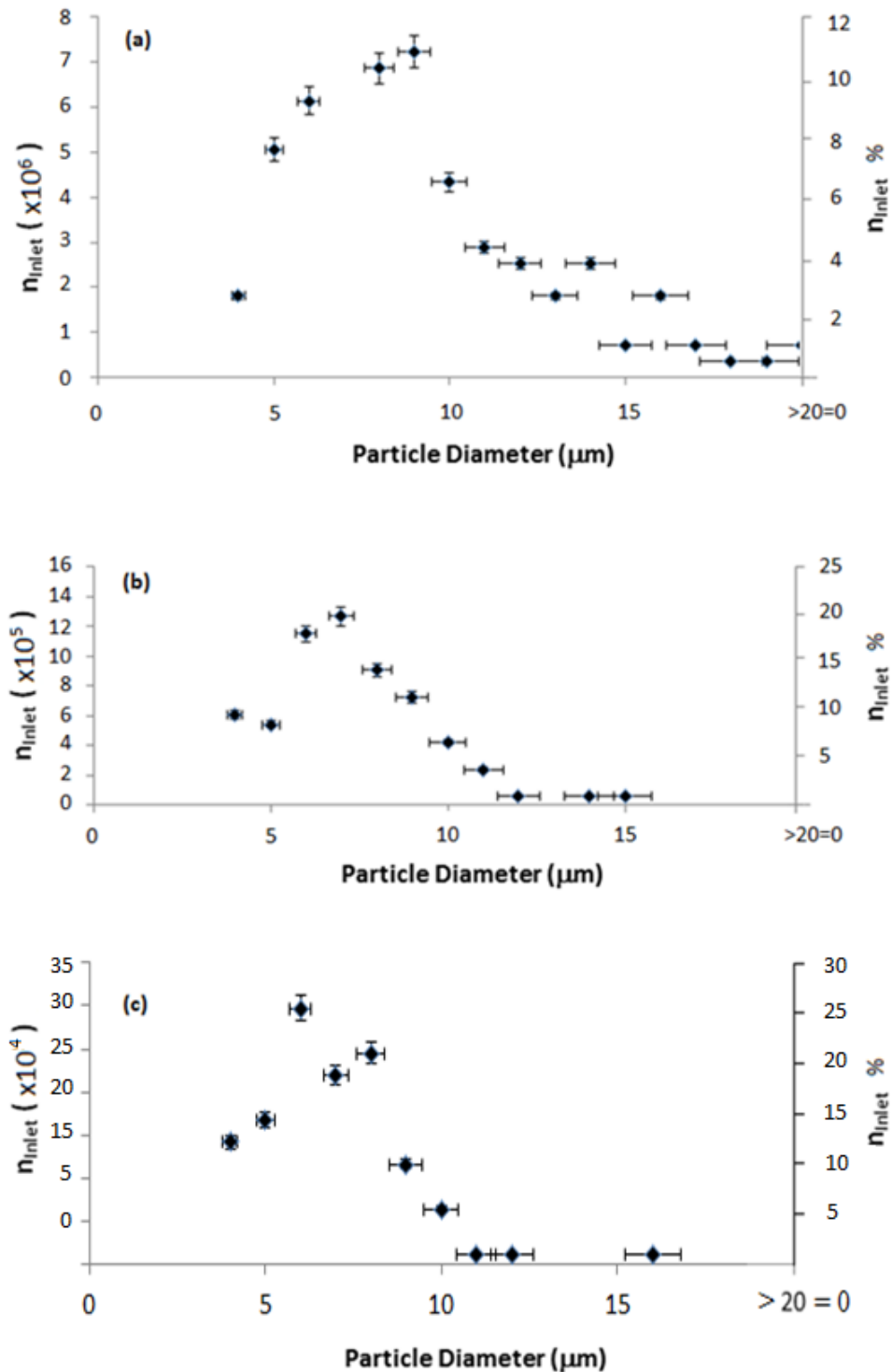


Figure 5-4: Count and percentage of the particle size distribution at the (a) inlet, (b) outlet of the conventional cyclone, and (c) outlet of the cyclone with the ferrous coating

Similar to dry sand particles, the characterization of the outlet ferrous powder-coated dust particles is investigated with error bars representing a 95% level of confidence (see Figure 5-4 (c)). The magnetic force is expected to enhance the capturing efficiency of the conventional cyclone, as it adds attraction forces to the escaping solid particles. Similar to the inlet pattern, the minimum size collected at the outlet is 4 μm . The scaled up experimental estimation for the conventional cyclone separator with a magnetic field indicate a maximum count of 25% of the total escaping particles at 6 μm particle size. In addition, all particles larger than 16 μm are separated from the gas stream when they went through the cyclone process.

Finally, the efficiency curves of the solid particle capturing using the conventional design and the proposed approach are shown in Figure 5-5 with error bars representing a 95% level of confidence. The efficiency values obtained here for the conventional cyclone design is also compared to those reported by Ji et al. [71]. It is seen that the maximum error between our experimental values and those reported by Ji et al. [71] is 7% at the particle size of 6 μm . The proposed ferrous powder coating exposed to a magnetic field is particularly very effective in enhancing the removal of fine particles (smaller than 10 μm). On the other hand, due to the increase of the centrifugal forces for larger particles, the effect of the magnetic forces on enhancing the separation is not as effective for larger particles. Therefore, the proposed method has a lower efficiency enhancement for particles larger than 12 μm . Also, in a co-axial jet pipeline mixer used in chemical reactors [85], the two reactants/streams are allowed to mix through a pipe-in-pipe process such as the one used in Figure 5-5. The mixing efficiency in such process has a 98% uniformity within the pipeline [85]. The mixing efficiency reduces the actual ferrous-coated dust efficiency. Therefore, the practical ferrous-coated dust efficiency shown in Figure 5-5 represents 98%

of the ideal ferrous coated-dust efficiency. This reduction is due to the use of co-axial mixing chamber.

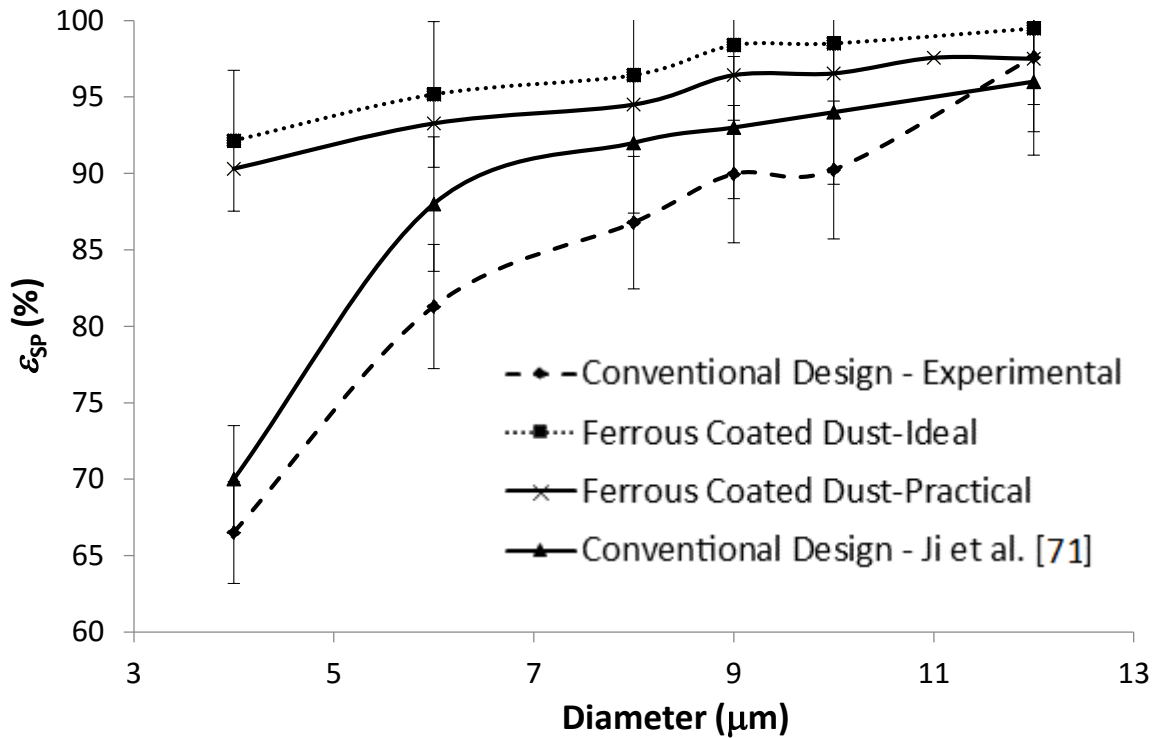


Figure 5-5: Capture efficiency values obtained based on the conventional cyclone design, the conventional cyclone design of the Ji et al. [71], and the magnetic-based cyclone design proposed in this section. The symbols present the average values of three runs.

The error bars were obtained at a 95% confidence level.

Overall, spraying the sand particles with an adhesive ferrous powder enhances the solid-gas separation under the effect of a magnetic field in the conventional cyclone separators. The enhancement occurs by reducing the number of smaller particles escaping with the gas (e.g., a reduction of 25% and 10% for 4 μm and 8 μm, respectively). This method in particular offers higher efficiency for smaller particles (compared to the conventional approach) which is of interest in the current studies conducted for the industrial gas treatment. Therefore, the implementation of this separation mechanism into current cyclone

designs could provide a powerful tool for separation of the smaller sized particles with a higher efficiency.

Chapter 6: Passive modification by adding tangential collecting chambers*

The separation efficiency, ε_{sp} , pressure drop and erosion rate are used as ways to evaluate the performance of the proposed approach. The larger the value of ε_{sp} , the larger the enhancement in cyclone capturing. On the other hand, the smaller the pressure drop and the smaller the erosion rate, the higher the enhancement in the cyclone separator's performance life.

6.1 Capturing efficiency

The effect of the particle diameter on the separation efficiency (ε_{sp}) is investigated here for i) the conventional (referred to as Stairmand cyclone) design, and ii) the cyclone with the proposed geometrical modification. As indicated by previous studies [71, 72], the conventional cyclones have generally higher efficiency for larger particles. In essence, larger particles experience larger centrifugal forces, and hence, are expected to reach the outer walls faster. As a particle hits the outer walls of the cyclone, its momentum declines and it falls down the collecting chamber. Similarly, smaller particles can also reach outer walls by increasing centrifugal forces through the conical section. However, very fine particles can still escape with the gas stream as they can be picked up by the gas easily. The goal of the proposed geometrical modification is to capture these fine particles prior to their escape through the gas stream.

Model verification and mesh independency analysis – To verify the CFD modeling results, the separation efficiency values obtained using the model are compared against the experimental results reported by Ji et al. [71] (see Figure 6-1). The modeling results were determined for three different mesh cell counts to determine mesh independency. The results show that the maximum error between the experimental [86] and CFD results (regardless of the number of the meshing elements) occurs for 3 μm particles. The smaller

particles (1-2 μm) have high tendency to escape as they reach the exit; while larger particles (4-6 μm) have high tendency to settle at the bottom. The 3- μm particles, on the other hand, have high tendency to rotate inside the cyclone before they either escape or are captured. This can result in the observed difference between the CFD and experimental results for this size of the particles.

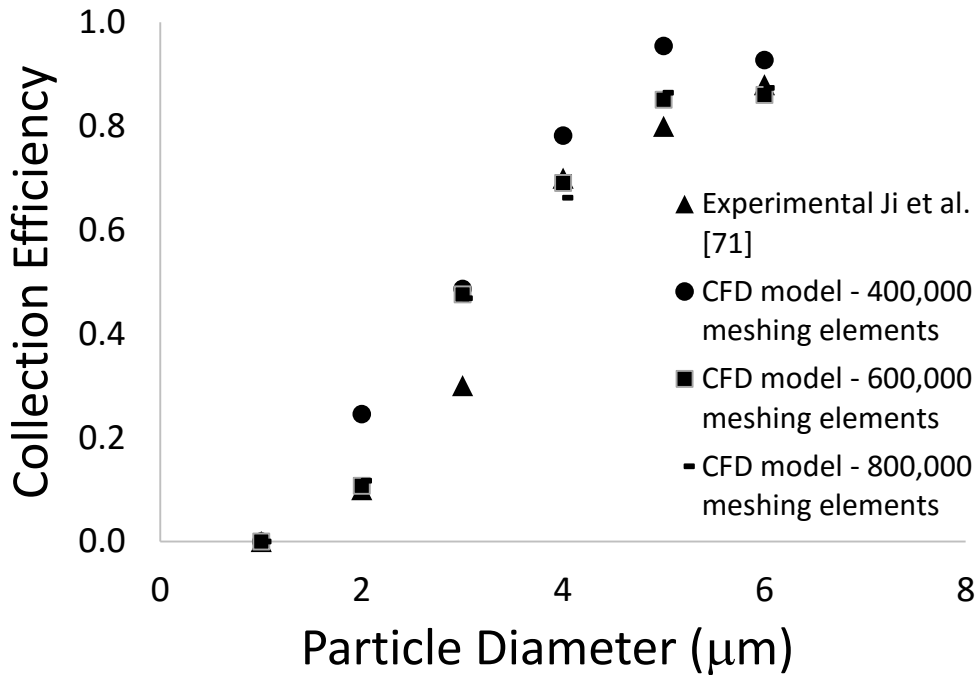
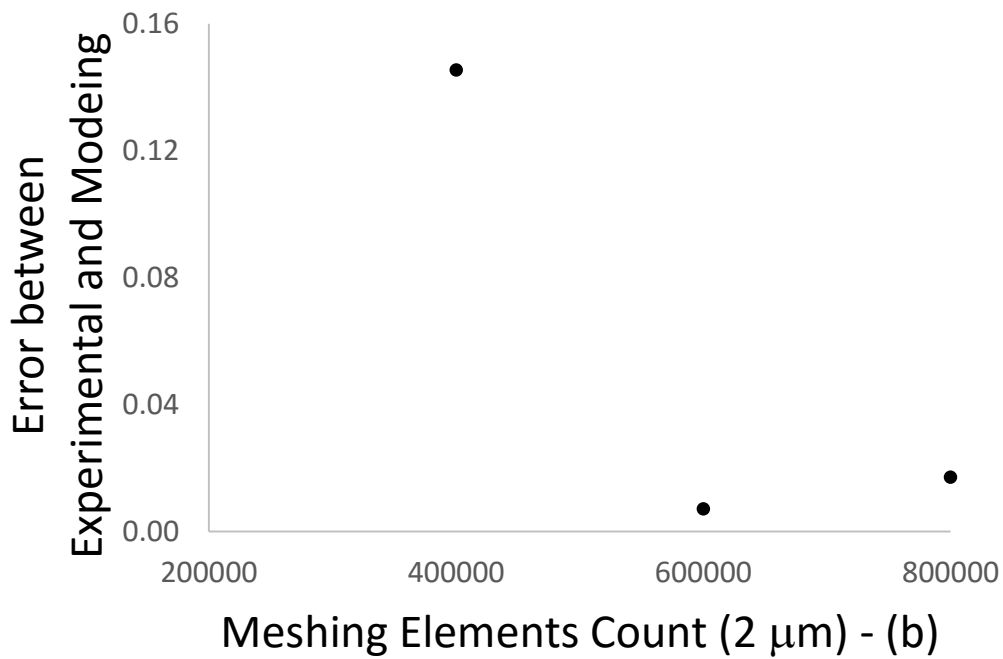
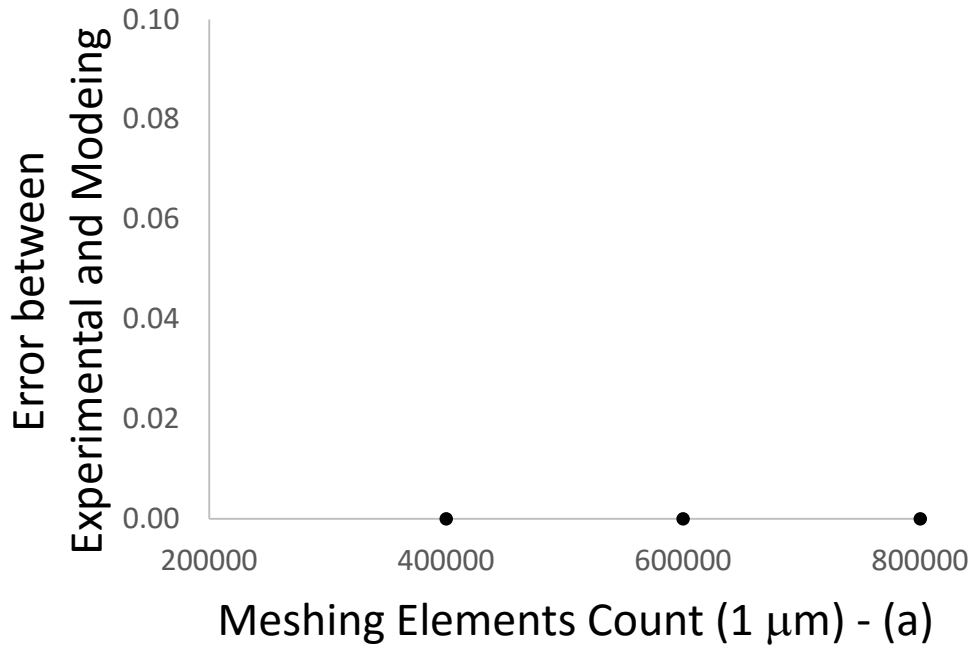
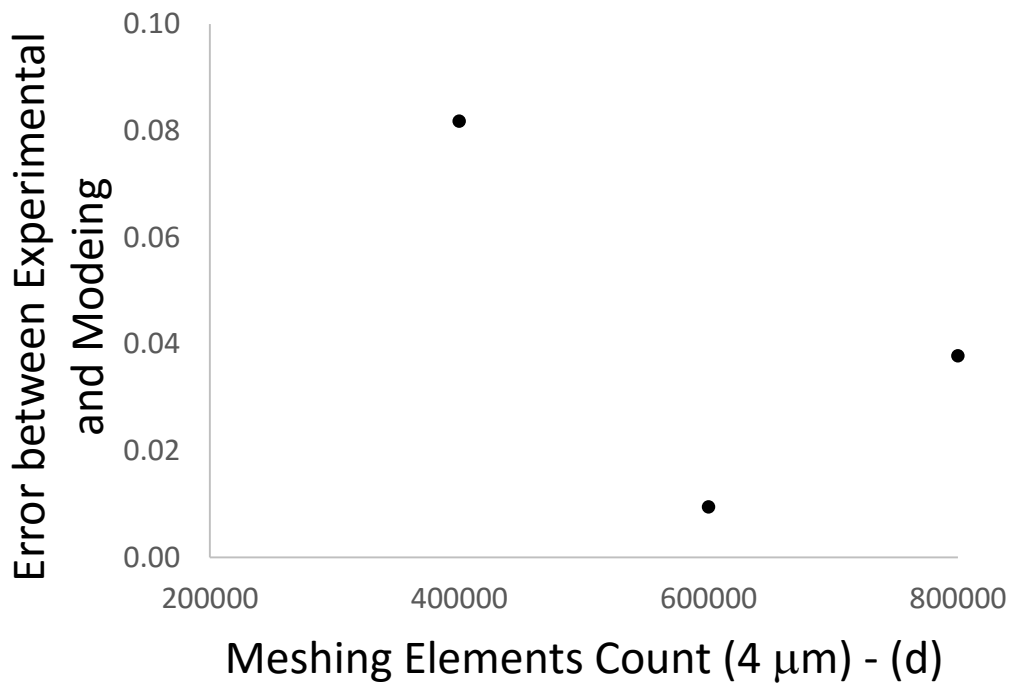
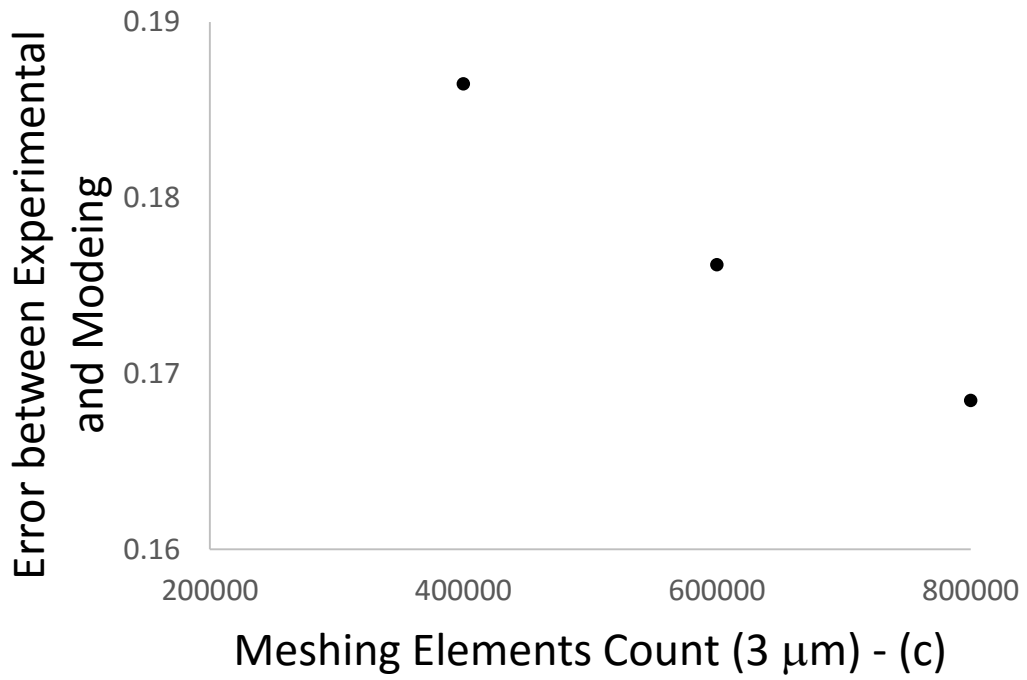


Figure 6-1: Comparison between the experimental separation efficiency (Ji et al. [71]), CFD modeling conducted at 400,000 meshing elements, 600,000 meshing elements and 800,000 meshing elements for a conventional design

To conduct the mesh independency analysis, the difference between the CFD and experimental results for each mesh resolution is quantified. The difference between the 400,000 and 600,000 element cases are too large. For example, for 5- μm particles, the difference between the errors obtained for two meshing elements is 10% which is in the same order of the magnitude of the separation efficiency enhancement being considered here. Figure 6-2 shows a reduction in the total error between the numerical results as the meshing grid elements count increases. Increasing the mesh counts from 600,000 to

800,000 elements reduces the magnitude of the error by less than 2.1% for 4- μm particles but at the expense of increasing significantly the computational time (by 150%). Thus, 600,000 meshing elements is chosen for further analysis.





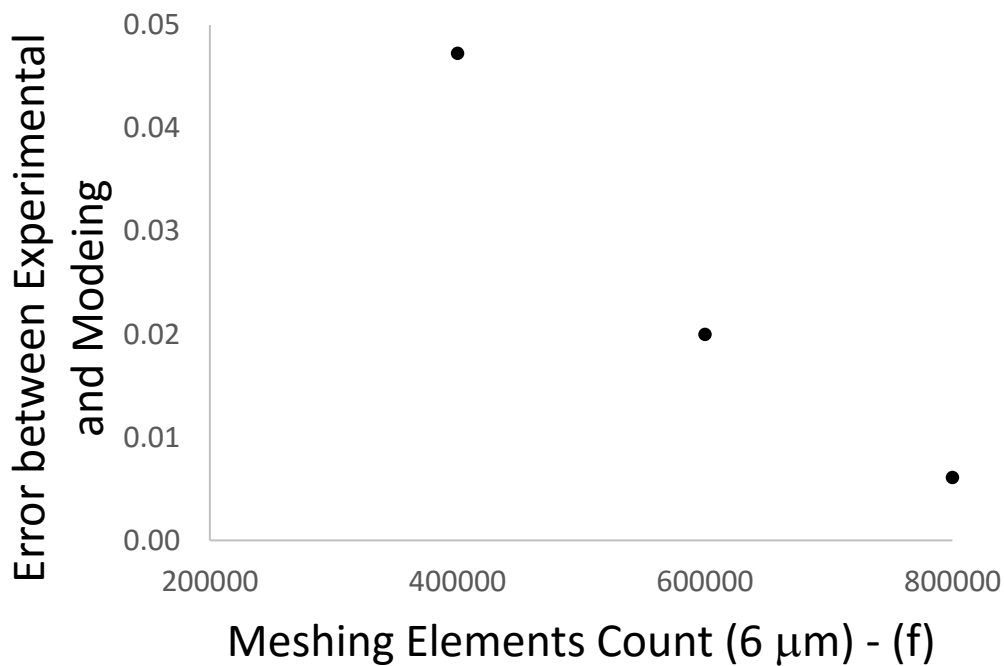
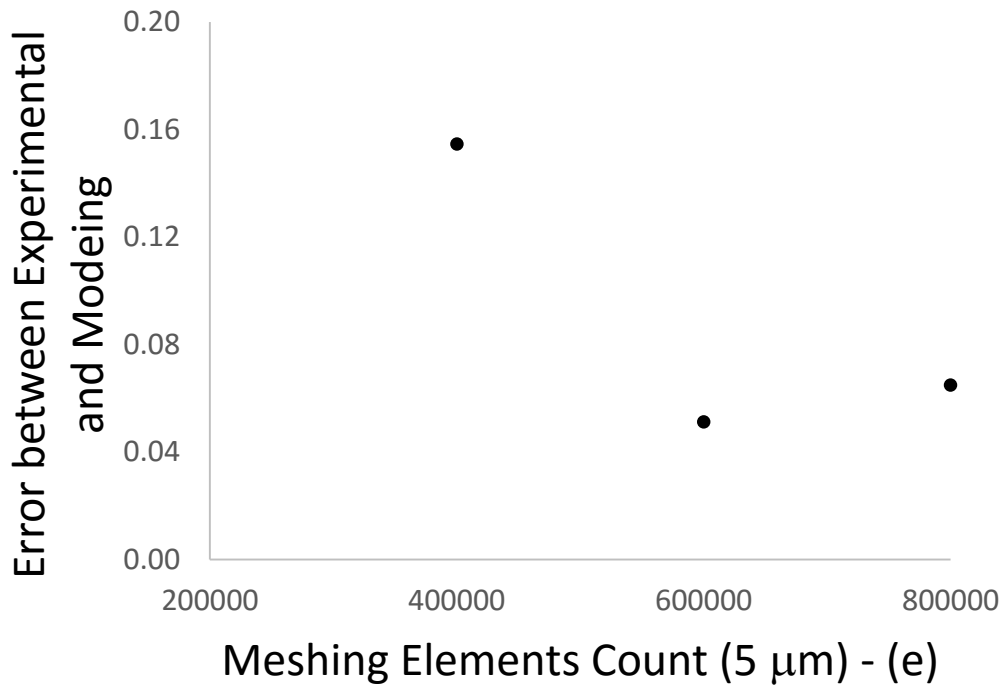


Figure 6-2: Errors obtained for different meshing grids

Number of the tangential chambers – Using 600,000 meshing elements, the separation efficiency of the proposed geometrical modification (involving the addition of a tangential chamber) is determined for the range of the particle sizes mentioned above. The addition

of the tangential chamber at the conical section of the cyclone is expected to enhance the separation efficiency of smaller particles as they reach the walls. As particles enter the conical section, their radial velocities increase due to the decrease of the rotational radius. Furthermore, the centrifugal forces applied at the particles increase due to the increased tangential velocities. Thus, particles from all ranges have higher tendencies to reach the outer walls of the conical section. Moreover, the location to place the tangential chamber is chosen to be just above the lowest part of the conical section. Further optimization of the location of the tangential chamber is needed and has been proposed as future work (see Chapter 8).

In this proposed modification, the small-sized particles are trapped and collected inside the tangential chamber before they have a chance to gain their momentum again. Figure 6-3 shows the separation efficiency of the proposed modification as compared to those reported by Ji et al. [71]. Also, the effect of the number of the tangential number on the efficiency is shown in this figure. In general, the addition of the tangential chambers increases the separation efficiency as compared to that reported by Ji et al. [71]. However, the number of the chambers affects the separation efficiency; it is observed that adding one tangential chamber to the conical section results in higher efficiency than the case of two or three tangential chambers. This is attributed to the increased turbulence at the inlet of each of the chambers. Figure 6-4 shows the turbulence eddy dissipation rate at the cross section of the chambers. Since the turbulence dissipation rate increases as the fluid velocities increase, the turbulence dissipation rate increases as the Reynolds number of the fluid increases. It is observed that for the case of one chamber, the maximum value of the turbulence dissipation rate at the inlet of the tangential chamber is smaller ($12770 \text{ m}^2/\text{s}^3$) than the two and three chamber cases ($15580 \text{ m}^2/\text{s}^3$ and $14220 \text{ m}^2/\text{s}^3$, respectively). For the case of three chambers, the eddy value is smaller, and hence the separation efficiency is higher, than

those values obtained for the case of adding two chambers. This is likely due to the reduced distance between the openings.

Figure 6-5 shows that at the inlet of the chambers the largest velocity corresponds to the case of one chamber (7.686 m/s), followed by three and two chambers (6.52 m/s and 4.8 m/s, respectively). It is obvious from the velocity contours that the fluid flow has the farthest propagation inside the chamber for the case of one chamber. For the case of adding two chambers, on the other hand, the fluid flow seems to have the least propagation inside the chamber. Due to the increased turbulence dissipation rate at the inlets of the chambers in the two- and three-chamber cases, it seems the velocity near the walls and the chambers decreases, yielding the reduced flow penetration into the chamber in those cases. As noted before, the decrease in the velocity directly reduces the centrifugal forces. The reduction in centrifugal forces reduces the ability of solid particles (especially smaller ones) to reach the outer walls and the collection chambers.

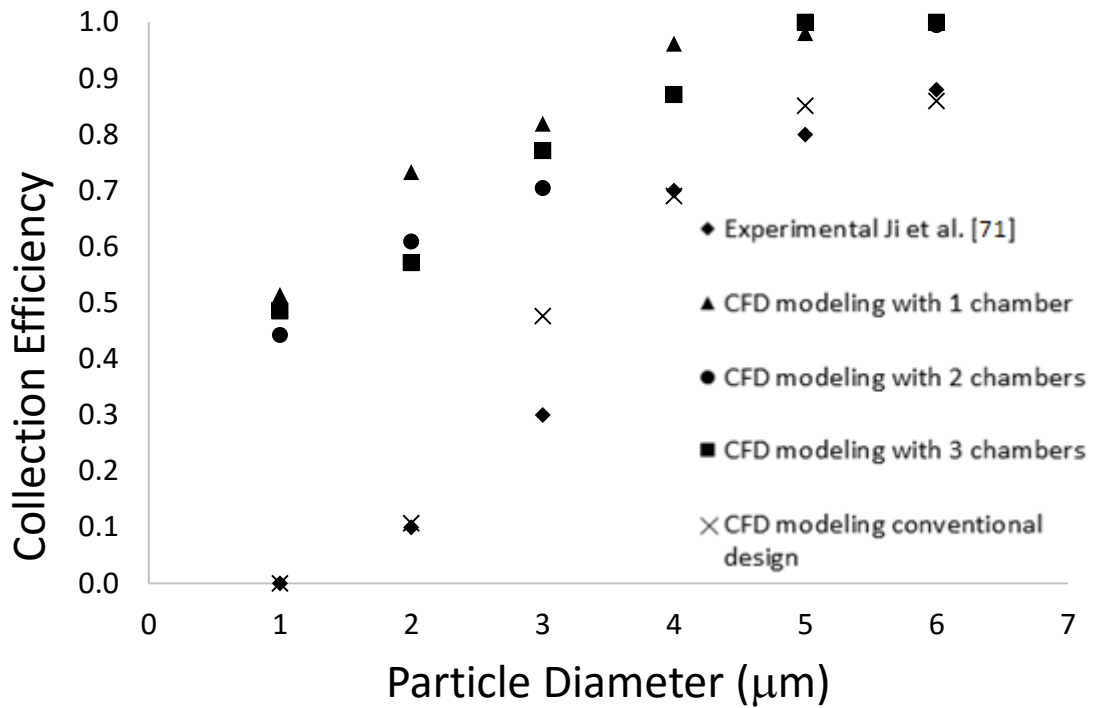


Figure 6-3: The comparison between the experimental results reported by Ji et al. [71], CFD results of a conventional design, CFD results for the proposed geometrical modification involving the addition of one tangential chamber, CFD results for the case of two chambers, CFD results for the case of three chambers

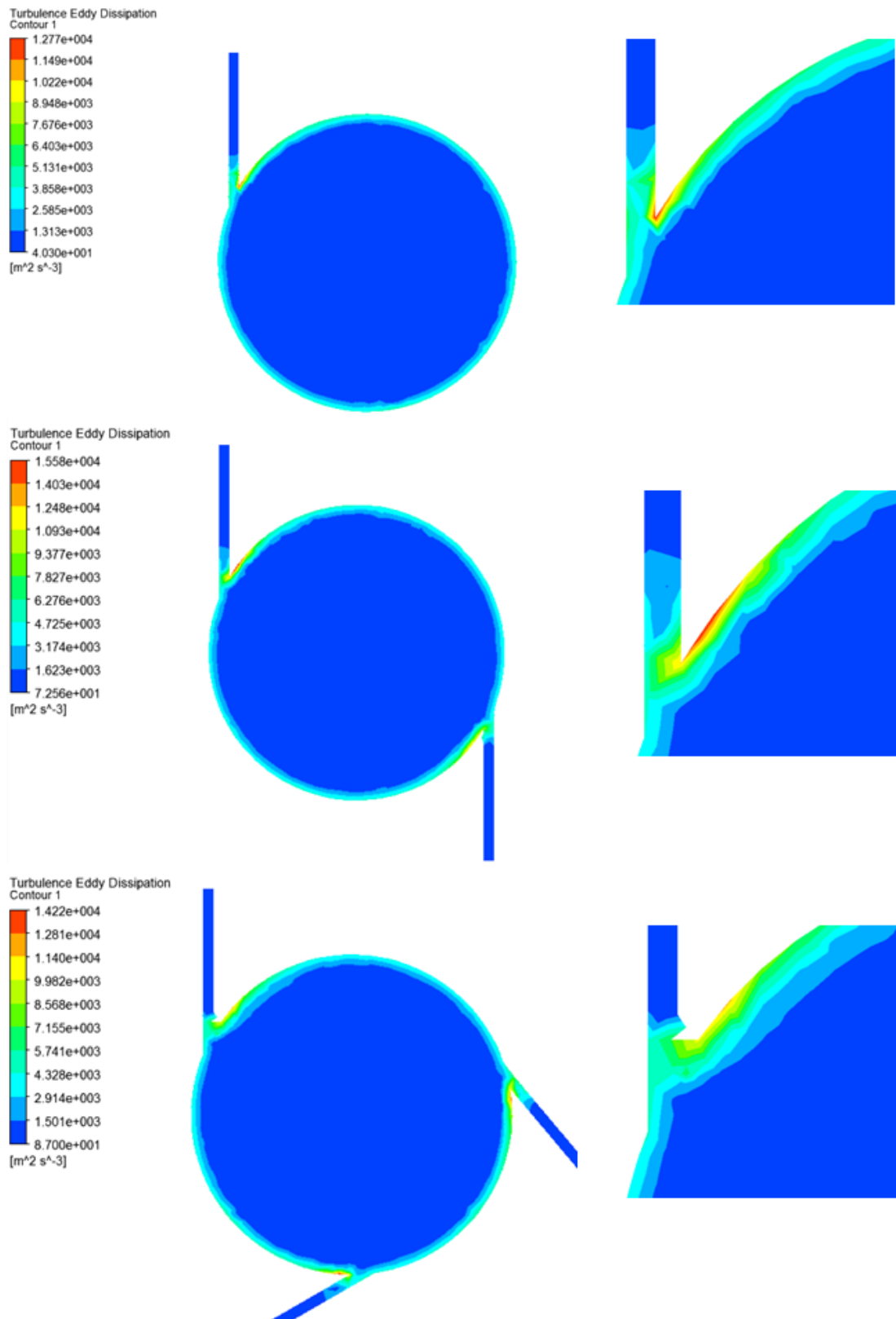


Figure 6-4: The turbulence eddy dissipation for the cases of adding one, two, or three tangential chambers

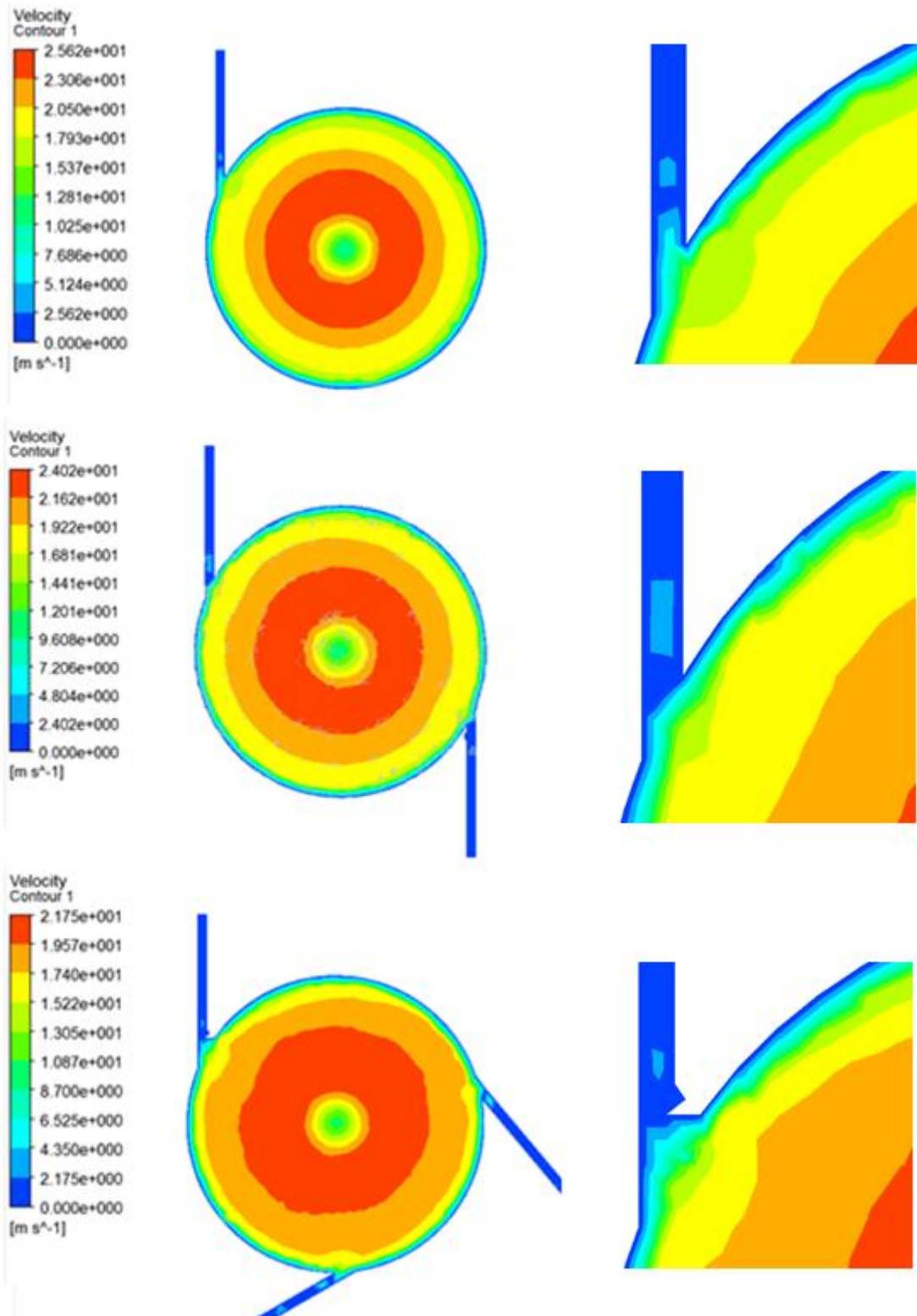


Figure 6-5: The fluid velocity contours for the cases of adding one, two, or three tangential chambers

Velocity at the inlet of the cyclone - Increasing the inlet velocity increases the separation efficiency as mentioned in Introduction. Using the numerical model, this effect was studied for two inlet velocity values of 14 and 20 m/s applied to the geometrical modification with one tangential chamber. These results, shown in Figure 6-6, were compared against the experimental results of Ji et al. [71] reported for these two inlet velocities. The results show that increasing the inlet velocity from 14 to 20 m/s increases the separation efficiency for the design with one tangential chamber for all particle sizes. The largest increase of 25% is achieved for the 2 μm particles and the smallest increase of 1% is achieved for the 6 μm particles. However, this improvement incurs a significant rise in the pressure drop, with increases of up to 132% as shown in Section 6.2.

Length of the conical section – Among different geometrical modifications reported in literature (see Introduction), the vertical length of the conical section seems to yield the highest separation efficiency gains [55]. The CFD model is used to compare the separation efficiency for the range of the particles studied here of the cases of: i) the conventional cyclone design, ii) the design with an elongated vertical cone, and iii) the design with one tangential chamber. The results shown in Figure 6-7 demonstrates that elongating the cone enhances the efficiency for particle sizes larger than 5 μm as compared to the conventional design. The addition of one tangential chamber, however, enhances the efficiency for all ranges of particles (especially the small particles) compared to the conventional and elongated designs. Specifically, the addition of a tangential chamber at the conical section of the cyclone increases the separation efficiency for particles less than 3 μm by 50% compared to the conventional and the elongated designs and 15% for particles larger than 5 μm compared to the conventional design.

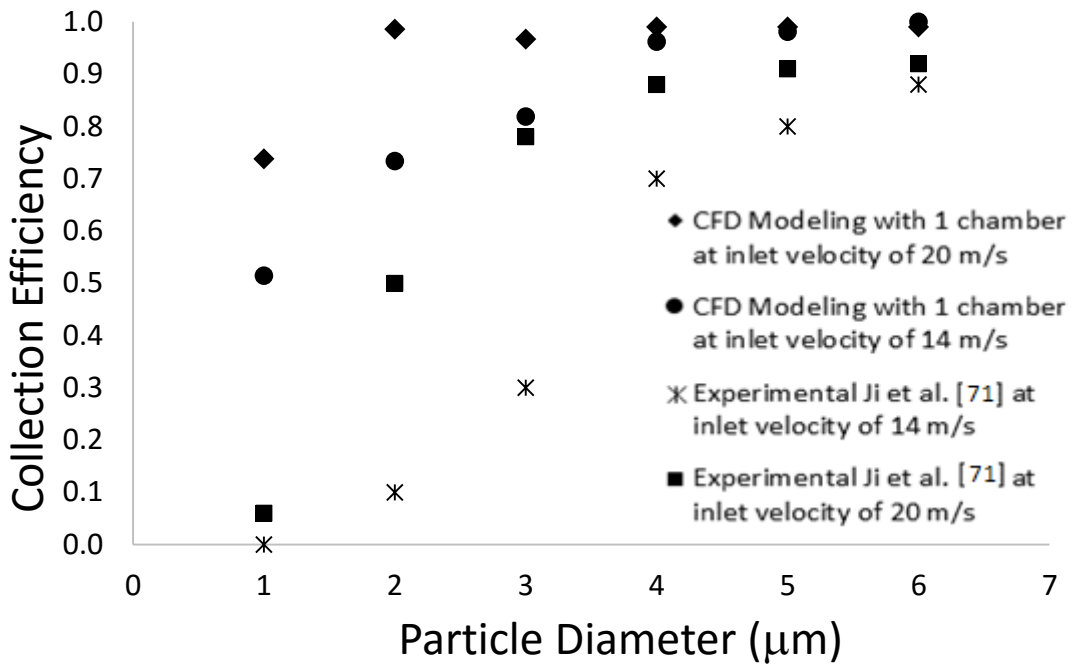


Figure 6-6: The effect of the velocity at the inlet of the cyclone on the separation efficiency for the conventional design, and the design with one tangential chamber

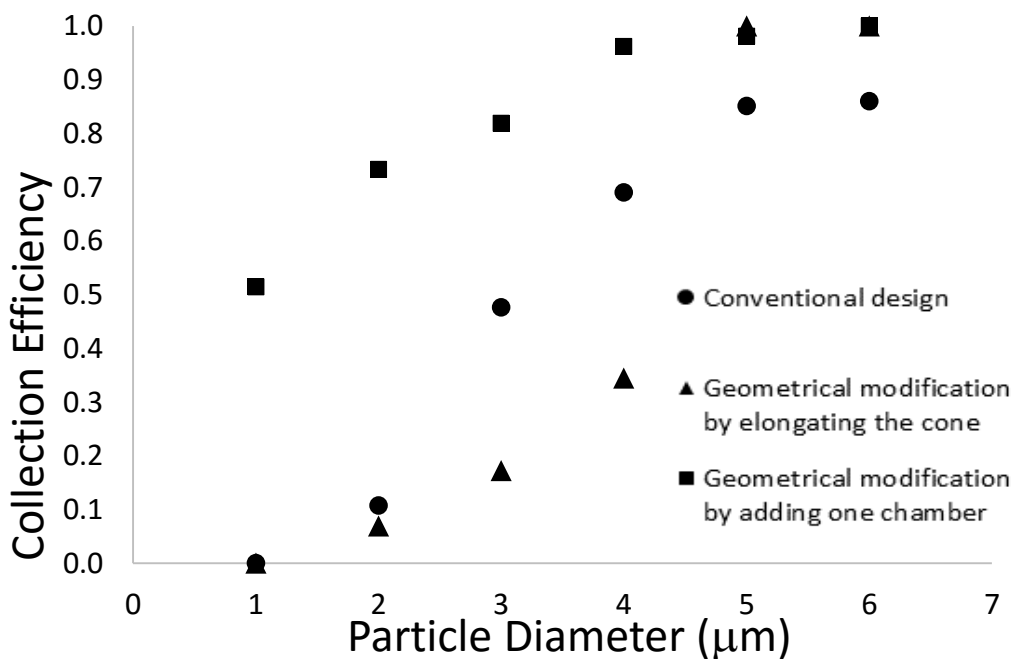


Figure 6-7: Efficiency comparison between conventional cyclone design, conventional cyclone design with an elongated cone length, and the design with a tangential chamber

6.2 Pressure drop

The effect of the proposed model on the pressure drop inside the cyclone separator is investigated here using CFD analysis. Table 6-1 represents the pressure drop of i) the experimental results of Ji et al. [71] reported for the conventional cyclone at the inlet velocity of 14 m/s, ii) the CFD modeling results for the conventional design at 14 m/s, iii) the CFD results for the case of adding one tangential chamber at 14 m/s, and iv) the CFD results obtained for the case of adding one tangential chamber at 20 m/s. The efficiency enhancement using one tangential chamber at 14 m/s inlet velocity is 50% for 1- μm particles (see Figure 6-7) at the cost of only an 8% increase in the pressure drop. On the other hand, the efficiency enhancement using one tangential chamber at 20 m/s inlet velocity reaches 74% for 1- μm particles size with a significant pressure drop increase of 132%.

Table 6-1: Pressure drop for i) the experimental results reported in [70] for conventional cyclone ran at the inlet velocity of 14 m/s, ii) the CFD modeling result for the conventional design at 14 m/s, iii) the CFD result with the addition of one tangential chamber at 14 m/s, and iv) the CFD result with the addition of one tangential chamber at 20 m/s

Pressure Drop (Pa)			
14 m/s Inlet Velocity			20 m/s Inlet Velocity
Ji et al. [71]	CFD modeling for a conventional design	CFD modeling with one chamber added	CFD Modeling with one chamber added
1000	1044	1127	2424

6.3 Erosion rate

The effect of the proposed model on the erosion rate inside the cyclone separator is investigated numerically. Figure 6-8 and Figure 6-9 represent the erosion rates of the walls due to the particles impact and the velocity profiles inside the cyclone, respectively. The

erosion rate is evaluated using the pitting rate of particles on the walls. In this study, the material of the walls was not specified. However, the overall reduction in pitting identifies the reduction in the overall erosion rate regardless of the material. The erosion rate analyzed here refers to radial erosion (due to radial velocity and impact) and sliding erosion (due to tangential velocities)

The results are presented for the cases of the conventional and proposed designs. In essence, the addition of the tangential chamber reduces the maximum erosion rates inside the cyclone (from 5.4×10^{-8} kg/m²s obtained for the conventional design to its half value of 2.5×10^{-8} kg/m²s obtained by adding a tangential chamber) in the addition to the enhancement in the separation efficiency. This decrease in the erosion rate can be explained due to the decrease in the absolute velocity at the walls of the cyclone (specified with a 0.5 slip condition) from 5.6 m/s to 5.2 m/s (see Figure 6-5). The decrease of the absolute velocity at the cyclone walls is a result of the turbulence created near the chambers.

Overall, adding the tangential chamber at the conical section to the Stairmand conventional cyclone design would enhance the separation efficiency, increase the pressure drop and reduce the erosion rate. The efficiency enhancement occurs by reducing the number of smaller particles escaping with the gas as they reach the walls (e.g., an enhancement of 50% for 1 μ m). This method in particular offers higher efficiency for smaller particles (compared to the conventional approach) which is of interest in the current studies conducted for the industrial gas treatment. Therefore, the implementation of this separation mechanism into current cyclone designs could provide a powerful tool for separation of the smaller sized particles with a higher efficiency.

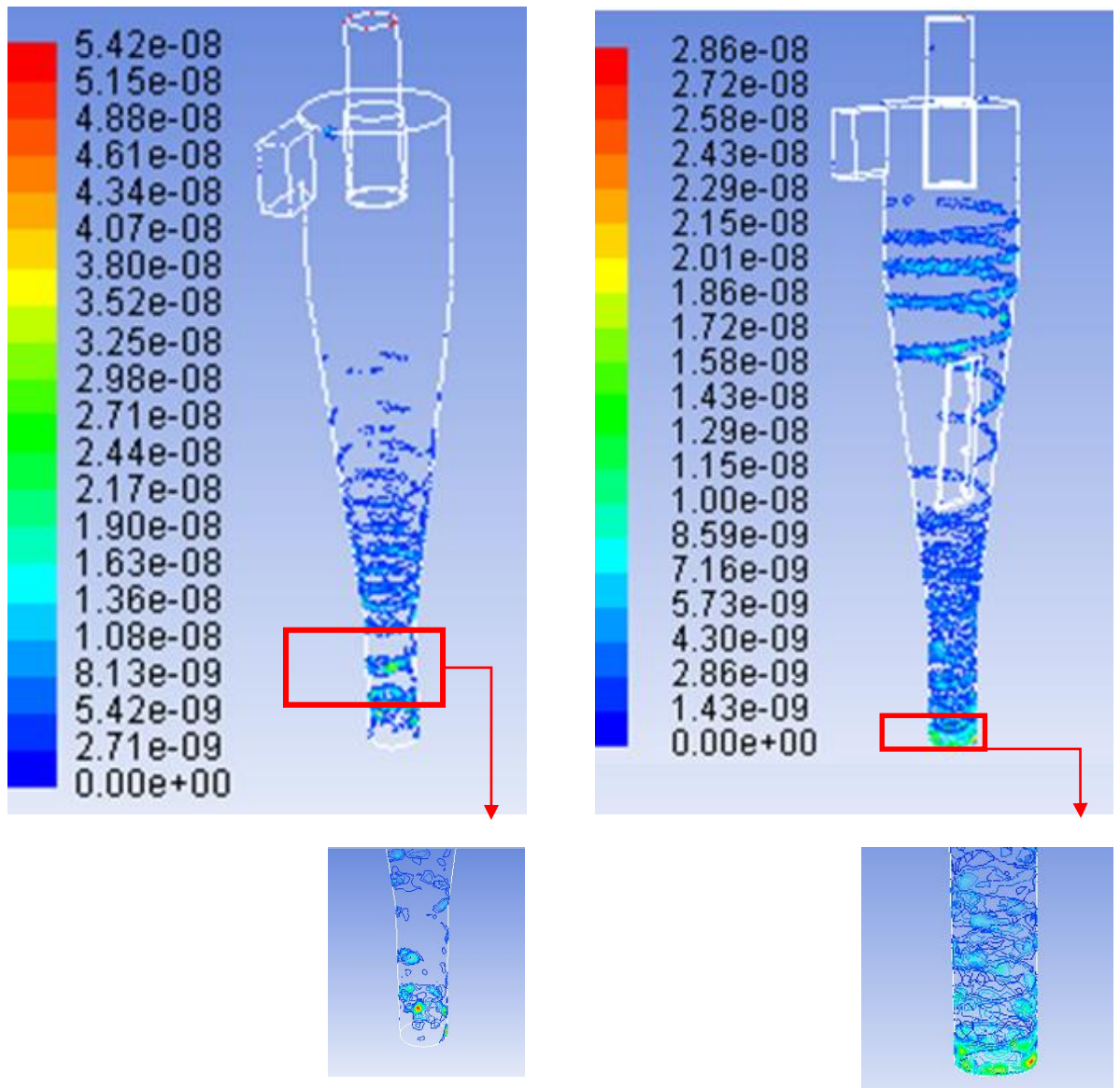


Figure 6-8: Locations of erosion in (a) conventional, and (b) the proposed design including one tangential chamber. The maximum erosion rates for (a) and (b) designs are

$5.4 \times 10^{-8} \text{ kg/m}^2\text{s}$ and $2.5 \times 10^{-8} \text{ kg/m}^2\text{s}$, respectively.

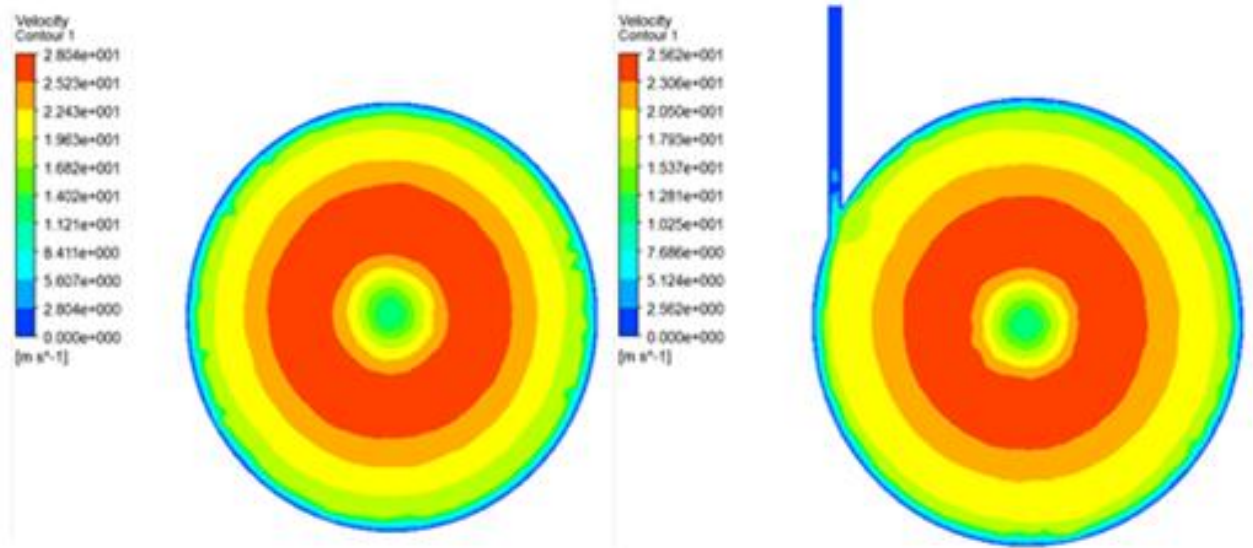


Figure 6-9: Velocity profile for (a) conventional, and (b) the design chamber added

6.4 Experimental results

To increase the separation efficiency, a tangential chamber is added at the conical section of the cyclone separator. The tangential chamber consists of a tangential 3 mm x 100 mm (i.e. same length as the conical section). In the proposed design, solid particles are entered with the gas stream. The increased radial velocity at the conical section due to the decrease in the radius enhances the centrifugal forces of smaller particles. This increase allows the particles reach the walls of the tangential chamber. In conventional cyclones, although the smaller particles reach the walls, they may not be filtered as they might still gain momentum with the escaping air flow coming from the bottom chamber. Therefore, the tangential collecting chamber would collect those particles as soon as they reach the walls. The escaped solid particles are collected on a membrane (Whatman membranes, GE Healthcare) at the outlet stream and analyzed under the Qualitest Digital Microscope (Hardness Tester). The MH_VK_E software package is used for determining the particle dimension.

The number of sampled particles at the inlet and outlet are chosen as the minimum number of particles needed to achieve a 10% change in the mean value. The size distribution within

the sampled particles is used to estimate the volume (and consequently the mass using sand density of 1780 kg/m^3) of the sampled particles. For the details please refer to Chapter 2. The characterization of the inlet sample and its size distribution is presented in Figure 6-10(a) with error bars representing a 95% confidence level. The range of the particle sizes obtained from the collected sample starts from $4 \text{ }\mu\text{m}$ – $150 \text{ }\mu\text{m}$ with a peak counting value at $9 \text{ }\mu\text{m}$.

The effect of the additional collecting chamber on the solid-gas separation is investigated here for the conventional cyclone design. Since larger particles experience larger centrifugal force, they are expected to reach the outer walls and be readily filtered using the conventional cyclone design. Fine particles (smaller than $8 \text{ }\mu\text{m}$), on the other hand, might reach the walls of the cyclone, but their momentum can be picked up quickly as they follow the gas stream. Similar to the inlet, the size distribution of the dust particles from the outlet of the conventional cyclone was determined and is presented in Figure 6-10 (b) with error bars representing a 95% confidence level. The minimum size collected at the outlet is $4 \text{ }\mu\text{m}$. Experimental evaluations for the conventional cyclone separator indicate an overall count of 1,300,000 escaping particles with the maximum of 19% at the $7\text{-}\mu\text{m}$ particle size. In addition, all particles larger than $15 \text{ }\mu\text{m}$ are separated from the gas stream when they went through the separation process. The results suggest that capturing fine particles (less $7 \text{ }\mu\text{m}$) would require additional techniques to prevent them from escaping with the gas stream.

Similar to the conventional cyclone design, the proposed geometry modification (i.e., the addition of a tangential collecting chamber) is investigated based on the sand characterization method presented above (see Figure 6-10 (c)). The results show that the minimum size collected at the outlet is $4 \text{ }\mu\text{m}$. The scaled-up experimental estimations for

the conventional cyclone separator with the addition of the tangential chamber indicate an overall count of 600,000 (less than half of that obtained for the design without the tangential chamber) escaping particles with the maximum of 18% at the 7- μm particle size. In addition, all particles larger than 12 μm are separated from the gas stream when they went through the cyclone process.

Finally, the collection efficiency plots of the captured particles using the conventional and that with an additional chamber are shown in Figure 6-11 (the error bars present a 95% confidence level). The collection efficiencies achieved for the conventional cyclone design are also compared to those reported in [71] for the same size of the cyclone. It is observed that the maximum error between our experimental values (for the conventional design) and those reported by Ji et al. [71] is 7% occurring at a particle size of 6 μm . The proposed tangential chamber is highly effective in removal of fine particles (i.e., smaller than 6 μm). This enhancement could be due to the increase in the centrifugal forces applied to the smaller particles at the conical section, where they are pushed towards the walls.

Overall, adding the tangential collection chamber at the conical section of the cyclone enhances the collection efficiency performance. The enhancement occurs by reducing the number of smaller particles escaping with the gas (e.g., a reduction of 21% and 2% for 4- μm and 8- μm sizes, respectively). This method in particular offers higher efficiency for smaller particles (compared to the conventional design) which is of interest in the current gas treatment industries. Therefore, the implementation of this design into the 'existing' cyclones could provide a powerful tool for separation of smaller sized particles with a higher efficiency.

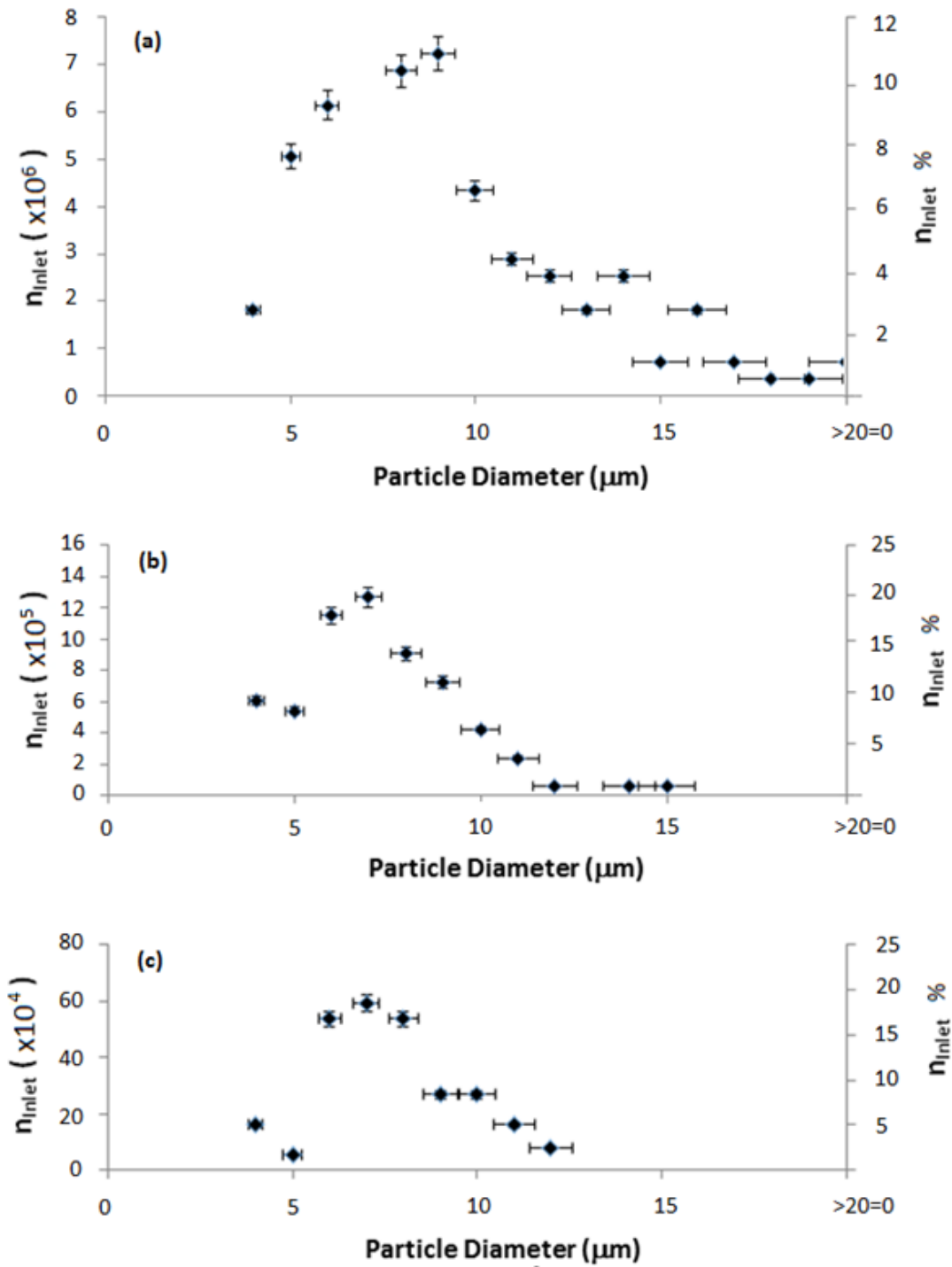


Figure 6-10: Count and percentage of the particle size distribution at the (a) inlet, (b) outlet of the conventional cyclone, and (c) outlet of the cyclone with the tangential chamber

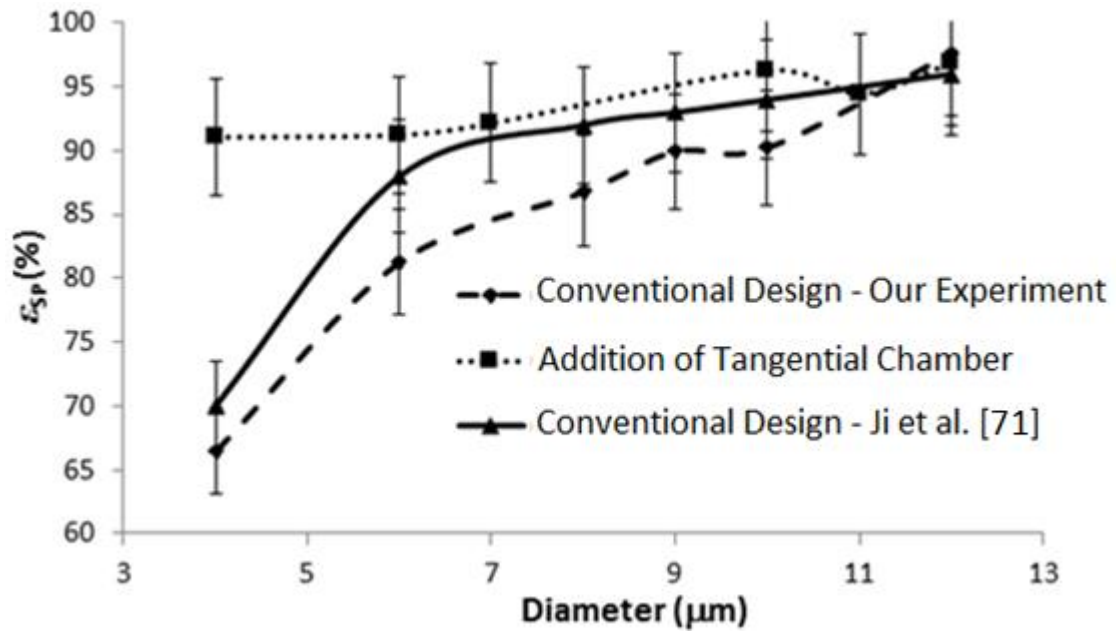


Figure 6-11: Experimental capture efficiency values obtained using our conventional cyclone design and that of Ji et al. [71] as well as those after adding the tangential chamber (the proposed modification in this paper). The symbols present the average values of three runs. The error bars were obtained at a 95% confidence level.

Chapter 7: Conclusions and future work

7.1 Summary

In this thesis, several innovative modifications were proposed to enhance the solid-gas separation in cyclone separators. These modifications are either passive (i.e., the addition of a chamber) or active (i.e., the addition of electro-hydro-magnetic forces). The separation efficiencies obtained based on these proposed modifications were validated using analytical, numerical, and experimental results. These modifications enhance the separation efficiency for a wide range of particles. The results of the analytical, numerical, and experimental results obtained here were first compared against the experimental values presented by Ji et al. [71]. It is observed that the maximum error is obtained at i) 7% for 6- μm particles from our experimental results, ii) 5% at the particle size of 3 μm for the numerical modeling results, and iii) 10% at the particle size of 10 μm for the analytical modeling results. After applying the modifications similar analysis has been conducted. The effect of each modification on separation efficiency is summarized below.

Active modifications

Effect of electrostatic forces – the feasibility of using the electrostatic forces to enhance the efficiency of the overall solid-gas separation in cyclone scrubbers was investigated both using an analytical model and experimental data. The experimental results indicate a total separation enhancement of 34%—at 4- μm particles. The analytical separation results obtained show a separation enhancement of 24.5% at 4 μm . It is observed that the separation efficiency enhancement reduces as the particle size increases. Mainly, this is due to the static charge degradation of the particles over time.

Effect of magnetic forces – the feasibility of using the magnetic forces to enhance the efficiency of the overall solid-gas separation in cyclone scrubbers was investigated

experimentally. The experimental results indicate a total separation enhancement of 23% at 4- μm particles.

Passive additions

The passive modification consists of an additional tangential collecting chamber attached to the conventional cyclone separator. The effect of the additional chamber on the separation efficiency was investigated both numerically and experimentally. It is observed that the maximum error between the numerical and experimental proposed tangential chamber is 4.5% at 4- μm particles. This approach provides a total enhancement of 21.5% to 4- μm particles.

7.2 Limitations

This research faces two main limitations in the cyclone. The first one is related to the operational limitations. For example, the addition of ferrous powders and its attraction through electrostatic and magnetic forces would create a sticky surface on the inner walls of the cyclone. Therefore, cleaning of the internal walls would be required. The second main limitation for using the proposed methods is recycling of the ferrous powder injected. In order to reduce the overall running cost of the proposed methods, the ferrous powder needs to be recycled. Therefore, cost-effective techniques for recycling the ferrous powder must be explored

7.3 Contributions

The first significant contribution in this thesis is the introduction of electro-coating and ferro-fluid spray to existing cyclone equipment used in the solid-gas separation in natural gas industries [90]. This novel approach improves the efficiency of capturing fine particles (with a diameter of less than 1 μm) by more than 20%. The solid particle removal from the

natural gas stream is very crucial in enhancing the efficiency of the overall natural gas production by reducing the erosion of downstream equipment such as compressors. The cyclone optimization has been experimented with the addition of adhesive ferrous powder on an air-dust stream. Results obtained a 25% enhanced solid capturing for 4- μm particle sizes.

The second major contribution in this thesis is a new geometrical modification (i.e., the addition of the tangential chamber at the conical section) of the cyclone that has never been considered before. This addition showed a 27% enhancement for 4- μm particle removal.

The third contribution of this study is the technical and market assessment review published for the current and forecasted future. This review paper provides a basic understanding of the processes used and potential technical approaches that should be developed in the near future (see Appendix B).

Finally, I have contributed in the analysis of liquefaction process and have proposed the addition of low cost equipment reducing the overall power consumption required in the liquefaction and solid-gas separation in the natural gas industry. The results of this study presented in Appendix A will provide a significant cost enhancement in the production of the natural gas.

7.4 Future work

The trade-off between the enhancement of the separation efficiency and the reduction of the pressure drop is an important factor. Current filtration systems would either have the advantage of having a relatively low separation efficiency at a relatively constant pressure drop (i.e., cyclone separators), or having a relatively high efficiency at an increasing pressure drop (i.e., cartridge filters). As one of the future work, internal directing vanes which would reduce the eddy currents at the bottom of the cyclone and the inlet of the

tangential chambers is highly recommended. More specific suggestions regarding the modifications presented in this thesis are presented below:

Tangential chamber – This process would require further studies to find the optimum shape and location of the chamber. One suggested solution is a curved tangential collecting chamber which would collect larger particle sizes.

Electrostatic charges – Providing an electrostatic charge to the solid particles with the addition of adhesive material on the cyclone walls would enhance the separation efficiency for larger particles.

Magnetic forces – This process would be enhanced further with a controlled magnetic field. For example, it is suggested to have a control based on user suitability (i.e., increasing the magnetic field to have higher separation values and decreasing the magnetic field to obtain lower separation values at lower operational costs). Moreover, recycling of the coated particles would lower operational cost after the separation process.

Flow Temperature - Other factors which could affect the separation efficiency (as suggested by Leith and Licht [44]) is the temperature. One could argue that temperature affects the flow density and hence the interactions between the fluid particles and solid particles would be affected. As one of the future study, experimental studies and numerical simulations must be conducted to evaluate the effect of the temperature on the separation efficiency.

Large Eddy simulation - Large Eddy simulations (LES) investigate the flow inside the cyclone more accurately than RANS. Large Eddy simulation models the small eddies and discretize the larger ones. This method is very effective in providing more accurate results in turbulent flows. However, the required run time for such a simulation is significantly higher than that of RANS methods. Hence, the separation efficiencies which would be

achieved from running large eddy simulations would give more accurate results compared to RANS. On the other hand, LES takes a very long simulation time to obtain the results. It would be a great addition to the numerical model developed here to include Large Eddy simulations.

Particle size effect on erosion rate – Studies have shown that the particle mass flowrate has a direct impact on the cyclone wall erosion rate (see Figure 7-1). Therefore, one possible future work could be related to heat treatment of the inner surface of the cyclone separator. The heat-treated surface would have a higher hardness value. The harder surface would have a lower erosion rate.

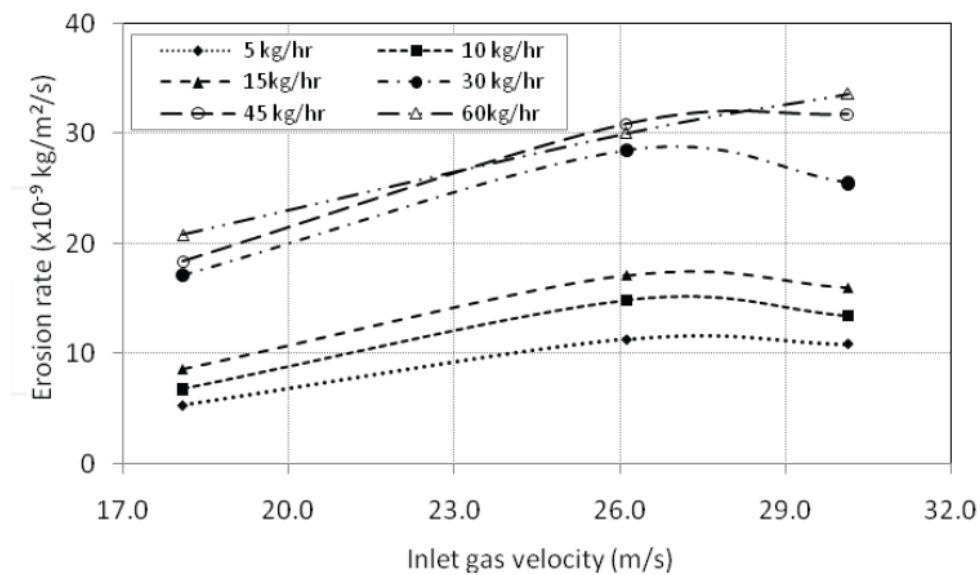


Figure 7-1: Particle size effect on the erosion rate (reproduced from [70] with permission from InTech)

References

- [1] M. Mei. "North American Natural Gas Market Dynamics". Canadian Energy Research Institute. Global LNG - A review study no. 123-Section II, June 2011.
- [2] Adventures in Energy. "Extracting Oil and Natural Gas". Online Source, retrieved on September 2014 from: <http://www.adventuresinenergy.org/exploration-and-production/Extracting-Oil-and-Natural-Gas.html>
- [3] United States Environmental Protection Agency, April 2013. "Water: Oil & Gas Extraction". EPA. Online Source, retrieved on October 2014 from: <http://water.epa.gov/scitech/wastetech/guide/oilandgas/index.cfm>
- [4] Z. Yuan, M. Cui, Y. Xie, C. Li. " Design and analysis of a small scale natural gas liquefaction process adopting single nitrogen expansion with carbon dioxide pre-cooling". *Applied Thermal Engineering*, Volume 64, pp. 139-146, 2014.
- [5] Consumer Energy Center. "Compressed Natural Gas (CNG) as a Transportation Fuel". Online source, retrieved on October 2014 from: <http://www.consumerenergycenter.org/transportation/afvs/cng.html>
- [6] M. Khamforoush, R. Moosavi, T. Hatami. "Compressed natural gas behavior in a natural gas vehicle fuel tank during fast filling process: Mathematical modeling, thermodynamic analysis, and optimization". *Journal of Natural Gas Science and Engineering*. Vol. 20, pp. 121-131, 2014.
- [7] M. Nikolaou. "Optimizing the logistics of compressed natural gas transportation by marine vessels". *Journal of Natural Gas Science and Engineering*. Volume 2, pp. 1-20, 2010.
- [8] D. Wood, S. Mokhatab, M. Economides. (2008). "Technology options for securing markets for remote gas," In: 87th Annual Convention, GPA, Grapevine, TX.

- [9] International Gas Union, 2013. "World LNG Report". News, views and knowledge on gas – worldwide.
- [10] R. Kebede, M. Anantharaman (E). "Exxon, BHP plan world's largest floating LNG plant off Australia". Great Minds think differently. Apr. 2, 2013, 7:07 am EDT. Online article: <http://www.reuters.com/article/2013/04/02/us-exxon-bhp-lng-idUSBRE9310C920130402>
- [11] J. C. Bronfenbrenner, M. Pillarella, J. Solomon. "Review the process technology options available for the liquefaction of natural gas." Air products and Chemicals, Inc., USA.
- [12] Refrigeration Basics and LNG. Online Source, retrieved on October 2014 from: www.ou.edu/.../Refrigeration%20Basics%20and%20LN
- [13] M. S. Khan, Y. D. Chaniago, M. Getu, M. Lee. "Energy saving opportunities in integrated NGL/LNG schemes exploiting: Thermal-coupling common-utilities and process knowledge Chemical Engineering and Processing". *Chemical Engineering and Processing*. Vol. 82, pp. 54-64, 2014.
- [14] Encana. "CNG from wellhead to fuel tank". Online source, retrieved on September 2014 from: <http://www.encana.com/natural-gas/transportation/compressed-natural-gas.html>
- [15] Encana. "LNG from wellhead to fuel tank". Online source, retrieved on September 2014 from: <http://www.encana.com/natural-gas/transportation/liquid-natural-gas.html>
- [16] The Maritime Executive. July 07, 2011. "Is LNG the Fuel of the Future? ". Online source, retrieved on September 2014 from: <http://www.maritime-executive.com/article/is-lng-the-fuel-of-the-future>

- [17] G. Vernengo, E. Rizzuto. "Ship synthesis model for the preliminary design of a fleet of compressed natural gas carriers". *Ocean Engineering*. Volume 89, pp. 189–199, 2014.
- [18] Liquefied Gas Carrier (2011). "Materials of cargo tank construction and insulation of modern liquefied gas carriers". Online source, retrieved on September 2014 from: <http://www.liquefiedgascarrier.com/construction-materials.html>
- [19] H. Sun, H. Zu, F. Liu, H. Ding. "Simulation and optimization of a novel Rankine power cycle for recovering cold energy from liquefied natural gas using a mixed working fluid". *Energy*, volume 70, pp. 317-324, 2014.
- [20] H. Ding, H. Sun, M. He. "Optimisation of expansion liquefaction processes using mixed refrigerant N₂-CH₄". *Applied Thermal Engineering*. Vol. 93, pp. 1053–1060, 2016.
- [21] J. Szargut, I. Szczygiel. "Utilization of the cryogenic exergy of liquid natural gas (LNG) for the production of electricity". *Energy*. Vol. 34, pp. 827-837, 2009.
- [22] J. Wang, Z. Yan, M. W., Y. Dai. "Thermodynamic analysis and optimization of an ammonia-water power system with LNG (liquefied natural gas) as its heat sink". *Energy*. Vol. 50, pp. 513-522, 2013.
- [23] Y. Hisazumi, Y. Yamasaki, S. Sugiyama. "Proposal for a high efficiency LNG power-generation system utilizing waste heat from the combined cycle". *Applied Energy*. Vol. 60, pp. 169-182, 1998
- [24] Y. Liu, K. Guo. "A novel cryogenic power cycle for LNG cold energy recovery". *Energy*. Vol. 36, pp. 2828-2833, 2011.
- [25] G. Angelino, C. Invernizzi. "Carbon Dioxide Power Cycles Using Liquid Natural Gas as Sink". *Applied Thermal Engineering*. 29, pp. 2935-2941, 2009.

- [26] K. Kaneko, K. Ohtani, Y. Tsujikawa, S. Fujii. "Utilization of the cryogenic exergy of LNG by a mirror gas-turbine". *Applied Energy*. Vol. 79, pp. 355-369, 2004.
- [27] T. Lu, K. S. Wang. "Analysis and optimization of a cascading power cycle with liquefied natural gas (LNG) cold energy recovery". *Applied Thermal Engineering*. Vol. 29, pp. 1478-1484, 2009.
- [28] H. Dong, L. Zhao, S. Y. Zhang, A. H. Wang, J. J. Cai. "Using cryogenic exergy of liquefied natural gas for electricity production with the Stirling cycle". *Energy*. Vol. 63, pp. 10-18, 2013.
- [29] C. A. Scholes, G. W. Stevens, S. E. Kentish. "Membrane gas separation applications in natural gas processing". *Fuel*. Vol. 96, pp. 15–28, 2012.
- [30] T. E. Rufford, S. Smart, G.C.Y.Watson, B.F.Graham, J.Boxall, J.C.Diniz da Costa, E.F.May. "The removal of CO₂ and N₂ from natural gas: A review of conventional and emerging process technologies". *Journal of Petroleum Science and Engineering*, Vol. 94-95, pp. 123–154, 2012.
- [31] H. Cong, M. Radosz, B.F. Towler, Y. Shen. "Polymer–inorganic nanocomposite membranes for gas separation". *Separation and Purification Technology*. Vol. 55, pp. 281–291, 2007.
- [32] R. Zolandz, G. Fleming. *Membrane Handbook, Design of gas permeation systems*. Editors: Ho, WSW, Sirkar KK. Kluwer Academic Publishers. Dordrecht. The Netherlands. pp. 54–77, 2001.
- [33] T. Cnop, D. Dortmund, M. Schott. "Continued Development of as Separation Membranes for Highly Sour Service". UOP LLC, Illinois 60017, USA.
- [34] "NATCO given go-ahead for balance of major membrane project". *Membrane Technology*. Vol. 4, 2009.

- [35] J. Haggin. "New generations of membranes developed for industrial separations". *Chemical Engineering News*. Vol. 66, pp. 7-16, 1988.
- [36] W. J. Schell, C. G. Wensley, M. S. K. Chen, K. G. Venugopal, B. D. Miller, J. A. Stuart. "Recent advances in cellulosic membranes for gas separation and pervaporation". *Gas Separation & Purification*. Vol. 3, pp. 162-169, 1989.
- [37] R. Zolanz, G. Fleming. *Membrane Handbook*. Editors: Ho, WSW, Sirkar KK. Kluwer Academic Publishers. Dordrecht, The Netherlands pp. 78–94, 2001.
- [38] L. White. "Evolution of natural gas treatment with membrane systems," In *Membrane Gas Separation*, ed. Y. Yampolskii, B. Freeman. Singapore: John Wiley & Sons; 2010. p. 313–32.
- [39] Gascat. "Natural Gas Filter Technology". Online source, retrieved on October 2014 from: <http://www.gascat.com.br/catalogos/ingles/newFILTERS.pdf>
- [40] Valerus. "Gas Filtration". Online source, retrieved on October 2014 from <http://www.valerus.com/products-services/production-equipment/gas-filtration/>
- [41] Bahadori A. *Natural gas processing-technology and engineering design*. Waltham, MA: Elsevier Inc., 2014.
- [42] Xiong Z, Ji Z, Wu X. Development of a cyclone separator with high efficiency and low pressure drop in axial inlet cyclone. *Powder Technology*. 2014; 253: 644-649.
- [43] B. Zhao. Prediction of Gas-Particle Separation Efficiency for Cyclones: A Time-of-flight Model". *Separation and Purification Technology*. 2012; 85: 171-177.
- [44] D. Leith, W. Licht. The Collection Efficiency of Cyclone Type Particle Collectors: A New Theoretical Approach, in: *Air Pollution and its Control*. AIChE Symposium. Series 68. 1972: 196-206.
- [45] W. Barth. *Design and Layout of the Cyclone Separator on the Basis of New Investigations*. BWK. 1956; 8: 1-9.

- [46] F. Qian, M. Zhang. Study of the natural vortex length of a cyclone with response surface methodology. *Computers & Chemical Engineering*. 2005; 29: 2155–2162.
- [47] A. C. Hoffmann, A. van Santen, R. W. K. Allen. Effects of Geometry and Solid Loading on the Performance of Gas Cyclones. *Powder Technology*. 1992; 70:83-91.
- [48] F. P. Qian, J. G. Zhang, M. Y. Zhang, J. Haz. Mat. 2006, in press. DOI: 10.1016/j.jhazmat.2006.01.028.
- [49] Xiong Z, Ji Z, Wu X. Investigation on the Separation Performance of a Multicyclone Separator for Natural Gas Purification. *Aerosol and Air Quality Research*. 2014; 14: 1055–1065.
- [50] Yang KS, Yoshida H. Effect of mist injection position on particle separation performance of cyclone scrubber. *Separation and Purification Technology*. 2004; 37: 221–230.
- [51] Yoshida H, Hayase Y, Fukui K, Yamamoto T. Effect of conical length on separation performance of sub-micron particles by electrical hydro-cyclone. *Powder Technology*. 2012; 219: 29–36.
- [52] Svoboda J, Coetzee C, Campbell QP. Experimental Investigation into the application of a Magnetic Cyclone for Dense Medium Separation. *Minerals Engineering*. 1998; 11: 501-509.
- [53] Park, C. W.; Song, D. H.; Yook, S. J. (2015). Development of a single cyclone separator with three stages for size-selective sampling of particles. *Journal of Aerosol Science*, 89: 18-25.
- [54] Kim, H. T.; Lee, K. W.; Kuhlman, M. R. (2001). Exploratory design modifications for enhancing cyclone performance. *Aerosol Science*, 32: 1135-1146.

- [55] Brar, L. S.; Sharma, R. P.; Elsayed, K. (2015). The effect of the cyclone length on the performance of Stairmand high-efficiency cyclone. *Powder Technology*. 286, 668:677.
- [56] Xiang, R.; Park, S. H.; Lee, K. W. (2001). Effects of cone dimension on cyclone performance. *Aerosol Science*. 32, 549:561.
- [57] Chuah, T. G.; Gimbut, J.; Choong, T. S. Y. (2006). A CFD study of the effect of cone dimensions on sampling aerocyclones performance and hydrodynamics. *Powder Technology*. 162, 126:132.
- [58] Bryant, H.; (1983). How dust in gas affects cyclone pressure drop. *Hydrocarbon Process*. 62.
- [59] Zhu, Y.; Lee, K. (1999). Experimental study on small cyclones operating at high flowrates. *Journal of Aerosol Science*. 30, 1303:1315.
- [60] Mothes, H. (1982). *Bewegung und Abscheidung der Partikeln im Zyklon* (PhD. Thesis). Technical University Karlsruhe, Germany.
- [61] Qian, F.; Zhang, J.; Zhang, M. (2006). Effects of the prolonged vertical tube on the separation performance of a cyclone. *Journal of Hazardous Materials*. B136, 822:829.
- [62] Bogodage, S. G.; Leung, A. Y. T. (2015). CFD simulation of cyclone separators to reduce air pollution. *Powder Technology*. 286, 488:506.
- [63] Gil, A.; Cortes, C. (2002). Gas-particle flow inside cyclone diplegs with pneumatic extraction. *Powder Technology*. 128, 78:91.
- [64] Lim, K. S.; Kwon, S. B.; Lee, K. W. (2003). Characteristics of the collection efficiency for a double inlet cyclone with clean air. *Aerosol Science*, 34: 1085 – 1095.
- [65] Kim, H. T.; Lee, K. W.; Kuhlman, M. R. (2001). Exploratory design modifications for enhancing cyclone performance. *Aerosol Science*. 32, 1135:1146.

- [66] Misiulia, M.; Andersson, A. G.; Lundstrom, T. S. (2017). Effects of the inlet angle on the collection efficiency of a cyclone with helical-roof inlet. *Powder Technology*, 305: 48-55.
- [67] Lim, K. S.; Kim, H. S.; Lee, K. W. (2004). Characteristics of the collection efficiency for a cyclone with different vortex finder shapes. *Aerosol Science*, 35: 743-754.
- [68] Jung, C. H.; Xiang, R. B.; Kim, M. C.; Lim, K. S.; Lee, K. W. (2004) Performance evaluation of a cyclone with granular packed beds. *Aerosol Science*, 35: 1483 – 1496.
- [69] Leith D, Licht W. The Collection Efficiency of Cyclone Type Particle Collectors – A New Theoretical Approach. AIChE, Symposium Series (126). 1972; 68: 196-206.
- [70] Utikar, R., Darmawan, N., Tade, M., Li, Q, Evans, G., Glennly, M. and Pareek, V. (2010). Hydrodynamic Simulation of Cyclone Separators, Computational Fluid Dynamics, Hyoung Woo Oh (Ed.), ISBN: 978-953-7619-59-6, InTech, Available from: <http://www.intechopen.com/books/computational-fluid-dynamics/hydrodynamic-simulation-of-cyclone-separators>
- [71] Ji, Z.; Xiong, Z.; Wu, X.; Chen, H.; Wu, H. (2009) Experimental investigations on a cyclone separator performance at an extremely low particle concentration. *Powder Technology*, 191: 254-259.
- [72] Wang, B.; Xu, D.; Chu, K.W; Yu, A.B.;(2006). Numerical study of gas solid flow in a cyclone separator. *Applied Technology*, 102:1326-1342.
- [73] Baker, T. H. W.; Kurfurst, P. J. (1985). Acoustic and mechanical properties of frozen sand. *National Research Council Canada*, 1: 227 – 234.
- [74] Avci A, Karagoz I. A Mathematical Model for the Determination of a Cyclone Performance. *Int. Comm. Heat Mass Transfer*. 2000; 27: 263-272.
- [75] Lapple CE. Processes use many collector types. *Chemical Engineering*. 1951; 58, 144-151.

- [76] N. Bock, M. A. Woodruff, D. W. Hutmacher, T. R. Dargaville. Electro spraying, a Reproducible Method for Production of Polymeric Microspheres for Biomedical Applications. *Polymers*. 2011; 3: 131-149.
- [77] George Lovell. Electrocoating Basics. BASF Corporation. Online Source. Retrieved on April 2016 from <http://infohouse.p2ric.org/ref/02/01458.pdf>
- [78] Kip AF. Fundamentals of Electricity and Magnetism (2nd edition). US: McGraw-Hill Inc., 1969.
- [79] CFD Online. Reynolds Stress Model. Online source. Retrieved on November, 2016 from [https://www.cfd-online.com/Wiki/Reynolds_stress_model_\(RSM\)](https://www.cfd-online.com/Wiki/Reynolds_stress_model_(RSM))
- [80] ANSYS. Introductory Fluent Training-Solver Settings. Fluent User Services Center. www.fluentusers.com
- [81] Park, C. W; Song, D. H.; Yook, S. (2015). Development of a single cyclone separator with three stages for size-selective sampling of particles. *Journal of Aerosol Science*, 89: 18-25.
- [82] Kim, J. C.; Lee, K. W. (2007). Experimental Study of Particle Collection by Small Cyclones. *Aerosol Science and Technology*.
- [83] Xiang, R.; Park, R.; Lee, S. H.; Lee, K. W. (2001). Effects of cone dimension on cyclone performance. *Journal of Aerosol Science*, 32: 549 – 561.
- [84] Mazyan WI, Ahmadi A, Jesus RD, Ahmed H, Hoorfar M. Use of Ferrous Powder for Increasing the Efficiency of Solid Particle Filtration in Natural Gas Cyclones. *Separation Science and Technology*. 2016; 51: 2098-2104.
- [85] E.L. Paul, V.A. Atiemo-Obeng, and S.M. Kresta (Eds.), Handbook of Industrial Mixing, Wiley-Interscience, New York, 2004.

- [86] Mazyan, W.; Ahmadi, A.; Brinkerhoff, J.; Ahmed, H.; Hoorfar, M. (2017). Enhancement of cyclone solid particle separation performance based on geometrical modification: numerical analysis. *Physics of Fluids*. (Submitted)
- [87] Paint & Coating Industries (2004). Understanding the Total Cost of Electrocoating. Online Source, retrieved on April, 2016 from <http://www.pcimag.com/articles/93684-understanding-the-total-costs-of-electrocoating>
- [88] Bare Conductive Ltd. Electric Paint Application Notes. Online Source retrieved on April 2016 from bareconductive.com
- [89] [GHG Institute. Compressor Station Efficiency Improvement GHG Project using the Performance Standard Baseline Procedure. Online Source. Retrieved on April 2016 from](http://member.ghginstitute.org/ghgcourses/Course2/downloads/NaturalGasCompressor.pdf) <http://member.ghginstitute.org/ghgcourses/Course2/downloads/NaturalGasCompressor.pdf>
- [90] Mazyan, W.; Ahmadi, A.; Jesus, R. D.; Ahmed, H.; Hoorfar, M. (2016). Use of ferrous powder for increasing the efficiency of solid particle filtration in natural gas cyclones. *Separation Science and Technology*, 51: 2098-2104
- [91] G. Venkataratham (2008). *Cryogenic Mixed Refrigerant Processes: Need for Refrigerant Mixtures*. Colorado: Springer.
- [92] M. Barclay, N. Denton. "Selecting offshore LNG processes". *LNG Journal*. Vol. 10, pp. 34-36, 2005.
- [93] C. Howard, P. Oosthuizen, B. Peppley. "An investigation of the performance of a hybrid turboexpander-fuel cell system for power recovery at natural gas pressure reduction stations". *Applied Thermal Engineering*. Vol. 31, pp. 2165-2170, 2011.

- [94] Song, Y, Wang, J, Dai, Y, Zhou, E. (2012). Thermodynamic analysis of a transcritical CO₂ power cycle driven by solar energy with liquefied natural gas as its heat sink. *Applied Energy*. 92, 194-203.
- [95] The University of Manchester. Cryoman-SMR: A revolution in gas liquefaction technology.
- [96] P. Rodgers, A. Mortazavi, V. Eveloy, S. Al-Hashimi, Y. Hwang, R. Radermacher. "Enhancement of LNG plant propane cycle through waste heat powered absorption cooling". *Applied Thermal Engineering*. Vol. 48, pp. 41-53, 2012.
- [97] A. Mortazavi, C. Somers, Y. Hwang, R. Radermacher, P. Rodgers, S. Al-Hashimi. "Performance enhancement of propane pre-cooled mixed refrigerant LNG plant". *Applied Energy*. Vol. 93, pp. 125–131, 2012.
- [98] M. S. Khan, S. Lee, G.P. Rangaiah, M. Lee. "Knowledge based decision making method for the selection of mixed refrigerant systems for energy efficient LNG processes". *Applied Energy*. Vol. 111, pp. 1018 - 1031, 2013.
- [99] N. B. N. Khan, A. Barifcani, M. Tade, V. Pareek. "A case study: Application of energy and exergy analysis for enhancing the process efficiency of a three stage propane pre-cooling cycle of the cascade LNG process". *Journal of Natural Gas Science and Engineering*. Vol. 29, pp. 125-133, 2016.
- [100] K. J. Park, T. Seo, D. Jung. "Performance of alternative refrigerants for residential air-conditioning applications". *Applied Energy*. Vol. 84, pp. 985–991, 2007.
- [101] K. J. Park, Y. B. Shim, D. Jung. "Performance of R433A for replacing HCFC22 used in residential air-conditioners and heat pumps". *Applied Energy*. Vol. 85, pp. 896–900, 2008.

- [102] V. La Rocca, G. Panno. "Experimental performance evaluation of a vapour compression refrigerating plant when replacing R22 with alternative refrigerants". *Applied Energy*. Vol. 88, pp. 2809–2815, 2011.
- [103] C. Aprea, R. Mastrullo, C. Renno, G. P. Vanoli. "An evaluation of R22 substitutes performances regulating continuously the compressor refrigeration capacity". *Applied Thermal Engineering* Vol. 24, pp. 127–139, 2004.
- [104] X. Xu, J. Liu, C. Jiang, L. Cao. "The correlation between mixed refrigerant composition and ambient conditions in the PRICO LNG process". *Applied Energy*. Vol. 102, pp. 1127–1136, 2013.
- [105] A. Alabdulkarem, A. Mortazavi, Y. Hwang, R. Radermacher, P. Rogers. "Optimization of propane pre-cooled mixed refrigerant LNG plant". *Applied Thermal Engineering*. Vol. 31, pp. 1091-1098, 2011.
- [106] A. Cavallini. "Working fluids for mechanical refrigeration". *International Journal of Refrigeration*. Vol. 19, pp. 485-496, 1996.
- [107] C. Gabriellii, L. Vamling. "Replacement of R22 in tube-and-shell condensers: experiments and simulations". *International Journal of Refrigeration*. Vol. 20, pp. 165-178, 1997.
- [108] C. Aprea, A. Greco. "An exergetic analysis of R22 substitution". *Applied Thermal Engineering*. Vol. 22, pp. 1455–1469, 2002.
- [109] J. L. C. Fannou, C. Rousseau, L. Lamarche, S. Kajl. "A comparative performance study of a direct expansion geothermal evaporator using R410A and R407C as refrigerant alternatives to R22". *Applied Thermal Engineering*. Vol. 82, pp. 306-317, 2015.
- [110] Y. Cengel, M. A. Boles (2001). *Thermodynamics: An Engineering Approach*. Ed 7. Boston: McGraw-Hill.

- [111]A. D. Fares (2013). Hysys workbook. Propane Refrigeration Cycle. Retrieved on January 2015 from: <http://www.adeyab.com/HysysWorkBook.pdf>.
- [112]J. Bukowski, Y. Liu, M. Pillarella, S. Boccella, W. Kennington. "Natural Gas Liquefaction Technology for Floating LNG Facilities". Air products and Chemicals, Inc., USA.
- [113]British Stainless Steel Association. "Selection of stainless steels for handling sulphur dioxide (SO₂) and sulphur trioxide (SO₃)". Retrieved on March 2016 from <http://www.bssa.org.uk/topics.php?article=37>.
- [114]MEPS International Ltd. "MEPS – World Carbon Steel Prices – with Individual Product Forecasts". Retrieved on March 2016 from <http://www.meps.co.uk/World%20Carbon%20Price.htm>.
- [115]B. Songhurst." LNG Plant Cost Escalation". The Oxford Institute for Energy Studies. 2014.
- [116]W. J. Rao, L. J. Zhao, C. Liu, M. Zhang. "A combined cycle utilizing LNG and low-temperature solar energy". *Applied Thermal Engineering*. Volume 60, pp. 51-60, 2013.
- [117]J. Wollan, G. W. Swift, S. Backhaus, D. L. Gardner. (2002). "Development of a Thermoacoustic Natural Gas Liquefier". *AIChE New Orleans Meeting*. Presented in New Orleans, LA March 11-14.
- [118]American Petroleum Institute. "Natural Gas Hydrates May Help Fuel the Future". Online source, retrieved on October 2014 from: <http://www.api.org/environment-health-and-safety/environmental-performance/innovation/natural-gas-hydrates-may-help-fuel-the-future>.

- [119] B. K. Abdalla, N. A. Abdullatef. "Simulation and economic evaluation of natural gas hydrates [NGH] as an alternative to liquefied natural gas [LNG]". *Catalysis Today*. Chemical Engineering Department, University of Qatar.
- [120] Natural Gas, September 2013. "Natural Gas Supply". Online source, retrieved on October 29, 2015 from: <http://naturalgas.org/business/supply/>
- [121] Canadian Association of Petroleum Producers. "An Overview of the World LNG Market and Canada's Potential for Exports of LNG". CAPP. January 2014.
- [122] A. Martinelli. "Natural Gas Investing After Paris 2015". An online source, retrieved on December 2015 from <http://www.energyandcapital.com/articles/natural-gas-investing-after-paris-2015/4977>.
- [123] R. A. Ritz. "Price discrimination and limits to arbitrage: An analysis of global LNG markets". *Energy Economics*. Vol. 45, pp. 324–332, 2014.
- [124] GIIGNL (The International Group of Liquefied Natural Gas Importers), 2012. *The LNG Industry in 2011*. International Group of Liquefied Natural Gas Importers, Paris.
- [125] Energy Information Administration. "What are the major factors affecting natural gas prices?" Online source, retrieved on October 2014 from: <http://www.eia.gov/tools/faqs/faq.cfm?id=43&t=8>
- [126] Energy Information Administration. "How much does it cost to produce crude oil and natural gas?" Online source, retrieved on October 2014 from: <http://www.eia.gov/tools/faqs/faq.cfm?id=367&t=8>
- [127] "Canadian LNG risks losing out to the US". *Global LNG Monitor*. Issue 336, Week 36, September 2014.
- [128] M. S. Khan, S. Lee, M. Hasan, M. Lee. "Process knowledge based opportunistic optimization of the N₂-CO₂ expander cycle for the economic development of

- stranded offshore fields". *Journal of Natural Gas Science and Engineering*. Vol. 18, pp. 263-273, 2014.
- [129] M. S. Khan, S. Lee, M. Getu, M. Lee. "Knowledge inspired investigation of selected parameters on energy consumption in nitrogen single and dual expander processes of natural gas liquefaction". *Journal of Natural Gas Science and Engineering*. Vol. 23, pp. 324-337, 2015.
- [130] Gazprom. "How is natural gas produced". Gaz Prom Info. Retrieved on 27/09/2014. Online source, retrieved on September 2014 from: <http://www.gazprominfo.com/articles/production-of-natural-gas/>
- [131] TNT Energy Services. "Drilling Rig Companies Canada". Retrieved on 27/09/2014. Online source, retrieved on September 2014 from: <http://tntenergy.ca/drillingcanada/>
- [132] Yahoo. "Industry Center - Oil & Gas Drilling & Exploration". Retrieved on 27/09/2014. Online source, retrieved on September 2014 from: https://biz.yahoo.com/ic/123_cl_all.html
- [133] S. C. Lee. "Technology Selection in Gas Processing Plant". Turkmenistan Gas Congress, 2010.
- [134] K. Tanaka, K. Okamoto. (2006). *Structure and transport properties of polyimides as materials for gas and vapor membrane separation*, In: *Materials science of membranes for gas and vapor separation*, ed Y. Yampolskii, I. Pinnau, B. Freeman. Chichester: John Wiley & Sons. p. 271–91.
- [135] R. W. Baker. "Future directions of membrane gas separation technology". *Industrial & Engineering Chemistry Research*. Vol. 41, pp. 1393-1411, 2002.
- [136] A. Tokarev, K. Friess, J. Machkova, M. Sipek, Y. Yampolskii. "Sorption and diffusion of organic vapors in amorphous teflon AF2400". *Journal of Polymer Science Part B: Polymer Physics*. Vol. 44, pp. 832-844, 2006.

- [137] E. Squire. "Cladding, optical fibers, electronics, films, molding materials". US Patent 4754009; June 28, 1988.
- [138] T. Merkel, I. Pinnau, R. Prabhakar, B. Freeman. (2006). *Gas and transport properties of perfluoropolymers*, In: *Materials science of membranes for gas and vapor separation*. Ed. Y. Yampolskii, I. Pinnau, B. Freeman. Chichester: John Wiley & Sons.
- [139] L. Y. Yen, G. Lopatin. "Fluorocarbon membranes and process for making fluorocarbon membranes." US Patent 4906377; Mar 6, 1990.
- [140] Y. Mutoh, M. Miura. "Mixing and Extraction of Pore-formers." US Patent 4623670, Nov 18, 1986.
- [141] Y. Mutoh, M. Miura. "Porous fluorine resin membrane and process for preparing the same." US Patent 4702836; Oct 27, 1987.
- [142] A. Jansen, R. Klaassen, P. Ferron, J. Hanemaaijer, P. Meulen. "Membrane Gas Absorption Processes in Environmental Applications". TNO Institute of Environmental and Energy Technology: 7300 AH Apeldoorn. The Netherlands.
- [143] W.J. Lau, A. F. Ismail, N. Misdan, M. A. Kassim. "A recent progress in thin film composite membrane: A review". *Desalination*. Vol. 287, pp. 190–199, 2012.
- [144] E. M. Mahdi, J. C. Tan. "Mixed- matrix membranes of zeolitic imidazolate framework (ZIF-8)/Matrimid nanocomposite: Thermo-mechanical stability and viscoelasticity underpinning membrane separation performance". *Journal of Membrane Science*. Vol. 498, pp. 276–290, 2016.
- [145] M. A. Aroon, A. F. Ismail, T. Matsuura, M. M. Montazer-Rahmati. "Performance studies of mixed matrix membranes for gas separation: A review". *Separation and Purification Technology*. Vol. 75, pp. 229–242, 2010.

- [146]N. M. Wara, L.F. Francis, B.V. Velamakanni, "Addition of alumina to cellulose acetate membranes". *Journal of Membrane Science*. Vol. 104, pp. 43–49, 1995.
- [147]G. Corvini, J. Stiltner, K. Clark. “Mercury Removal from Natural Gas and Liquid Streams”. UOP LLC, Houston, Texas, USA.
- [148]Exterran. “Hydrocarbon Stabilizer Unit”. Production Solutions. Online source, retrieved on October 2014 from: <http://www.exterran.com/Content/Docs/Products/Hydrocarbon-Stabilizer-English-Letter.pdf>
- [149]United Nations. Paris Climate Change Conference. An online source, retrieved on December 2015 from: http://unfccc.int/meetings/paris_nov_2015/meeting/8926.php/Christiana Figures, Executive Secretary UNFCCC.
- [150]J. Bukowski, Y. N. Liu, S. Boccella, L. Kowalski. (2011). "Innovations in natural gas liquefaction technology for future LNG plants and floating LNG facilities". *International Gas Union Research Conference*.
- [151]KLM Technology Group, Online Source, retrieved on October 2014 from: www.klmtechgroup.com
- [152]J. Javanmardi, Kh. Nasrifar, S.H. Najibi, M. Moshfeghian. “Economic evaluation of natural gas hydrate as an alternative for natural gas transportation”. *Applied Thermal Engineering*, volume 25, pp. 1708-1723, 2005.
- [153]D. Wolman, 2003. “Gas Goes Solid”. Energy News. Online source, retrieved on October 2014 from: <http://www.technologyreview.com/news/401887/gas-goes-solid/>
- [154]NatGas, Sep 2013. “The Transportation of Natural Gas”. Online source, retrieved on September 2014 from: <http://naturalgas.org/naturalgas/transport/>

- [155]X. Wang, M. Marongiu-Porcu. (2008). “The potential of compressed natural gas transport in Asia,” In: International Petroleum Technology Conference (IPTC), Kuala-Lumpur, Malaysia, IPTC 12078.
- [156]G. swift, J. Wollan. “Thermoacoustics for Liquefaction of Natural Gas”. *Gas Tips*. Pp. 21-26, 2002.
- [157]EPA. “Natural Gas Dehydration, Lessons Learned from Natural Gas Star Program”. Producers Technology Transfer Workshop College Station, Texas, May 17, 2007. Online source, retrieved on October 2014 from: <http://epa.gov/gasstar/documents/workshops/college-station-2007/8-dehydrations.pdf>
- [158]Gascat, Natural Gas Filter Technology-Gascat, Filters catalogue.
- [159]Peerless MFG CO., Vane Type Separators, Retrieved on 11/11/2014 from: <http://www.peerlessmfg.com/solutions/separation-filtration/vane-type-separators.html>
- [160]J. M. Beekmans, C. J. Kim. Analysis of the Efficiency of Reverse Flow Cyclones. *Canadian Journal of Chemical Engineering*. 1977; 55: 640-643.
- [161]Cortes C, Gil A. Modeling the gas and particle flow inside cyclone separators. *Progress in Energy and Combustion Sciences*. 2007; 33: 409-452.

Appendix A: Performance of Refrigeration Cycle in Natural Gas Liquefaction Process*

A.1. Introduction

This appendix presents the feasibility of using low-cost techniques to enhance the coefficient of performance (*COP*) of the refrigeration cycle used in natural gas liquefaction. The effect of mixing the propane refrigerant with ammonia, sulfur dioxide and carbon dioxide on the performance and the work of the compressor is studied. It is shown that the mixture of ammonia-propane and sulfur dioxide-propane enhances the overall *COP* by 7% and 9%, respectively. The addition of ammonia and sulfur dioxide to the propane refrigerant reduces the overall compressor work by reducing the overall mass flowrate required to absorb a constant heat from the natural gas. On the other hand, the mixture of carbon dioxide-propane degrades the overall *COP* by 70%. The addition of carbon dioxide increases the overall mass flowrate required to absorb a constant heat from the natural gas. Interestingly, the proposed method requires small capital and running costs, and hence, can be used as an enhancement to existing liquefaction plants.

The preparation to transport involves storing natural gas in containers by either compressing it or liquefying it [4]. Liquefaction is a vital process in the natural gas transport as it is considered to have a lower overseas transportation cost compared to other transportation forms [4].

There are many technologies available for liquefaction of natural gas. Current technologies include i) single refrigerant processes (cascade [12]), ii) mixed refrigerant processes (DMR [12], Linde [12]) and iii) combined refrigerant processes (APCI [12]). The efficiency of these liquefaction processes generally depends on the working fluid, the arrangement of the refrigeration cycles, and the number of elements used in the cycle. The working

principle of each one of these liquefaction processes is different. The cascade processes use a single refrigerant (single working fluid) in multi-stage refrigeration cycles connected in series. Each refrigeration cycle has a single refrigerant and cools the natural gas partially until the natural gas liquefies at $-160\text{ }^{\circ}\text{C}$. DMR/Linde processes use mixed refrigerants in the refrigeration cycles to have a better fit with the natural gas cooling curve, and hence, reduce the power consumption of the compressors in the cycles. The APCI liquefaction processes, the mostly used worldwide, use a combination of a single refrigerant refrigeration cycle (using propane) to pre-cool the natural gas. The natural gas is then cooled down to $-160\text{ }^{\circ}\text{C}$ using a mixed refrigerant cycle. Due to their simpler propane pre-cooling cycle, the APCI liquefaction processes offer a higher liquefaction performance (i.e. high coefficient of performance (*COP*)) with lower running cost compared to the DMR/Linde processes. APCI consists of three stages for cooling down the treated natural gas [12]. The first stage is by cooling the natural gas to $1.7\text{ }^{\circ}\text{C}$ using chilled propane. This stage takes place after cooling down the natural gas from $38\text{ }^{\circ}\text{C}$ to $15.5\text{ }^{\circ}\text{C}$ using air and water coolers. The second stage in the APCI process involves feeding the precooled natural gas to a two-staged heat exchanger tower. The first stage of the heat exchanger tower uses a mixed refrigerant consisting cold heavy propane and butane to cool the precooled natural gas down to $-50\text{ }^{\circ}\text{C}$. The second stage of the heat exchanger (i.e., the third stage in APCI) sprays a mixture of light gases (such as methane, ethane and nitrogen) over the natural gas. The valves are used to cool down further the natural gas to $-160\text{ }^{\circ}\text{C}$. In some plants, an additional working fluid is added to the above cooling cycle. The most common additional refrigerant added is nitrogen which enhances the efficiency of the liquefaction process. Such a cycle is referred to as the AP-X cycle.

The main drawback of the natural gas liquefaction processes is the high power consumption by the compressors and the size of the plant for offshore facilities. Based on the current

designs of the refrigeration cycles, the coefficient of performance (*COP*) of the cycle increases with the increase in the power consumption (as multiple compression stages required) and adding additional elements such as compressors and turbo-expanders. However, having higher power consumption and adding more elements increase the operating cost. Also, larger and complex plants are not suitable for offshore natural gas plants. In recent years, many researchers have focused on increasing the *COP* of the refrigeration cycle while minimizing the capital and operating costs. The efforts made in this regard can be summarized in two categories: In the first category, major additions (and hence changes) have been implemented in the refrigeration cycles [91]; whereas other groups have focused on applying minor changes resulting in enhancement of the overall efficiency of the cycles. Examples of the attempts in the first category include the work of Barclay and Denton [92] have shown that pre-cooling of propane, propylene or CO₂ in the liquefaction process further reduces the power consumption of the compressors, and hence the energy consumption during the natural gas liquefaction process. Among the three gases, CO₂ is the most desirable choice in the offshore plants due to its safe nature, availability, non-toxicity, and non-combustibility. Yuan et al. [4] presented a refrigeration process with the combination of CO₂ precooling and single nitrogen (N₂) expansion. In their cycle, the natural gas is essentially cooled by N₂ and CO₂ cycles. Nitrogen is compressed in two stages and pre-cooled by water coolers and cold CO₂. Then, it is expanded to achieve low pressure and low temperature required for cooling down the natural gas in the heat exchangers. In essence, the CO₂ refrigerant cycle aims to cool further the natural gas; while the nitrogen cycle is to reduce the energy consumption in the gas liquefaction process. Other innovative cycles proposed include the fuel cell hybrid turbo-expander which has been developed to investigate the effects of available exergy in the natural gas pressure reduction stations [93]. The results showed a 10% improvement in the efficiency of the

turbo-expander after the addition of the fuel cell. In recent years, solar power has also been proposed to increase the refrigeration cycle performance. For instance, Song et al. [94] investigated the feasibility of utilizing the solar power in the evaporator of the CO₂ power cycles. They achieved a 6.5% efficiency improvement. Another novel refrigeration cycle design which was proposed by the researchers at the University of Manchester [95] consists of a single mixed refrigerant that splits to light and heavy refrigerants in a separator located after a multistage compressor. This design causes the refrigerants to evaporate at different temperatures which are aligned better with the hot and cold cooling curves of the natural gas, resulting in less compression power. This design has shown a 7% improvement compared to the basic single mixed refrigerant cycles.

The second category of the efforts made towards enhancement of the liquefaction process includes the work of Rodgers et al. [96] who emphasized that the use of turbo-expanders replacing the Joules Thompson expansion valves enhances the performance of the refrigeration cycle. This is due to the partial power utilization from the turbines that is fed back to the compressors. They also used part of the turbine exhaust waste heat as a regenerative power to the compressor which resulted in a 12% improvement in the cycle's efficiency. Similarly, Mortazavi et al. [97] investigated the effect of replacing expansion valves with two phase expanders, liquid turbines and gas turbines. Their model achieved a 7.07% reduction in power consumption by the expansion work recovery. Khan et al. [98] investigated the optimization of the Single Mixed Refrigerant (SMR) liquefaction process based on non-linear modeling of exergy. They were able to enhance the process efficiency based on optimum composition of the refrigerant, flowrate, suction pressure and evaporation pressure. In another study, Khan et al. [99] optimized the propane precooling liquefaction process by identifying optimum operating conditions using HYSYS. Their results showed 15.51% *COP* enhancement and 18.76% exergy enhancement due to lower

cooling duty requirement at the intermediate cooling stage. As for their optimal operating conditions, they selected temperatures of 5 °C, 0 °C and -40 °C for the high pressure, intermediate pressure and low pressure evaporator stages, respectively.

Lately, a special attention has been given to the use of mixed refrigerants as they provide flexibility in matching the multiple thermodynamic properties of the gas being cooled [90] and can replace the high efficient, though ozone depleting, HCFCs. For example, Park et al. [100] studied the effect of mixed refrigerants as a replacement for the HCFC 22 refrigerant in air conditioning units. Their results indicated a 5.7% increase in the *COP* when they used a refrigerant blend consisting of 45% R1270, 40% R290 and 15% DME [100]. Park et al. [101] measured the thermodynamic performance of R433A (30% propylene and 70% propane) and HCFC 22 in a broadband type heat pump/air conditioner. Their study concluded that R433A enhances *COP* by 4.9-7.6% as compared to HCFC 22. Rocca and Pano [102] proposed HFC and HC mixed refrigerants as a replacement for R22 HCFC. They compared the *COP* of the R22 refrigerant with their proposed blended refrigerants including R417A (46.6% R125, 50% R134a and 3.4% R600a), R422A (85.1% R125, 11.5% R134a and 3.4% R600a) and R422D (65.1% R125, 31.5% R134a and 3.4% R600a). Their cycle's *COP* showed its highest values when they used R22, and then followed by R417A, R422A and R422D, consecutively. In another study, Aprea et al. [103] investigated a possible alternative for R22 refrigerant. They studied the effect of the blended refrigerants on the reduction of the compressor's power consumption. In their analysis, R22 refrigerant showed a *COP* value of 2.8 at the 30 Hz motor current supply frequency; whereas the second highest *COP* (2.5 at the same frequency) was achieved using R407C (23% R32, 25% R125 and 52% R134a). In all of the studies conducted for the mixed refrigerants, the percentage of pure elements in the mixed refrigerants is determined in accordance to the ambient temperature of the refrigeration cycle [104]. In a

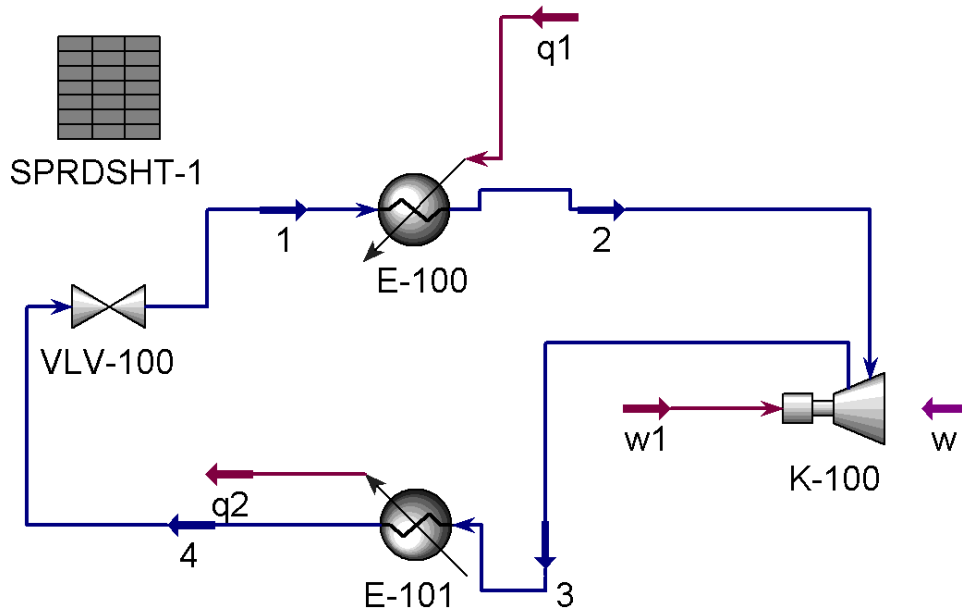
similar study, Alabdulkarim et al. [105] used a genetic algorithm to optimize the C3MR cycle. In their study, the MR cycle was enhanced by 13.28% using new mixed refrigerants with mass fractions of 0.1027 nitrogen, 0.218 methane, 0.5306 ethane, and 0.1487 propane. Ding et al. [19] utilized the advantages of the high specific refrigeration effect of methane, and the low boiling temperature of nitrogen to optimize the expansion process using ASPEN HYSYS. They used this mixture in the propane pre-cooled N₂-CH₄ expansion liquefaction process. This refrigerant mixture produced 36.06% less unit power as compared to the single stage nitrogen expansion cycle. Wang et al. [22] presented four different objective functions for the optimization of C3MR liquefaction process. They were able to reduce the total shaft work by 44.5% using the mixture (in terms of mole fraction) of 8.5% nitrogen, 50.5% methane, 33.8% ethane, 7.1% propane, 0.1% i-butane.

Among all the refrigerants studied in the literature, pure natural fluids (i.e. hydrocarbons, ammonia, carbon dioxide, air, etc.) have potential to be used as pure refrigerants in future LNG plants [106-109]. This paper investigates the feasibility of mixing propane, a hydrocarbon used in all C₃MR natural gas liquefaction plants [12], with non-hydrocarbon natural fluids. Excluding the CFC's and HCFC's due to their potential environmental effects, the most promising gases which would provide an improvement in the overall *COP* are ammonia (NH₃), sulfur dioxide (SO₂) and carbon dioxide (CO₂). These gases (NH₃, SO₂, and CO₂) are already being used in the industry as pure refrigerants and have boiling temperatures around the operating temperatures in the pre-cooled refrigeration cycle investigated in this study. By mixing the propane refrigerant with the industrially approved gases, the coefficient of performance (*COP*) will alter resulting in observing either an increase or a decrease in operating costs. The goal of this study is to investigate the possibility of improving *COP* using the refrigerant mixture at low cost to eliminate the

need of running a separate refrigeration cycle prior to the propane cycle as studied in literature.

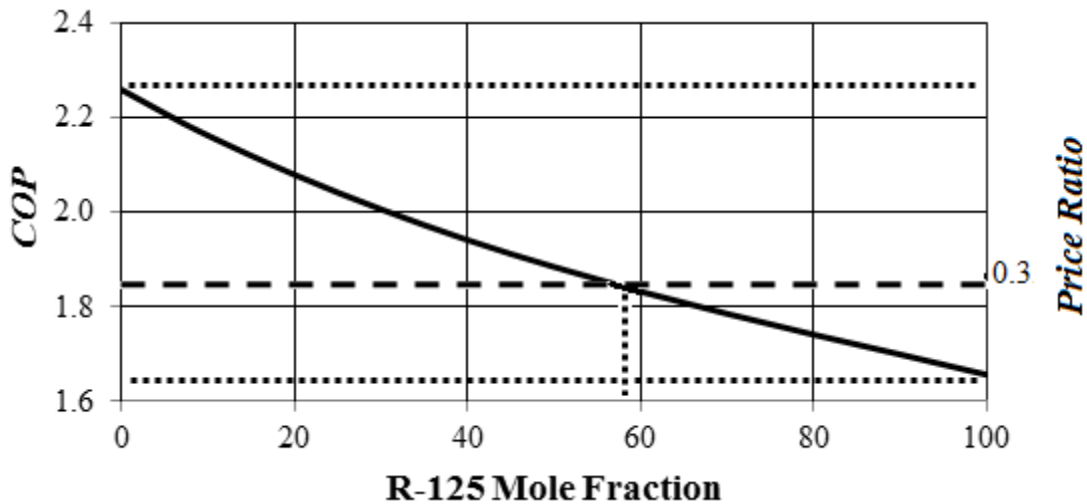
A.2. Material and methods

the proposed method consists of blending refrigerants with propane. This addition has no running cost and can be added to provide an improvement in the basic refrigeration cycle shown in Figure A-1. The industrially used software HYSYS is used to simulate the refrigeration cycle and to evaluate the enthalpy values in the cycle. To assess the reliability of the software used, an example of an industrially-used refrigerant consisting of a mixture of R-134a and R-125 is analyzed. The *COP* curve of this mixture is shown in Figure A-1. Although pure R-134a is a more efficient refrigerant to be used (with a *COP* of 2.21 as compared to R-125 *COP* of 1.657), industry uses the mixture blend of 42% R-134a and 58% of R-125 to obtain a balance between the efficiency and cost (the cost of R-134a is three times that of R-125). As shown in Figure A-1, the 58% mole fraction of R-125 is associated with the cost ratio discussed above.



(i) Figure A-1: A schematic of a basic propane refrigeration cycle

Using the software package, three gases are blended with propane to study the effectiveness of blend refrigerants in increasing *COP* of the refrigeration cycle. An increase in the *COP* of the propane-gas mixed refrigerant will essentially save the capital and running cost of having a separate pure gas component refrigeration cycle prior to the propane cycle.



(ii) Figure A-2: The *COP* curve of a basic R-134a refrigeration cycle as a function of the mole fraction of the R-125 refrigerant

A.3. Theory

A refrigerant going through a refrigeration cycle experiences compression, evaporation, expansion and condensation. In the basic refrigeration cycle shown in Figure A-1, the compression is caused by the compressor (for the pressure increase), and expansion (for the pressure reduction) is caused by the expansion valve. The equation for the work done by the compressor can be calculated as [110]

$$W_{in} = m(h_{2a} - h_1), \quad (A-1)$$

where m is the mass flowrate of the refrigerant, h_{2a} is the actual refrigerant enthalpy at the compressor outlet and h_1 is the refrigerant enthalpy at the compressor inlet. The actual compressor exit enthalpy is calculated as [110]

$$h_{2a} = \frac{(h_{2s} - h_1)}{\eta_{Compressor}} + h_1, \quad (A-2)$$

where h_{2s} is the isentropic refrigerant enthalpy at the exit of the compressor and evaluated at the compressor exit pressure and entropy equals to that of the compressor inlet entropy.

$\eta_{Compressor}$ is the isentropic efficiency of the compressor.

The equation of the heat absorption from the evaporator is calculated as [110]

$$Q_{out} = m(h_4 - h_1), \quad (A-3)$$

where h_4 is the refrigerant enthalpy at the evaporator inlet, h_1 is the refrigerant enthalpy at the evaporator outlet.

To evaluate the overall cycle coefficient of performance, the *COP* equation used is

$$COP = \frac{Q_{absorbed}}{W_{compressor}} \quad (A-4)$$

$$COP = \frac{m(h_4 - h_1)}{m(h_{2a} - h_1)}, \quad (A-5)$$

The work of the compressor depends on the change in the outlet and inlet enthalpies and can be estimated as follows:

$$W_{compressor} = m\Delta h \quad (A-6)$$

Equation (A-6) can be written as

$$W_{compressor} = m(TdS + VdP) \quad (A-7)$$

Therefore, the average mass flowrate, the average temperature, change in the entropy and change in the pressure at the inlet and outlet of the compressor determine the *COP* of the cycle. It would be essential that the thermodynamic properties of the propane-gas mixture have a lower average temperature, lower fluid volume, lower pressure change and lower entropy change to reduce the enthalpy change and hence, increase the overall *COP*. Thus,

the key parameters affecting the *COP* of the refrigeration cycle are the boiling temperature, the critical temperature, and mass flowrate of the refrigerants mixed with propane.

Boiling Temperature - It is possible to obtain a high critical temperature and hence high specific refrigeration effect by mixing hydrocarbons with components with high boiling point [110]. The higher the component's boiling point the faster the evaporation rate and hence the higher the refrigeration capacity. The boiling temperatures of the gases investigated in this study are shown in Table A-1. Due to their higher boiling temperature values, NH₃ and SO₂ are expected to improve *COP* of the cycle when they are mixed with propane.

Critical Temperatures - Critical temperatures of the refrigerant blend changes according to the mole fraction composition of the two gases due to the change in the boiling temperatures. Therefore, the *T-s* and *P-v* diagrams will show changes as the gas composition is altered. Critical temperatures of the gases listed in Table A-1 show that the *COP* of the cycle could be improved for the refrigerant blends of propane-NH₃ and propane-SO₂.

Table A-1: Boiling and critical temperatures of Propane, NH₃, SO₂ and CO₂

Gas	Boiling Temp. (°C)	Critical Temp. (°C)
Propane	-42.10	96.75
Ammonia	-33.45	132.40
SO ₂	-9.95	157.65
CO ₂	-78.55	30.95

Mass Flowrate - According to Equations (A-6) and (A-7), the required mass flowrate to achieve the required cooling effect determines the *COP* of the cycle. Since the mass flowrate term appears at the denominator of the *COP* equation, it is required to choose a

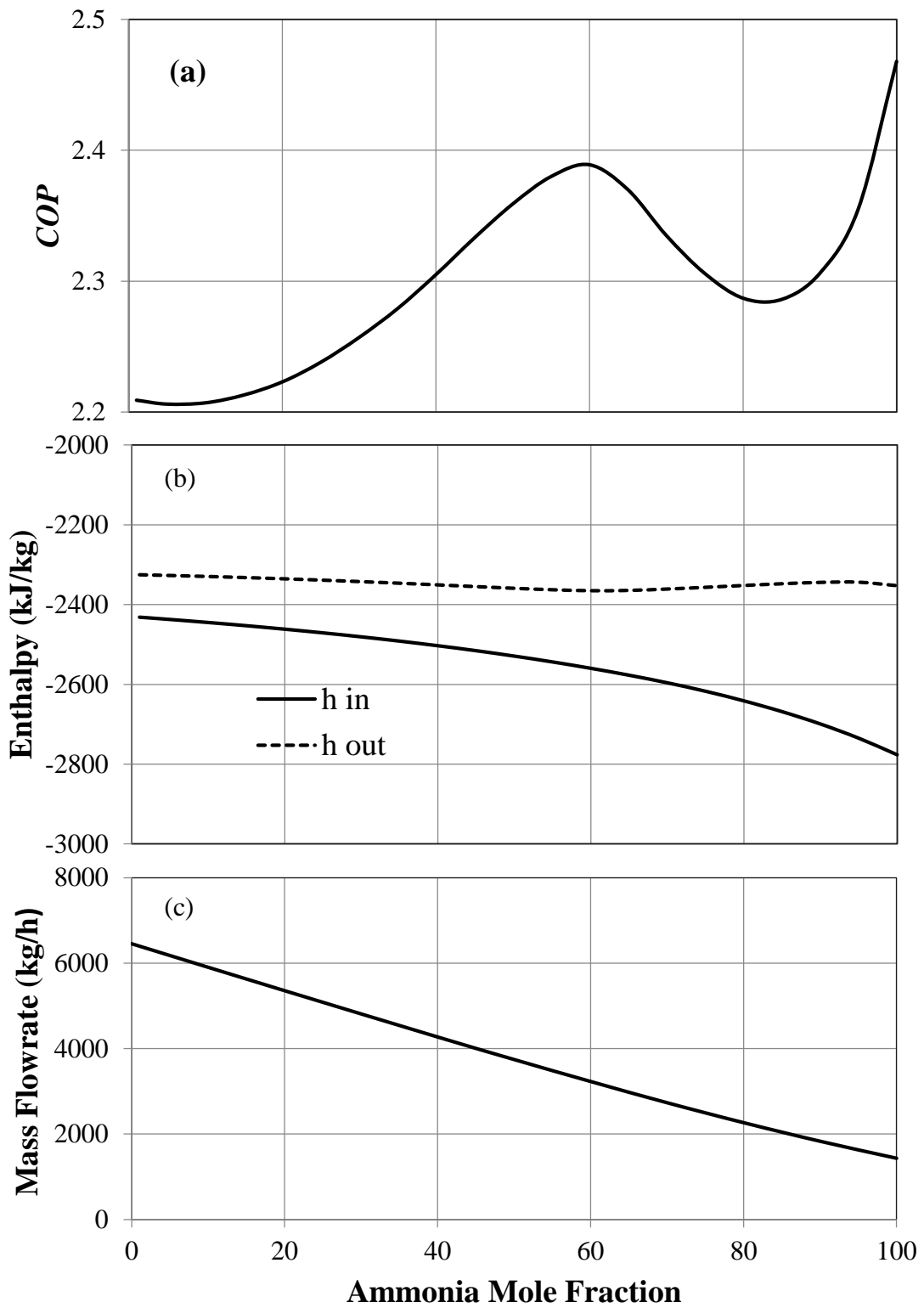
gas blend which provides a low mass flowrate. The blended refrigerants will consist of the combined single element densities and their combined volume flowrates. Both of these properties depend on the pure substances and their blending ratios.

A.4. Results and discussion

The coefficient of performance, *COP*, is studied here to evaluate the performance of the refrigeration cycle operating with different blends of refrigerants. The *COP* of the refrigeration cycle was determined using HYSYS. In this study, a basic refrigeration cycle operating using with pure propane was first evaluated. The propane refrigerant is fed to the evaporator to absorb 1.5×10^6 kJ/hr from the natural gas [111], and then it exits the evaporator as saturated vapour with a 5 kPa pressure drop. Propane is then compressed adiabatically with the efficiency of 75%. Inside the condenser, there is a pressure drop of 30 kPa, where propane leaves as a saturated liquid at 45°C. Finally, the propane is throttled using a throttling valve [111]. The *COP* value obtained for this basic refrigeration cycle is 2.21. The use of different refrigerants has shown different effects on the *COP* of the cycle [3, 4, 92]: mixed refrigerant such as nitrogen, methane, ethane and propane [112] have shown to improve *COP* while cycles running with nitrogen and carbon dioxide as pure refrigerants have low *COP* [111]. The latter are usually used in offshore plants as they are considered to be safer than hydrocarbon refrigerants. In the following sections, the mixture of three gases (ammonia (NH₃), sulfur dioxide (SO₂) and carbon dioxide (CO₂)) with propane is analyzed to study their effect on the *COP* of the propane cycle.

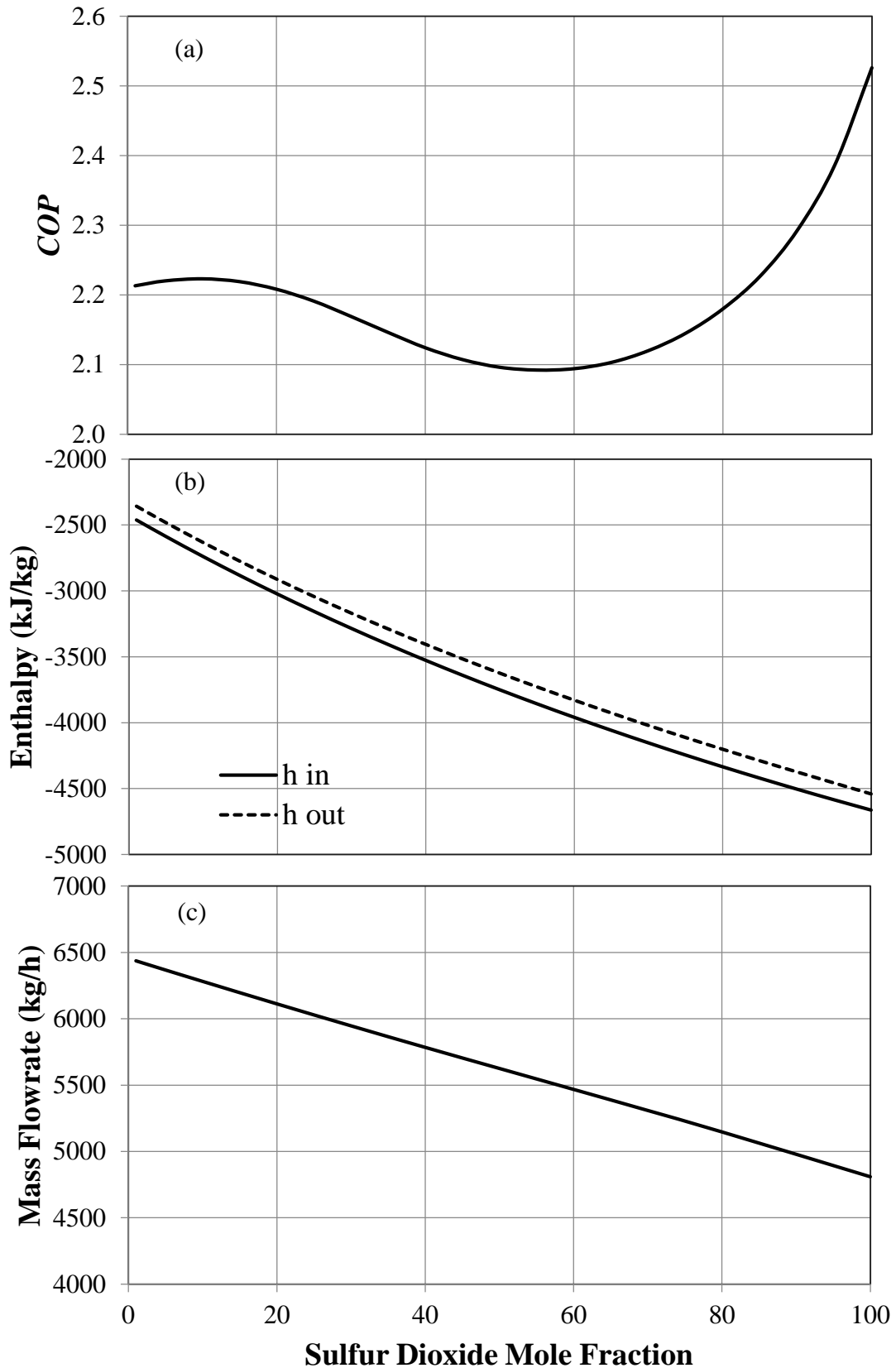
Refrigeration cycle with NH₃-propane mixed refrigerant - The overall *COP* change of the NH₃-propane mixture as a function of NH₃ mole fraction is shown in Figure A-1 (a). The added ammonia in the HYSYS analysis ranges between 1% to 100% mole fractions. The *COP* of the ammonia-propane mixture shows an increasing trend for the mole fraction up to 60%. This increase is due to the combination of i) a small increase in the difference

between the compressor's inlet and outlet enthalpies, from 106 kJ/kg at 0% ammonia to 423 kJ/kg at 100% ammonia (See Figure A-1 (b)), and ii) a large decrease in the mass flowrate, from 6454 kg/h at 0% ammonia to 1433 kg/h at 100% ammonia (See Figure A-1 (c)). Since the density of pure ammonia (1.9 kg/m^3 obtained from HYSYS) at the given temperature and pressure is lower than that of pure propane (6.48 kg/m^3), adding NH_3 to the propane refrigerant was expected to reduce the mass flowrate required to absorb the heat due to the fact that the mass flowrate of the mixture is directly proportional to its density. On the other hand, the change in the enthalpy depends on the blended refrigerants T - s and P - v diagrams, changing due to the change in the critical point of the refrigerant. For the mole fraction values between 60% and 80%, however, the COP of the cycle decreases. One possible reason for the sudden drop in the COP could be related to the high polarity of NH_3 as opposed to non-polar propane. In essence, the high polarity of ammonia molecules attracts the propane molecules and leads to higher energy requirements to cause condensation and evaporation of the mixed refrigerant; hence, higher compressor work is required to achieve the cooling effect at these ammonia-propane percentages. After the mole fraction of 80%, the COP of the cycle increases which shows the dominant effect of NH_3 which has larger absorption heat compared to that of propane.



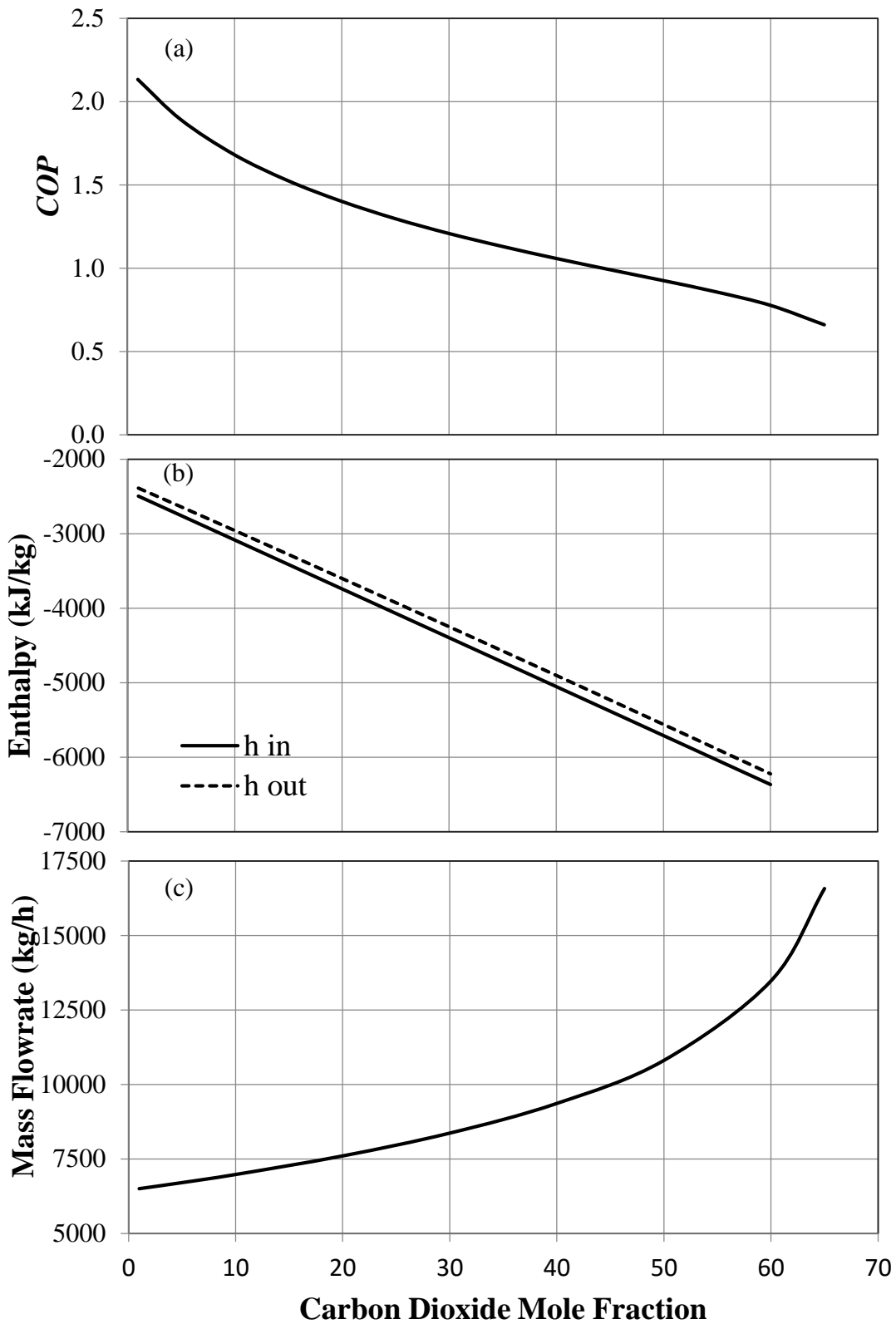
(i) Figure A-3: NH₃-Propane mixture as a function of the NH₃ mole fraction (a) COP curve; (b) Inlet and outlet enthalpy of the compressor; (c) mass flowrate

Refrigeration cycle with SO₂-propane mixed refrigerant - The overall *COP* change of the SO₂-propane mixture as a function of SO₂ mole fraction is shown in Figure A-1 (a). The added sulfur dioxide in the HYSYS analysis ranges between 1% to 100% compositions. The *COP* of the sulfur dioxide-propane mixture shows an increasing trend for the mole fraction up to 15%. This increase is due to the combination of a small increase in the difference between the compressor's inlet and outlet enthalpies, from 106 kJ/kg at 0% sulfur dioxide to 123 kJ/kg at 100% sulfur dioxide (See Figure A-1 (b)), with the fast mass flowrate decrease, from 6454 kg/h at 0% sulfur dioxide to 4808 kg/h at 100% sulfur dioxide (See Figure A-1 (c)). Similar to ammonia, the density of pure sulfur dioxide at the given temperature and pressure (2.46 kg/m³) is lower than that of pure propane (6.48 kg/m³). Thus, adding SO₂ to the propane refrigerant reduces the mass flowrate required to absorb the heat defined in Section 3. On the other hand, the change in the enthalpy depends on the *T-s* and *P-v* diagrams of the blended refrigerants. For the mole fraction values between 15% and 80%, however, the *COP* of the cycle decreases. One possible reason for the sudden drop in the *COP* could be related to the high polarity of SO₂ as opposed to non-polar propane (similar to ammonia). After the mole fraction of 80%, the *COP* of the cycle increases which shows the dominant effect of SO₂ which has larger absorption heat compared to that of propane. A special attention is required when using SO₂ as it being corrosive. Therefore, stainless steel pipes would be required in the refrigeration cycle.



(ii) Figure A-4: SO₂-Propane mixture as a function of the SO₂ mole fraction (a) COP curve; (b) Inlet and outlet enthalpy of the compressor; (c) mass flowrate

Refrigeration cycle with CO₂-propane mixed refrigerant – CO₂ is safe to store and available in large quantities in the environment. The overall *COP* change of the CO₂-propane mixture as a function of CO₂ mole fraction is shown in Figure A-1 (a). The added carbon dioxide in the HYSYS analysis ranges between 1% to 66% mole fractions. Exceeding the 66% mole fraction will cause the CO₂ to reach its critical temperature, preventing it to liquefy in the condenser. The *COP* of the carbon dioxide-propane mixture shows a decreasing trend for all mole fractions. This decrease is due to the combination of a small increase in the difference between the compressor's inlet and outlet enthalpies, from 106 kJ/kg at 0% carbon dioxide to 137 kJ/kg at 65% carbon dioxide (See Figure A-1 (b)), with a large increase in the mass flowrate, from 6454 kg/h at 0% carbon dioxide to 16576 kg/h at 65% carbon dioxide (See Figure A-1 (c)). In essence, the density of 66% carbon dioxide at the given temperature and pressure (18.74 kg/m³) is higher than that of pure propane (6.48 kg/m³). Therefore, adding CO₂ to the propane refrigerant increases the mass flowrate required to absorb the heat.



(iii) Figure 0: CO₂-Propane Propane mixture as a function of the CO₂ mole fraction (a) *COP* curve; (b) Inlet and outlet enthalpy of the compressor; (c)

mass flowrate

A.5. Cost analysis

To evaluate the feasibility of the proposed study, the prices of each gas in addition to the operational cost savings are compared. The cost of ammonia would range between \$1500-\$2000 USD per ton. Whereas, the cost of sulfur dioxide would range between \$1600-\$4800 USD per ton. A suitable material for the ammonia-propane and sulfur dioxide-propane mixtures would be SS304 stainless steel [113]. Carbon steel material price would cost around \$529 USD/ton [114], whereas stainless steel would cost around \$2590 USD/ton. Assuming each refrigeration cycle would require 100 tons of steel, the overall capital cost addition due to the replacement of carbon steel with stainless steel would be around \$206,000 USD. Additionally, a typical LNG plant capital cost would be around \$1400 USD per tonnes per annum (tpa) [115]. Therefore, the 7% and 9% operating cost savings from the addition of ammonia and sulfur dioxide per the plant life span would be around \$98 USD per tonnes per annum and \$126 USD per tonnes per annum, respectively. Since the refrigerant price is minimal compared to the material replacement cost, the proposed study would provide overall savings of around \$6,750,000 USD and \$8,750,000 USD (i.e. for a plant producing 71,000 tonnes per annum of natural gas).

A.6. Emerging technologies

There are several studies proposing emerging technologies for enhancing the efficiency of the liquefaction or re-gasification processes. Three of these emerging technologies are introduced here.

A.6.1. Solar power

Rao et al. [116] suggested an LNG re-gasification process which includes the utilization of solar power in the Rankine cycle to increase its power generation efficiency. The cold energy in the solar-based Rankine cycle is essentially from the cryogenic energy of LNG.

In this cycle, the working fluid (which could be N₂, CO₂, or hydrocarbons) is first compressed from a saturated-liquid state to a sub-cooled liquid state (State 2). The working fluid then exchanges its cold energy with the hot fluid entering the regenerator from the turbine (reaching State 2a). The addition of the solar heat to the flow transforms the working fluid to saturated or superheated vapor (State 3) after which it produces power in the turbine. Then, it goes back to the regenerator to cool down (State 4a), and then it is transferred to the saturated liquid state in the condenser which obtains its cold energy from the LNG process. Rao et al. [116] showed that the solar-LNG combined cycle enhances the efficiency by approximately 22% and the exergy by 10.62% compared to the efficiency and exergy of each system used separately.

A.6.2. Thermoacoustic

Wollan et al. [117] in collaboration with Praxair and Los Alamos National Laboratory suggested a new technology where thermo-acoustic heat engines and refrigerators are used. Helium is used as the working fluid in a tube oscillating back and forth due to the movement of a piston. Helium enters the hot reservoir, where it exchanges heat with a porous-plug regenerator. Then, it comes out with low temperature but still high pressure. Its pressure reduces as the helium particles expand due to the piston movement, reducing further the particles temperature. In essence, this technology uses a thermo-acoustic Stirling heat engine to convert heat energy to acoustic energy with high amplitude. Orifice pulse tube refrigerators convert the high amplitude oscillating wave into refrigeration energy, cooling down helium to -240 °C. Despite the fact that this technology has been first proposed in the 1980's, it can still be considered as an emerging technology in the natural gas liquefaction processes. Wollan et al. [117] have claimed that this new technology is the only technology that can benefit from the cryogenic energy with no moving parts. They

have already developed prototypes producing 500 gallons/day. Improvements have been made to increase this capacity to 20000 gallons/day.

A.6.3. Natural gas solidification

Due to the exponentially increasing demand for the natural gas, there are a prodigious number of attempts made towards implementing efficient storing methods such as liquefaction for storing a larger amount of natural gas compared to its alternatives like compressed gas. Another efficient storing method, which potentially could have higher storage capacity than liquefaction, is natural gas solidification (referred to as natural gas hydrates) which occurs naturally in cold areas (such as those in the Arctic and Antarctica). Several studies have been conducted to understand and control hydrates formation which contains natural gas and water frost. However, there are challenges associated with the hydrates, slowing down research and technology development in this area. The major issue is related to limitation in extraction of this type of natural gas due to i) their hostile environments (such as deep oceans and regions where seawater is at very low temperatures), and ii) the dispersion of the hydrates in large areas, making the extraction and recovering process difficult. Due to these challenges, there has been general lack of interests towards the hydrates technology (for storage and transportation). If these challenges are overcome, the hydrates have potential to meet the global large demands for the natural gas. A recent estimation has indicated that hydrates are available in approximately 20,000 trillion cubic meters which exceeds the global energy potential of oil, natural gas and coal combined [118].

Natural gas can be obtained from the hydrates by three suggested procedures. The first procedure is by heating and hence defrosting the hydrates using hot seawater, steam, electromagnetic radiation or electricity. The second procedure is melting the hydrates by lowering their pressure. The third suggested procedure is by injecting chemical inhibitors

used for melting the hydrates. All of the suggested procedures melt the hydrates, causing the natural gas to be released. Abdalla and Abdullatef [119] suggested that the natural gas be hydrated and solidified to enhance its storage and transportation capabilities. In this study, water is used as the carrier of the natural gas, and seawater is fed as the cooling agent in the refrigeration cycle. In this cycle, the natural gas is mixed with water where it is first cooled down by the second stage evaporator. The mixture is then separated and water is re-fed to the natural gas container, and the hydrates are sent to a dryer. Then, the hydrates are cooled down by the first stage evaporator causing the hydrate to freeze and then sent to the storage. Abdalla and Abdullatef [119] also investigated the production rates, storage and transportation from the production phase to the end consumer's stage. They suggested that the natural gas hydrates need larger transportation ships due to their larger weight compared to LNG.

Technical advances are the key points in determining the production cost of the natural gas. A lower production cost would make it viable for governments to sell natural gas at competitive prices and to compete with leading countries such as Qatar. Shale gas is one of those examples; before 2015, North America was not involved in exporting natural gas. Due to technical advances in the natural gas processing (mentioned above), North America is now expected to increase its exporting capacity between 2015 and 2019. To have a better understanding of the importance of all these technological advances on natural gas production, processes and exportation, a small-scale market analysis is presented in the following sections. An example showing the impacts of the advances on the global market of natural gas is given here: for instance, the increase in North American natural gas market was mainly due to the introduction of horizontal drilling [120]. Horizontal drilling has provided a significant opportunity for North American countries in extracting natural gas from difficult surfaces such as reservoirs located under the sea near the shores and

reservoirs located under the Rockies Mountains [120]. Another reason explaining why the countries in North America joined the market later than other regions is related to the financial situation occurred in 2007: in essence, the National Petroleum Council in North America estimated that production companies must invest \$4.3 trillion in capital between 2005 and 2030 in order to keep up with the demand growth [120]. This financial burden delayed the North American natural gas market due to the significant investment required for natural gas production [120].

Appendix B: Current and future markets of natural gas*

The market of the natural gas has increased dramatically in the past decade. The liquefied natural gas importing plants has increased from 10 in the year 2000, to 22 in the year 2009, to 73 in the year 2013 [121]. In addition to importers, exporters of the liquefied natural gas have increased by 77.3% from 2000 to 2009 [121]. New markets have emerged in North America including Mexico in 2007 which was followed by Canada in 2009. Other emerging markets in the world include those in Europe, Middle East, Central and Southern America, Asia Pacific and Africa. According to the International Energy Agency's New Policies Scenario, it is expected that LNG trade will globally increase from 23.5 BCFPD (billion cubic foot per day) (i.e., 665.285 billion liters per day) to 48.4 BCFPD (1370.2 billion liters per day) between 2008 and 2035 [151]. In the following sections, the natural gas markets for LNG re-gasification (import) and liquefaction (export) are explained in detail. The data presented for LNG regasification is in the timeframe of 2009 to 2012; whereas, the liquefaction market data are presented from 2009 to 2019 showing the future capacities and projecting the competitiveness of this market.

Figure A-1 (a) and (b) show the global re-gasification capacities in terms of BCFPD and percentage by regions, respectively. It is expected that once the re-gasification projects that are under construction become operational by the year 2015, an additional 16.3 BCFPD (461.45 billion liters per day) will be added to the existing LNG regasification capacity in the combined regions of North America, Central/South America, Europe/Eurasia and Asia Pacific since 2010 [121]. The global re-gasification capacity is expected to reach around 127 BCFPD (3595.3 billion liters per day) by 2027 [121]. In 2012, Asia Pacific has been accounted for 70% of the global regasification capacity (see Figure A-1 (b)). It has been speculated that the Asia Pacific and Europe/Eurasia regions will be considered the largest

LNG importing regions accounting for 45% (56.7 BCFPD (1605.2 billion liters per day)) and 32% (40.5 BCFPD (1146.55 billion liters per day)) of the global re-gasification capacity, respectively, by 2030 [121].

Figure A-1 (a) and (b) show the global liquefaction capacities in terms of BCFPD and percentage by regions, respectively. In 2013, Middle East has been accounted for 34% of the global liquefaction capacity (14 BCFPD (396.34 billion liters per day)). New plans for increasing liquefaction capacities are under construction. It is expected that the Asia Pacific region will be overtaking the Middle East export market in the global liquefaction capacity by 2019 during which Asia Pacific will be accounted for 33% of the global liquefaction capacity (see Figure A-1 (a)), increasing its liquefaction capacity from 12 BCFPD (339.72 billion liters per day) in 2013 to 27 BCFPD (764.37 billion liters per day) in 2019 (see Figure A-1 (b)). The global liquefaction capacity of the natural gas is speculated to reach 70.8 BCFPD (2004.348 billion liters per day) by 2028 [121]. By then, Middle East, Africa and Asia Pacific regions are expected to be the largest LNG exporters accounting for 75.6% of the total natural gas liquefaction capacity. Europe/Eurasia and Central/South America are speculated to have LNG export capacities of 5.8 BCFPD (164.198 billion liters per day) and 4.5 BCFPD (127.395 billion liters per day), respectively. The North American region is expected to be able to provide 7.2 BCFPD (203.832 billion liters per day) if new natural gas export plans from Canada and US move forward.

B.1. North America

Regasification Capacity – this region is mainly an importer of the natural gas from major natural gas suppliers. The number of the proposed projects for LNG import plants (i.e., regasification plants) in North America continuously increases and has reached 40 projects. Global issues in LNG production, however, have caused the global LNG output to be below panel capacities, affecting North America significantly. During the 2009 recession, the

overall demand and consumption of the natural gas decreased dramatically in North America except for power production plants. Analysts have speculated that importing unwanted LNG to North America has harmed the natural gas industry in this region by reducing the natural gas price to \$3.00/MCF. Also, the larger demands from Asian have limited the flow of the LNG imports towards North America.

The North America's historical regasification capacities of LNG are shown in Figure A-1 (a). In 2009, LNG re-gasification terminals in North America had a combined capacity of 1.8 BCFPD (50.958 billion liters per day) from total of 14 re-gasification plants for which 11 plants are in US which account for 68.9% of North America's total re-gasification capacity (see Figure A-1 (a)). It is expected that by the year 2030, the total Natural Gas consumption reaches 92.8 BCFPD (2627.168 billion liters per day) [121]. This consumption would be satisfied with the new natural gas fields that North America has invested for exploration.

Liquefaction Capacity – the LNG production has occurred in North America due to several technological advances in shale gas extraction and the horizontal drilling. These advances have increased the growth of the liquid natural gas production capacity in North America. Figure A-1 (b) shows the liquefaction capacity of North America between the years of 2011 and 2019. It is speculated that the total volume of liquid natural gas production in North America will reach 2.8 BCFPD (79.268 billion liters per day) in 2015 [121]. In 2019, the total volume of natural gas produced in Canada and US is expected to be 15.16 BCFPD (429.1796 billion liters per day). All of the new plans are aiming in reducing North America's dependency on the global natural gas. Also, the locations of these plants have made this region a secure alternative for LNG export (compared to unstable political situations in North Africa and the Middle East). LNG buyers such as South Korea and China have shown interests in investing in North American's shale gas. One of the

examples of shale gas extraction sites including a liquefaction facility will be constructed on the west coast of British Columbia, Canada. In addition to conventional gas extraction techniques, more attention is being given to new technologies for shale gas extraction [121]. For example, hydraulic fracturing is one technique which requires enhancement to reduce the environmental impact while extracting shale gas [121].

B.2. Central/South America

Regasification Capacity – Puerto Rico began importing LNG in the year 2000. After this period, plants for the LNG imports have increased steadily in Central/South America. The rate of increase in the LNG re-gasification plants (including the proposed ones) has reached 787 % which is much more than 250% regional demand increase. This increase in natural gas production would be a major cause for the natural gas production surplus.

The regasification capacity of Central/South America Countries is shown in Figure A-1 (a). The regasification capacities of Argentine, Brazil, and Chile are increasing over the years. The combined regional regasification capacity of the South/Central America is 1.2 BCFPD (33.972 billion liters per day) in 2012 as compared to 0.22 BCFPD (6.2282 billion liters per day) in 2009. In 2012, Argentine represents 41% of the region's regasification capacity followed by Chile representing 33%.

Liquefaction Capacity – liquefaction plants in this region are located in Trinidad and Tobago, and Peru. The combined liquefaction capacity of these two nations has reached 2.78 BCFPD (78.7018 billion liters per day) in 2011 (see Figure A-1 (b)). Part of this capacity is exported to regional regasification facilities in Puerto Rico and Chile, and the rest is supplied to European and North American markets. In 2019, it is expected that the region's combined liquefaction capacity reaches 3.5 BCFPD (99.085 billion liters per day).

B.3. Europe and Eurasia

Regasification Capacity – Europe/Eurasia is considered the second largest LNG importer in the world. Their regasification capacity has reached 29% of the global LNG market in 2010. In 2012, the combined regasification capacity of Europe/Eurasia has reached 6.6 BCFPD (186.846 billion liters per day) after the addition of one plant in France, two plants in Italy, and two plants in England.

The European LNG regasification capacities between 2009 and 2012 are shown in Figure A-1 (a). Spain is ranked first with its regasification capacity of 2.1 BCFPD (59.451 billion liters per day) in 2012: Spain alone has had an equivalent LNG import of 31.8% of the total European market. After Spain, UK has had a regasification capacity of 1.3 BCFPD (36.803 billion liters per day) in 2012. On the contrary, Greece has had zero regasification capacity in 2012 as they are more dependent on oil and coal for their energy source. Other nations such as France, Turkey, Portugal, Italy and Belgium have had a combined importing amount of 3.2 BCFPD (90.592 billion liters per day) in 2012.

Liquefaction Capacity – In 2007, the European region started its LNG export due to inception of the Norway's Shnovit facility exporting 0.6 BCFPD (16.986 billion liters per day) of LNG. Its main market is North America, Europe and to some extent some parts of Asia. Further, Russia doubled the Eurasian liquefaction capacity in 2009 by its plant called Sakhalin II supplying LNG to Japan, South Korea and India. The European/Eurasian projection of the LNG liquefaction capacity between 2011 and 2019 is shown in Figure A-1 (b). Russia is aiming to be one of the largest global LNG exporters by 2019 reaching a capacity of 5.3 BCFPD (150.043 billion liters per day).

B.4. Middle East

Regasification Capacity – Middle East region has seen an increase in oil prices in the past decade. As a result, local policies have imposed limitations on the use of oil, favoring the

use of the natural gas and increasing the oil exports. As a result, the LNG market has experienced a 4.4% increase each year in the past decade. It has been estimated that the demand growth in Middle East's natural gas will be accounted for 20% of the global natural gas demand by the year of 2035 [121].

The Middle East regasification capacity is shown in Figure A-1 (a). Kuwait became the first nation to import LNG in 2009 due to its insufficient natural gas supply. Followed by Kuwait, Dubai started importing LNG in 2010, and it has been transformed to an international center for re-gasification and transportation through pipelines to Northern Emirates. By 2012, the Middle East's regasification capacity has reached 0.4 BCFPD (11.324 billion liters per day).

Liquefaction Capacity – between the years of 2005 and 2010, the Middle East region has seen a significant growth in liquefaction processes and LNG exports [121]. The LNG export's capacity has increased by 140%. Qatar is considered to be the largest LNG exporter in the region: out of the total LNG capacity of 13.9 BCFPD (393.509 billion liters per day) in Middle East, Qatar has the capacity of 10.8 BCFPD (305.748 billion liters per day) (see Figure A-1 (b)). Iran, Iraq, UAE and Oman follow Qatar in their LNG export rankings. These nations have major supply contracts with Europe. It has been speculated that Middle East will be overtaken by the Asia Pacific region in the LNG exports by 2017 [121]. This surpass is due to the large number of proposed LNG projects in Australia.

B.5. Asia Pacific

Regasification Capacity – Japan and South Korea are considered to be the largest LNG importing nations in the world. Having the re-gasification capacities of 10.3 BCFPD (291.593 billion liters per day) and 4.7 BCFPD (133.057 billion liters per day) in 2011, respectively, the combined LNG demand in both nations has reached 15 BCFPD (424.65 billion liters per day) (see Figure A-1 (a)). After the Tsunami and earth quake that struck

Japan in 2011, nuclear plants were fully or partially out of operation, increasing the nation's natural gas demand by 1.3 BCFPD (36.803 billion liters per day). Followed by Japan and South Korea, China is aiming to increase its demand for natural gas consumption to 10% of its total energy consumption by the year of 2030 [121]. In 2012, China LNG regasification capacity rate was among the top four in its region reaching 1.9 BCFPD (53.789 billion liters per day) (Taiwan's and India's LNG regasification capacities are 1.6 BCFPD (45.296 billion liters per day) and 2 BCFPD (56.62 billion liters per day), respectively). China and India are planning to construct new regasification plants in order to meet their high demands. Their goal is to reach a capacity of 4.1 BCFPD (116.071 billion liters per day) and 3.1 BCFPD (87.761 billion liters per day), respectively. It has been estimated that China's demand will increase by 20% of the whole region's demand by the year of 2035 [121]. This demand will be met by local natural gas reserves and imports from Turkmenistan (the neighbor country). The total Asia Pacific natural gas demand is 40.8 BCFPD (1155.048 billion liters per day), which will be met by constructing 8 regasification facilities in the Asia Pacific's region.

Liquefaction Capacity – the Asia Pacific region is planning to have the largest global liquefaction capacity with the new exporting facilities being built in Australia and Papua New Guinea in near future. By 2019, the total liquefaction capacity of this region will reach 27.08 BCFPD (766.6348 billion liters per day) [121] (see Figure A-1 (b)). Almost all the produced liquefied natural gas in the region will be exported within the same region. LNG markets in China, India, Japan, and South Korea as well as new markets in Singapore, Malaysia and Indonesia are expected to reach 12.8 BCFPD (362.368 billion liters per day) by 2017 [121].

B.6. Africa

Regasification Capacity – in 2009, Africa's natural gas consumption was approximately 9.1 BCFPD (257.621 billion liters per day). By 2030, it is expected that the African demand be doubled to 19.9 BCFPD (563.369 billion liters per day). Although the regional production is estimated to increase to 48.1 BCFPD (1361.711 billion liters per day) by 2030, there is no plan for regasification plants in this region [121].

Liquefaction Capacity – Libya was the first LNG exporter in Africa with a capacity of 0.4 BCFPD (11.324 billion liters per day) in 1970. By 2011, new plants were constructed in Algeria, Egypt, Equatorial Guinea and Nigeria. This has increased the region's export capacity to 8.59 BCFPD (243.1829 billion liters per day). Current projects have increased the region's capacity to 10.2 BCFPD (288.762 billion liters per day) by the year 2014.

Africa's liquefaction capacity is shown in Figure A-1. In 2011, the top three African countries in the LNG exports were Algeria, Nigeria and Egypt having a combined 90% of the regions exports. By 2017, Nigeria's LNG liquefaction capacities are expected to reach 8.83 BCFPD (249.9773 billion liters per day) accounting for 50% of the region's liquefaction capacity.

There is no doubt that newer technology aims at reducing the production and maintenance cost of natural gas. Energy saving is a key point in current R&D sectors. The natural gas market is directly related to that of the petroleum market. Although it is very difficult to speculate the future trend of the market, political and future emerging technologies would play major roles in determining different regions' exportation capacity. Moreover, the Paris UN Climate Change Conference held in December of 2015 represented a historic opportunity for the world to meet the world's climate change challenges [1]. The outcomes discussed in the conference will be legally bound by April 2017 if all 55 countries that are responsible for global emission sign the agreement before the end of 2015 [1]. According

to Martinelli [122] the world generates more than 40% of its electricity from coal, and as being ranked as the top CO₂ emitter in the course of burning, coal must be replaced by a cleaner source of energy. Natural gas and nuclear energy will play major roles in power sources until the renewable energy sources accepted by environmentalists become cost effective with high efficiency. Since nuclear energy has waste hazards, the natural gas will be the top ranked option as an energy source for at least few decades [122]. It is also speculated that new future avenues due to the increasing demand in natural gas will boost up the natural gas prices and LNG exports [121].

B.7. Natural gas costs/prices

Despite the fact that LNG prices are set by the international trade, the LNG processes vary widely between countries around the world. For this reason, the transportation cost is different in various regions in the world [123]. For instance, the average gas price in Japan has been \$16/MMBtu (\$16/293 kWh), in US is \$3/MMBtu (\$3/293 kWh), and in Europe is \$9/MMBtu (\$9/293 kWh) in the year 2012. In the case of North America, there has been a large interest in the shale gas which has decreased the natural gas price. Also, the limitation for LNG export made the North America's gas price isolated from the world.

There is a theory suggesting that the gas prices around the world are related to the transportation cost. However, there are exceptions that do not follow this theory. GIIGNL (The International Group of Liquefied Natural Gas Importers) [124] studied the market and price of LNG export to Japan and UK. They presented a graph comparing the relationship between the transport cost and the gas price (see Figure A-1). The export cost to Japan is \$10/MMBtu (\$10/293 kWh) higher than that to UK although the transport cost to each of these regions are almost the same. A similar pattern is observed in the Peru's gas export sales to Asia and Europe. It is observed that the price of the gas exported to Asia is approximately \$2-3.5/MMBtu (\$2-3.5/293 kWh) higher than that to Europe. Ritz [123]

suggested that the differences in the market prices are due to the market power. For example, the Fukushima incident that effectively switched off large parts of the nuclear plants in Japan led to a sudden increase demand in the natural gas in Japan compared to UK (reaching up to 63% in Japan compared to 33% in UK). In essence, the more the demand the higher the price.

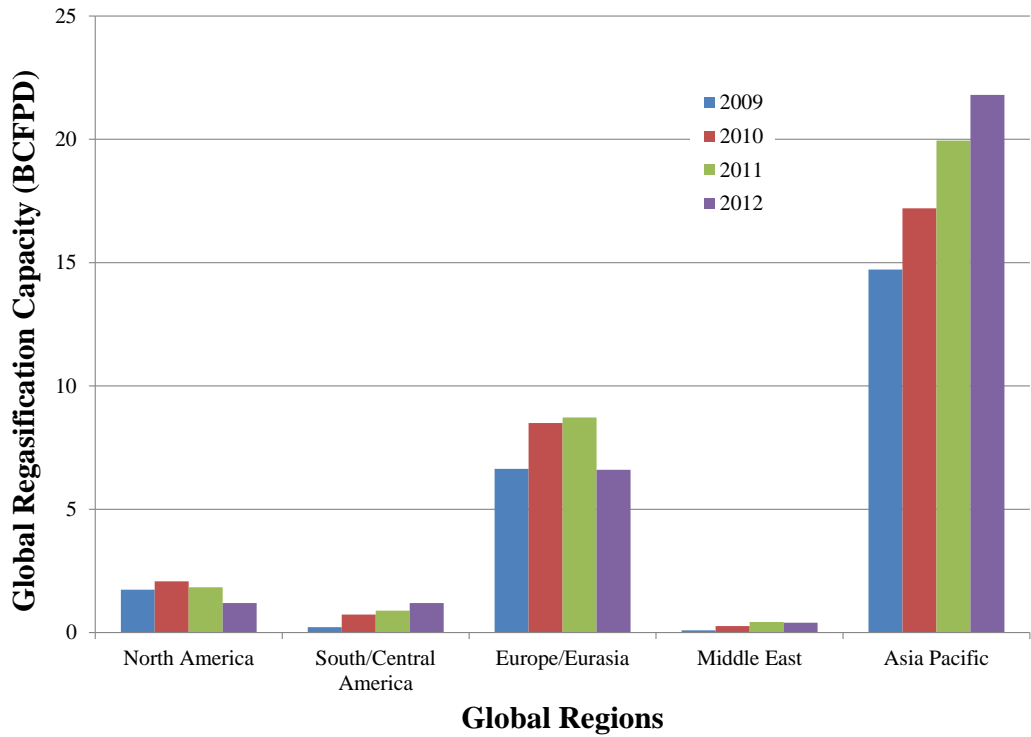
B.8. Major factors affecting NG prices

According to the US Energy Information Administration [125], natural gas prices across different countries are highly dependent on the supply and demand. The changes in the supply and demand over a short period of time often may result in a large price change. From the supply aspect, the amount of natural gas production, overall imports, and the level of available storage determine the overall price. When the supply increases, the prices tend to go down. From the demand aspect, the weather conditions (summer vs. winter), economic conditions of the market, and the petroleum prices (as a substitute for the natural gas) determine the price.

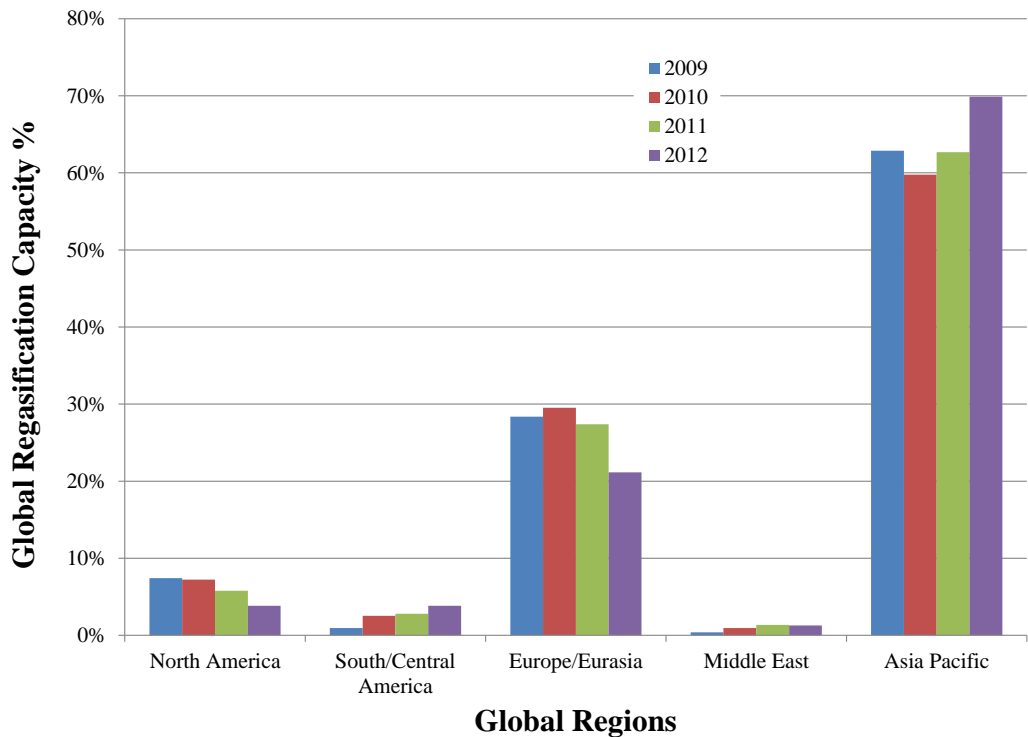
B.9. Cost of oil and gas production

Production costs (total upstream costs) include lifting and finding costs. The lifting costs are those related to operating and maintaining the oil and gas wells and the equipment and facilities used to extract oil and gas. Finding costs are the costs related to exploration and development of the well and additional costs compensating for leasing or purchasing properties.

Table B-1 illustrates the average costs (in US dollars per barrel, each barrel contains 5,618 cubic feet (159045.58 liters) of natural gas) for producing the crude oil and natural gas in different regions for the years of 2007, 2008 and 2009 [125].

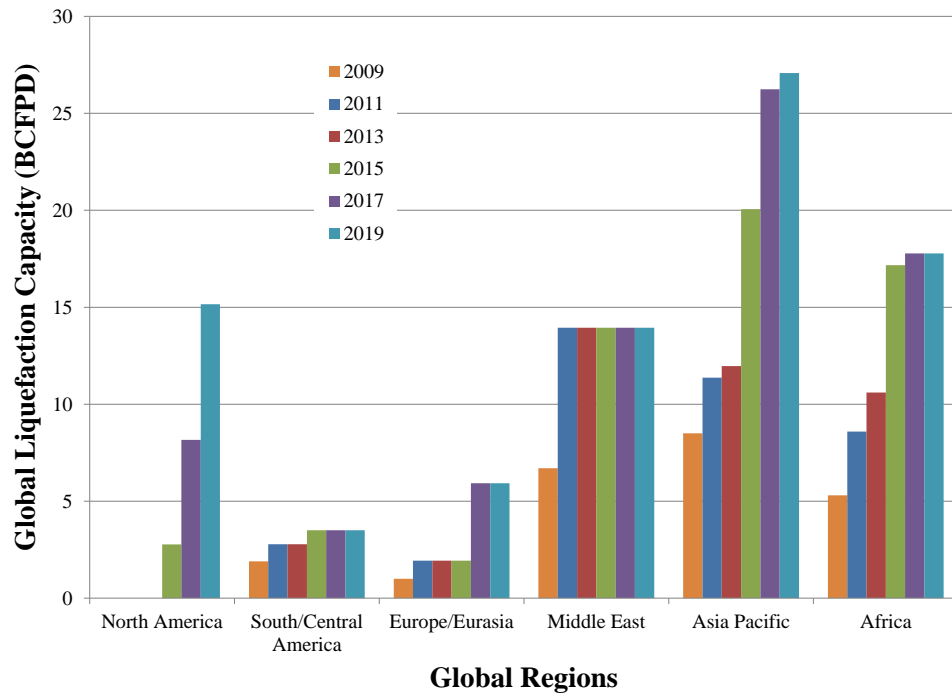


(a)

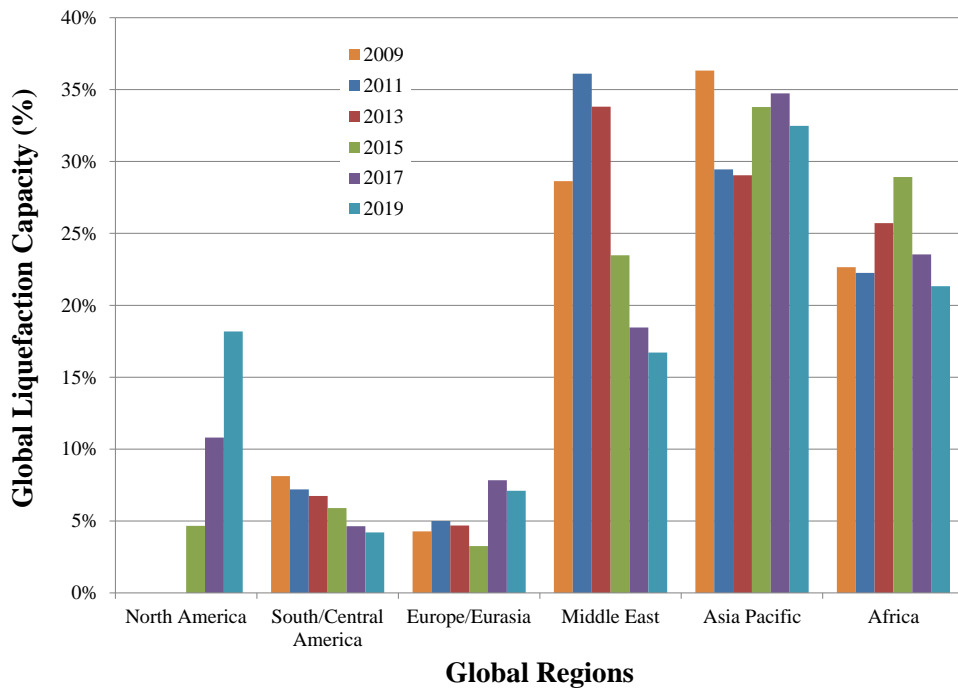


(b)

Figure B-1: (a) Global LNG regasification capacity, and (b) Global LNG regasification capacity percentage



(a)



(b)

Figure B-2: (a) Global LNG liquefaction capacity, and (b) Global LNG liquefaction capacity percentage

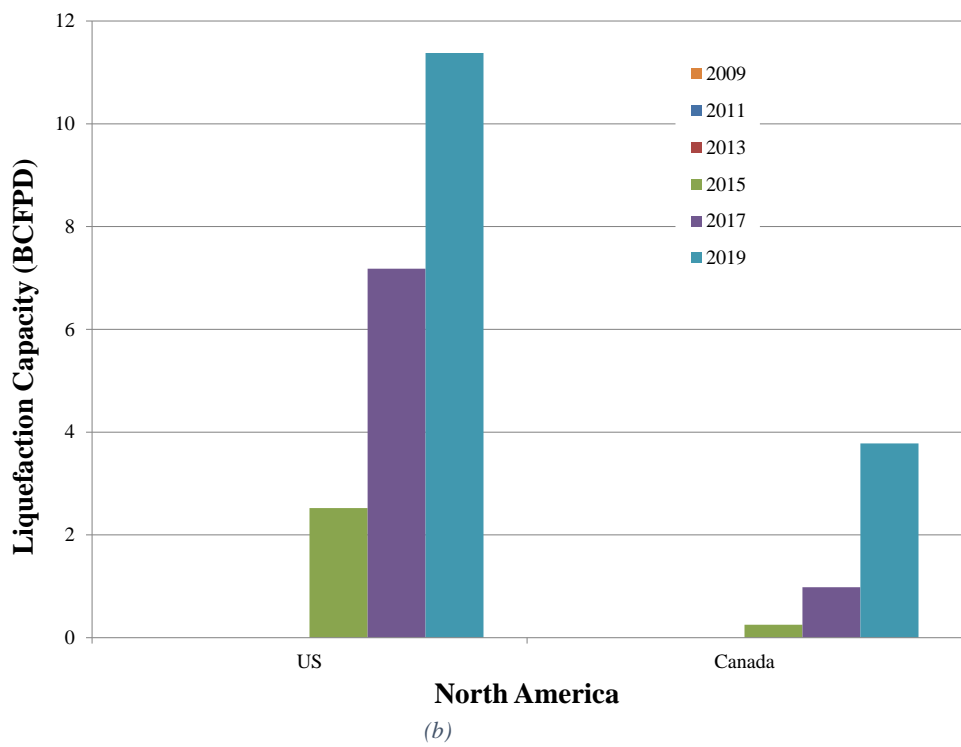
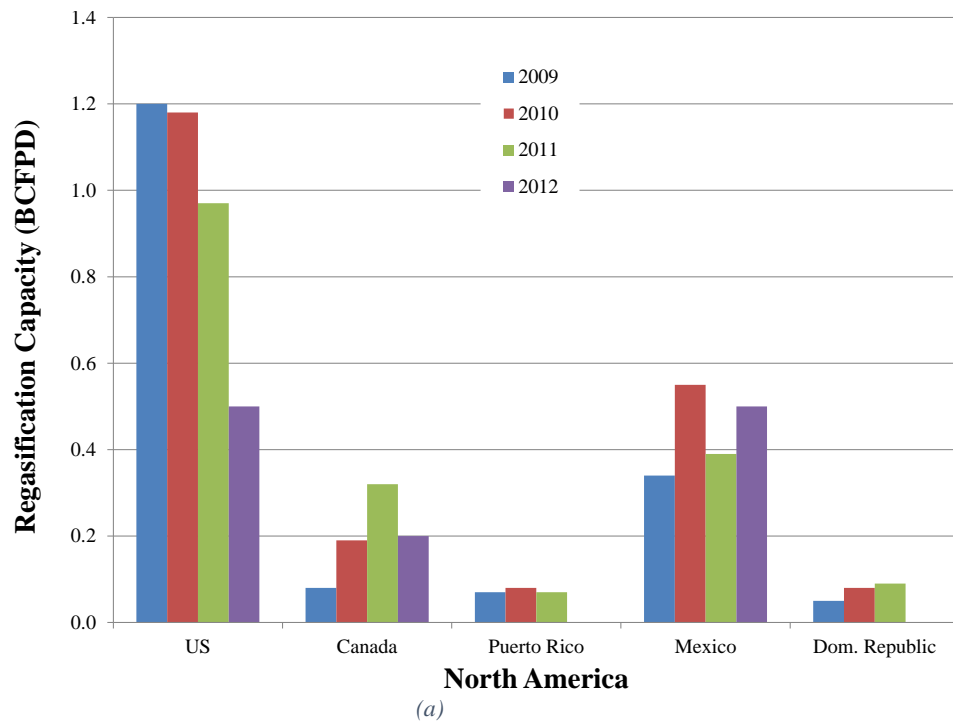
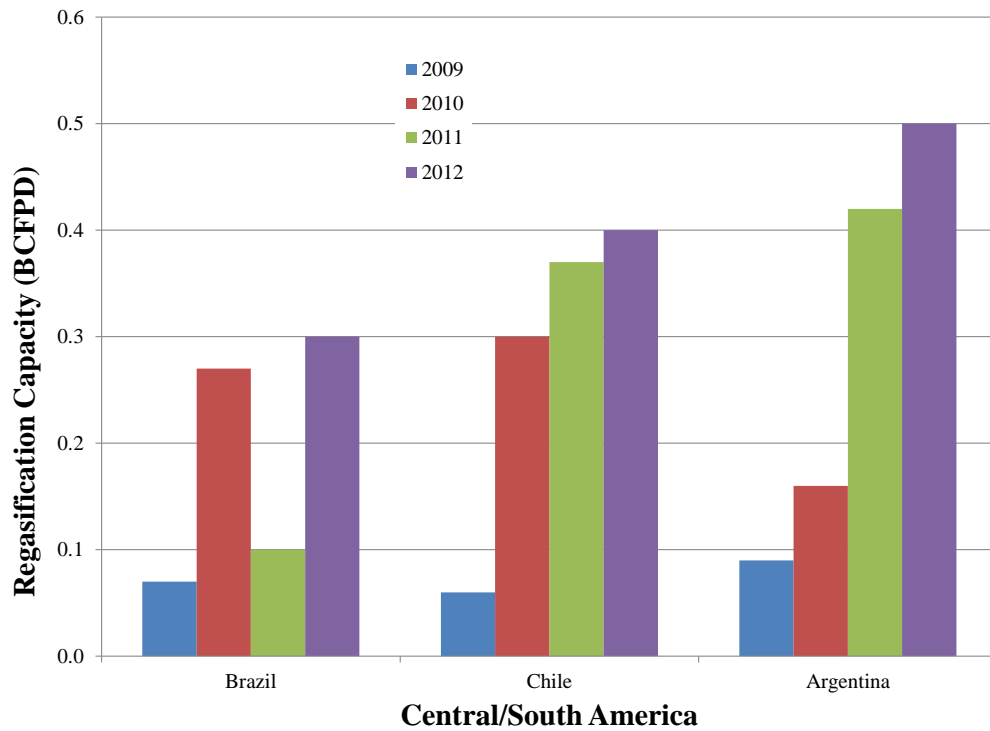
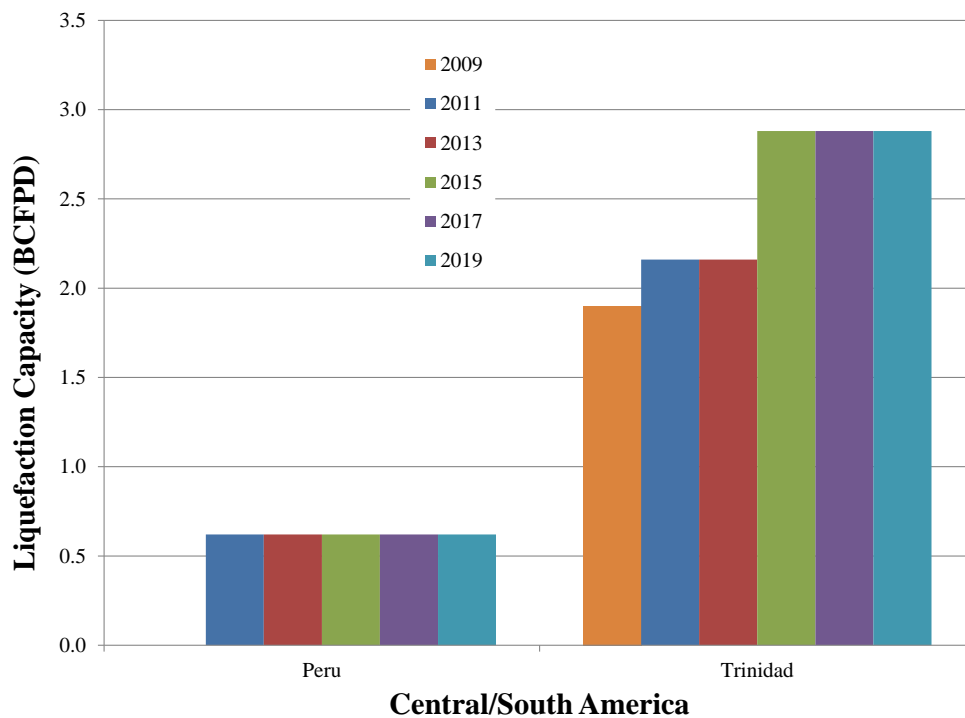


Figure B-3: North America (a) regasification capacity (2009-2012), and (b) liquefaction capacity (2011-2019)

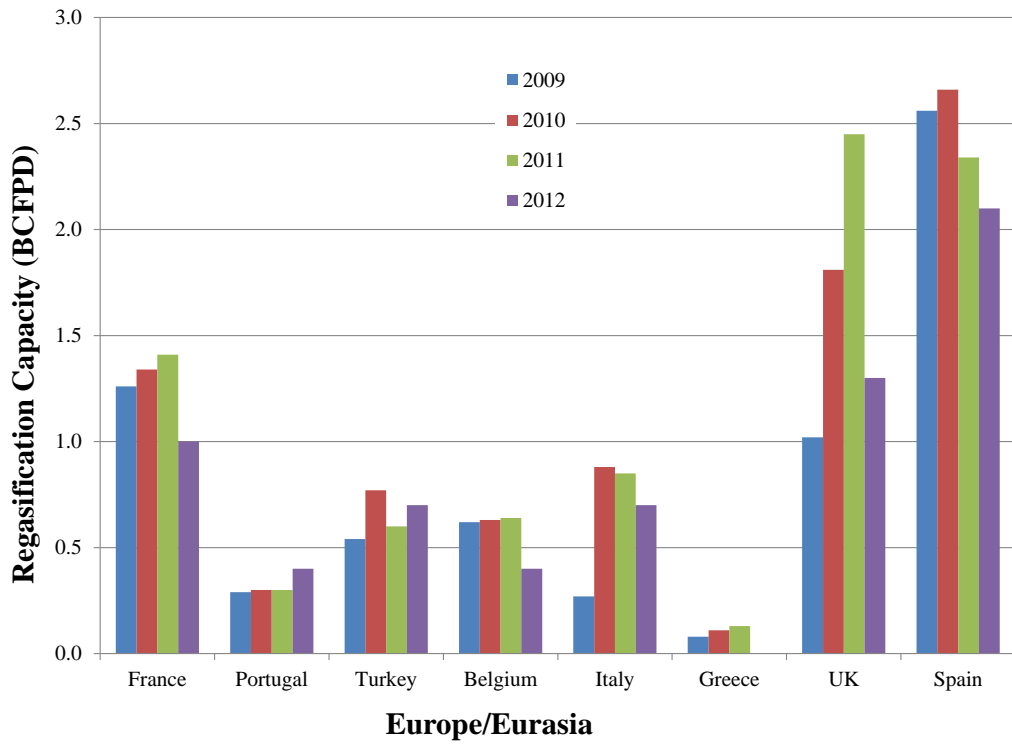


(a)

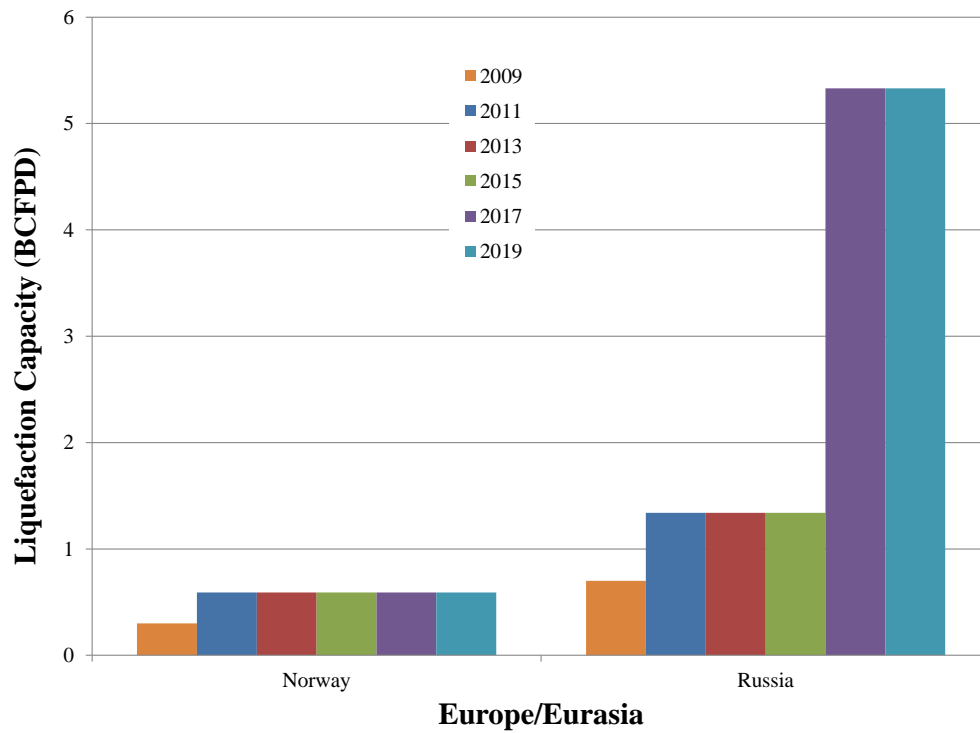


(b)

Figure B-4: Central/South America (a) regasification capacity (2009-2012), and (b) liquefaction capacity (2011-2019)

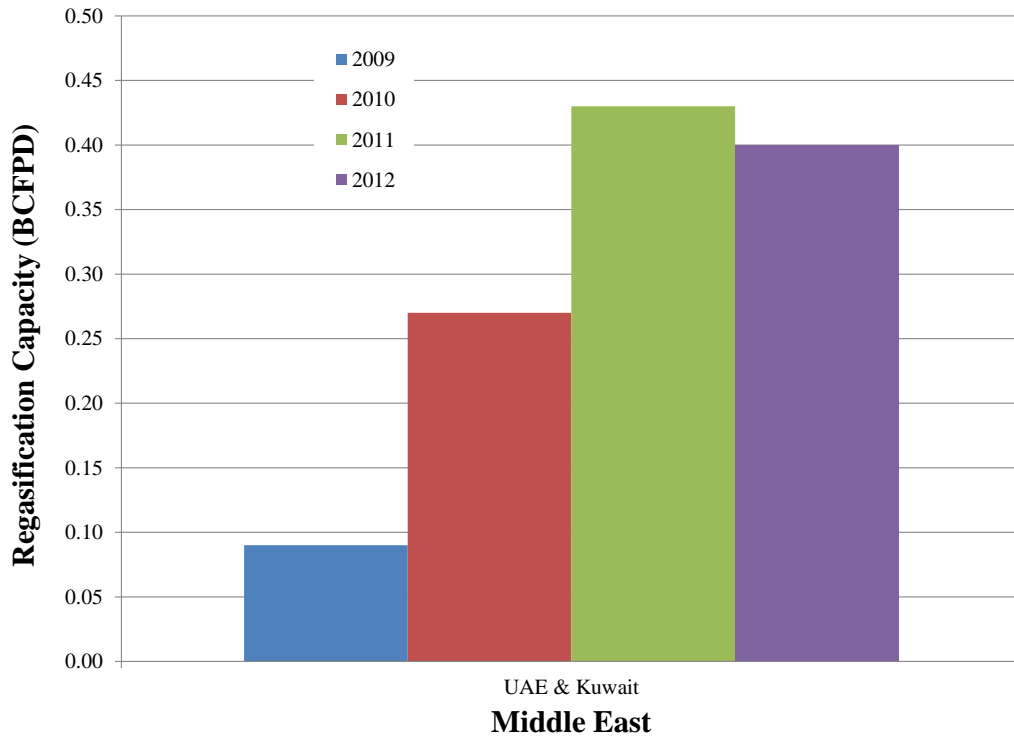


(a)

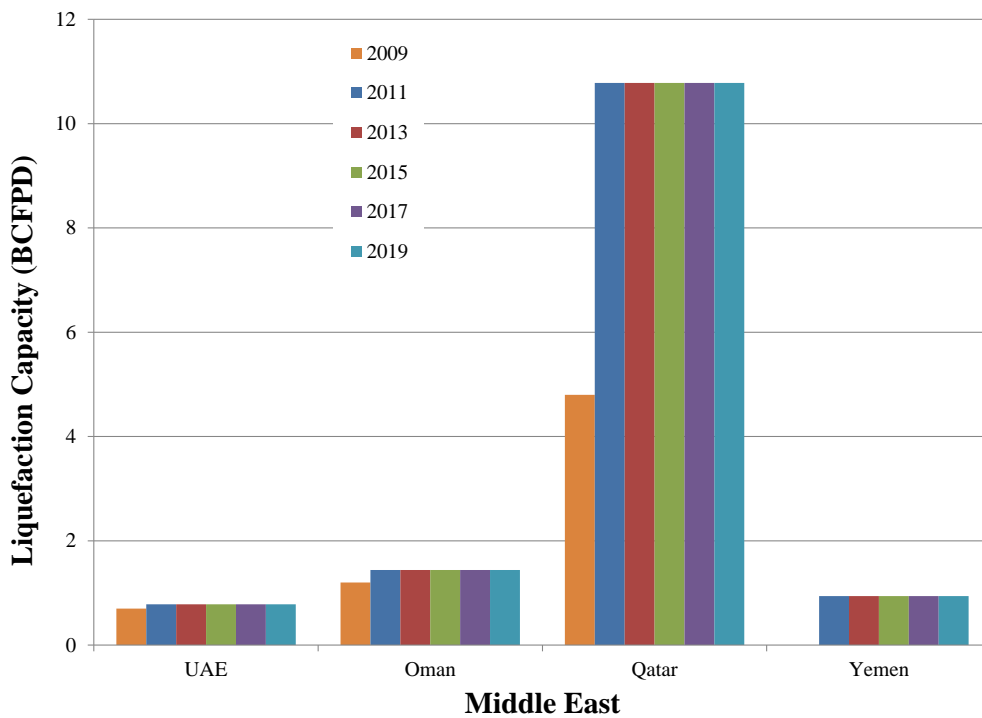


(b)

Figure B-5: Europe/Eurasia (a) regasification capacity (2009-2012), and (b) liquefaction capacity (2011-2019)

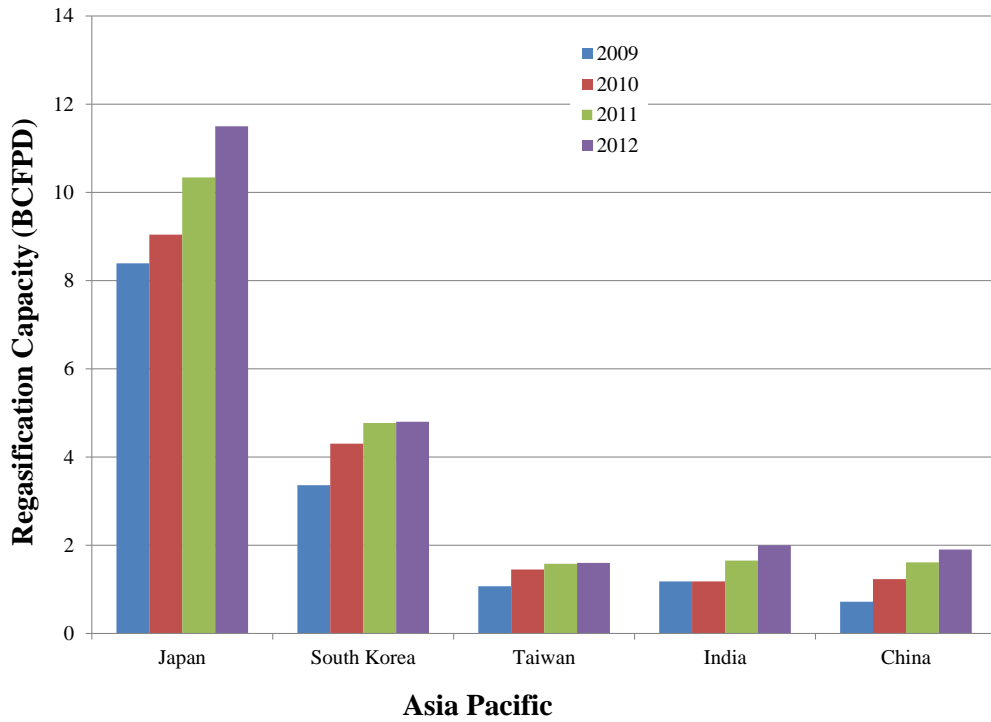


(a)

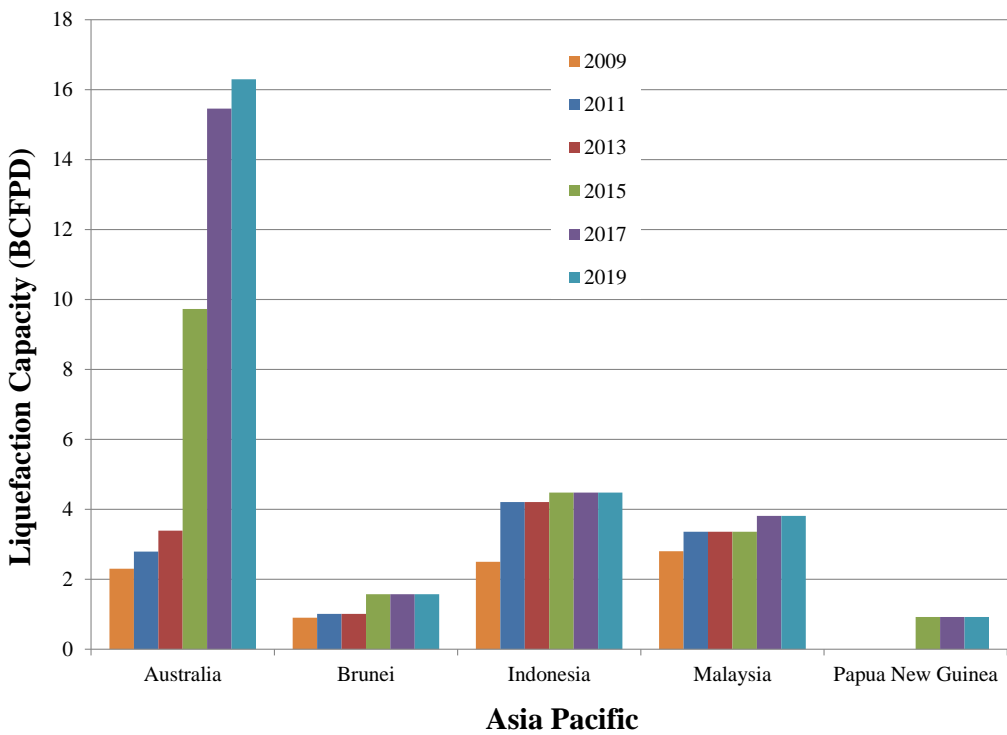


(b)

Figure B-6: Middle East (a) regasification capacity (2009-2012), and (b) liquefaction capacity (2011-2019)



(a)



(b)

Figure B-7: Asia Pacific (a) regasification capacity (2009-2012), and (b) liquefaction capacity (2011-2019)

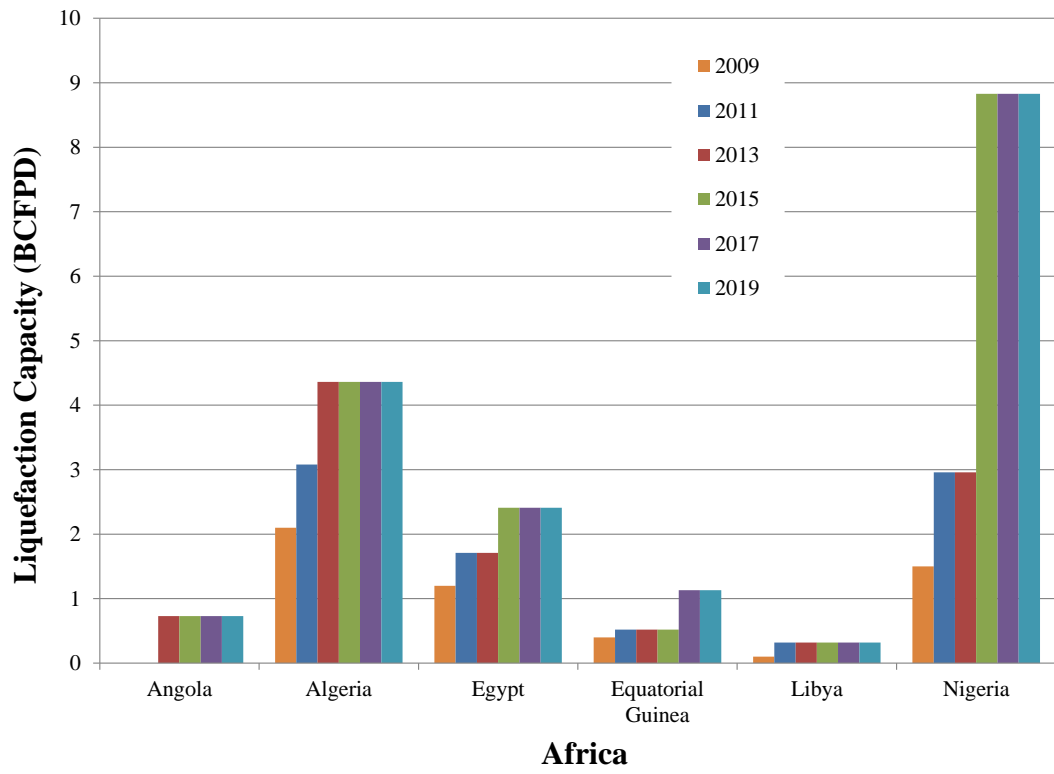


Figure B-8: Africa liquefaction capacity (2011-2019)

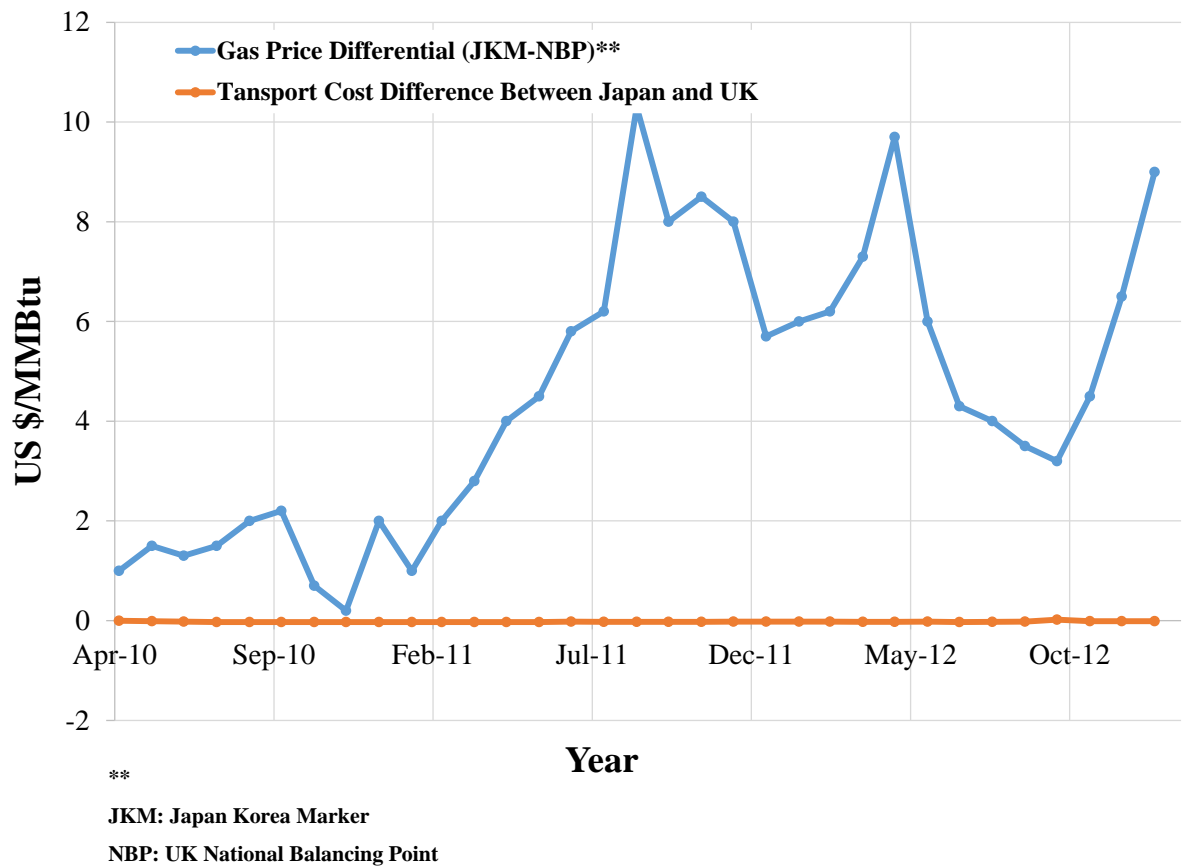


Figure B-9: Qatar LNG sales to Japan versus UK. Differences in the gas price are compared against the differences in the transports costs

Table B-1: Leading companies/current plants

Region	Company	Country	Year Founded
North America	Beaver Drilling	Canada	1965
	Brinkerhoff Drilling	Canada	1940
	Cora Lynn Drilling	Canada	1980
	Drillers Technology Corp.	Canada	1997
	Excalibur Drilling	Canada	1994
	Jade Drilling	Canada	1996
	Nabors	Canada/America	1952
	Apache Corporation	America	1954
	American Liberty Petroleum Corp.	America	2008
	CAMAC International Corporation	America	1986
	American Natural Energy Corporation	America	2001

Region	Company	Country	Year Founded
	Exxon Mobil Corp.,	America	1999
	ConocoPhillips Co.	America	2002
	Chevron Corporation	America	1984
South America	Petróleos de Venezuela, S.A.	Venezuela	1976
	ENARSA	Argentina	2004
	Petróleo Brasileiro S.A.	Brazil	1953
Middle East	Qatar Petroleum	Qatar	1974
	North Oil Company	Iraq	1987
	National Iranian Oil Company	Iran	1948
	Abu Dhabi National Oil Company	Emirates	1973
	Kuwait Oil Company	Kuwait	1934
	Bahrain Petroleum Company	Bahrain	1929

Region	Company	Country	Year Founded
	Missan Oil Company	Iraq	2008
	National Oil Corporation	Libya	1970
Europe/Eurasia	British Petroleum	England	1954
	Shell	England	1907
	Gazprom	Russia	1989
	Wintershall Holding GmbH	Germany	1894
	Edison S.p.A	Italy	1884
	Norwegian Energy Company ASA	Norway	2005
Asia Pacific	Japan Petroleum Exploration Company Limited (JAPEX)	Japan	1955
	BHP Billiton	Australia	2001
	Woodside Petroleum Limited	Australia	1954
	Cairn India	India	2007

Region	Company	Country	Year Founded
	China National Offshore Oil Corporation	China	1982
	Pakistan Petroleum Limited	Pakistan	1950
	Oil India Limited	India	1959
Africa	Vegas Oil and Gas S.A.	Egypt	2003
	Sonatrach	Algeria	1963
	Sudan National Petroleum Corporation	Sudan	1997
	Arabian Gulf Oil Company	Libya	1979
	National Petroleum Company of the Congo	Congo	1998

Table B-2: Current global liquefaction plants

Region	Country	Project Name	Year Operation Started	Capacity (MTPA)	Owner(s)	Process
North America	US	Kenai LNG	1969	1.5	ConocoPhillips	ConocoPhillips
South America	Trinidad	ALNG T4	2006	5.2	BP, BG, Repsol, NGC, Trinidad	ConocoPhillips
	Peru	Peru LNG	2010	4.45	Hunt Oil, Repsol, SK Corp, Marubeni	C3MR/Split MR
	Trinidad	ALNG T3	2003	3.5	BP, BG, Shell	C3MR
	Trinidad	ALNG T2	2002	3.5	BP, BG, Repsol	C3MR
	Trinidad	ALNG T1	1999	3.3	BP, BG, Repsol, CIC, NGC Trinidad, ConocoPhillips	C3MR
Middle East	Qatar	Qatargas II (T1)	2009	7.8	Qatar Petroleum, ExxonMobil	AP-X
	Qatar	Qatargas II (T2)	2009	7.8	Qatar Petroleum, ExxonMobil, TOTAL	AP-X
	Qatar	RasGas III (T1)	2009	7.8	Qatar Petroleum, ExxonMobil	AP-X

Region	Country	Project Name	Year Operation Started	Capacity (MTPA)	Owner(s)	Process
	Qatar	Qatargas III	2010	7.8	Qatar Petroleum, ConocoPhillips, Mitsui	AP-X
	Qatar	RasGas III (T2)	2010	7.8	Qatar Petroleum, ExxonMobil	AP-X
	Qatar	Qatargas IV	2011	7.8	Qatar Petroleum, Shell	AP-X
	Qatar	RasGas II (T1)	2004	4.7	Qatar Petroleum, ExxonMobil	ConocoPhillips
	Qatar	RasGas II (T2)	2005	4.7	Qatar Petroleum, ExxonMobil	ConocoPhillips
	Qatar	RasGas II (T3)	2007	4.7	Qatar Petroleum, ExxonMobil	C3MR
	Oman	Qalhat LNG	2006	3.7	Omani Govt, Petroleum Development Oman(PDO), Shell, Mitsubishi, Gas Natural,Fenosa, Eni, Itochu, Osaka Gas,	ConocoPhillips

Region	Country	Project Name	Year Operation Started	Capacity (MTPA)	Owner(s)	Process
					TOTAL, Korea LNG, Mitsui, Partex	
	Oman	Oman LNG T1	2000	3.55	Petroleum Development Oman (PDO), Shell, TOTAL, Korea LNG, Partex, Mitsubishi, Mitsui , Itochu	C3MR
	Oman	Oman LNG T2	2000	3.55	Petroleum Development Oman (PDO), Shell, TOTAL, Korea LNG, Partex, Mitsubishi, Mitsui , Itochu	C3MR

Region	Country	Project Name	Year Operation Started	Capacity (MTPA)	Owner(s)	Process
	Yemen	Yemen LNG T1	2009	3.35	TOTAL, Hunt Oil, Yemen Gas Co., SK Corp, KOGAS, GASSP, Hyundai	C3MR
	Yemen	Yemen LNG T2	2010	3.35	TOTAL, Hunt Oil, Yemen Gas Co., SK Corp, KOGAS, GASSP, Hyundai	C3MR/Split MR
	Qatar	RasGas I (T1)	1999	3.3	Qatar Petroleum, ExxonMobil, KOGAS, Itochu, LNG Japan	ConocoPhillips
	Qatar	RasGas I (T2)	2000	3.3	Qatar Petroleum, ExxonMobil, KOGAS, Itochu, LNG Japan	C3MR
	United Arab Emirates	ADGAS LNG T3	1994	3.2	ADNOC, Mitsui, BP, TOTAL	C3MR
	Qatar	Qatargas I (T1)	1997	3.2	Qatar Petroleum, ExxonMobil,	C3MR

Region	Country	Project Name	Year Operation Started	Capacity (MTPA)	Owner(s)	Process
					TOTAL,,Marubeni, Mitsui	
	Qatar	Qatargas I (T2)	1997	3.2	Qatar Petroleum, ExxonMobil, TOTAL,Marubeni, Mitsui	C3MR
	Qatar	Qatargas I (T3)	1998	3.1	Qatar Petroleum, ExxonMobil, TOTAL,Mitsui, Marubeni	C3MR
	United Arab Emirates	ADGAS LNG T1-2	1977	2.6	ADNOC, Mitsui, BP, TOTAL	C3MR
Europe/Eurasia	Russia	Sakhalin 2 (T1)	2009	4.8	Gazprom, Shell, Mitsui, Mitsubishi	DMR
	Russia	Sakhalin 2 (T2)	2009	4.8	Gazprom, Shell, Mitsui, Mitsubishi	DMR
	Norway	Snøhvit LNG T1	2007	4.2	Statoil, Petoro, TOTAL, GDF SUEZ, RWE	C3MR/Split MR

Region	Country	Project Name	Year Operation Started	Capacity (MTPA)	Owner(s)	Process
	Norway	Skangass LNG	2010	0.3	Skangass Linde LIMUM, Peru Peru LNG 2010 4.45 Hunt Oil, Repsol, SK Corp, Marubeni	Linde
Asia Pacific	Malaysia	MLNG Satu (T1-3)	1983	8.1	PETRONAS, Mitsubishi, Sarawak State government	C3MR
	Malaysia	MLNG Dua (T1-3)	1995	7.8	PETRONAS, Shell, Mitsubishi, Sarawak State government	C3MR
	Brunei	Brunei LNG T1- 5	1972	7.2	Government of Brunei, Shell, Mitsubishi	C3MR
	Malaysia	MLNG Tiga (T1-2)	2003	6.8	PETRONAS, Shell, Nippon, Sarawak State government, Mitsubishi	ConocoPhillips

Region	Country	Project Name	Year Operation Started	Capacity (MTPA)	Owner(s)	Process
	Indonesia	Bontang LNG T1-2	1977	5.4	Pertamina	C3MR
	Indonesia	Bontang LNG T3-4	1983	5.4	Pertamina	C3MR
	Australia	North West Shelf T4	2004	4.4	BHP Billiton, BP, Chevron, Shell, Woodside, Mitsub ishi, Mitsui	C3MR/Split MR
	Australia	North West Shelf T5	2008	4.4	BHP Billiton, BP, Chevron, Shell, Woodside, Mits- ubishi, Mitsui	C3MR
	Australia	Pluto LNG T1	2012	4.3	Woodside, Kansai Electric, Tokyo Gas	Shell propane pre-cooled mixed refrigerant design
	Indonesia	Tangguh LNG T1	2009	3.8	BP, CNOOC, Mitsubishi, INPEX, JOGMEC, JX Nippon Oil &	C3MR

Region	Country	Project Name	Year Operation Started	Capacity (MTPA)	Owner(s)	Process
					Energy, LNG Japan, Talisman Energy, Kanematsu, Mitsui	
	Indonesia	Tangguh LNG T2	2009	3.8	BP, CNOOC, Mitsubishi, INPEX, JOGMEC, JX Nippon Oil & Energy, LNG Japan, Talisman Energy, Kanematsu, Mitsui	AP-X
	Australia	Darwin LNG T1	2006	3.6	ConocoPhillips, Santos, INPEX, Eni, TEPCO, Tokyo Gas	C3MR
	Indonesia	Bontang LNG T8	1999	3	Pertamina	C3MR

Region	Country	Project Name	Year Operation Started	Capacity (MTPA)	Owner(s)	Process
	Indonesia	Bontang LNG T5	1989	2.9	Pertamina	C3MR
	Indonesia	Bontang LNG T6	1994	2.9	Pertamina	C3MR
	Indonesia	Bontang LNG T7	1998	2.7	Pertamina	C3MR
	Indonesia	Arun LNG T6	1986	2.5	Pertamina	C3MR
	Australia	North West Shelf T1	1989	2.5	BHP Billiton, BP, Chevron, Shell, Woodside,Mitsub ishi, Mitsui	C3MR
	Australia	North West Shelf T2	1989	2.5	BHP Billiton, BP, Chevron, Shell, Woodside, Mitsubishi, Mitsui	C3MR
	Australia	North West Shelf T3	1992	2.5	BHP Billiton, BP, Chevron, Shell, Woodside,Mitsub ishi, Mitsui	C3MR
	Indonesia	Arun LNG T1	1978	1.65	Pertamina	C3MR

Region	Country	Project Name	Year Operation Started	Capacity (MTPA)	Owner(s)	Process
	Malaysia	MLNG Dua Debottleneck	2010	1.2	PETRONAS, Shell, Mitsubishi, Sarawak State government	C3MR
	Indonesia	Senkang LNG T1	2013	0.5	Energy World Corporation	-
	Indonesia	Senkang LNG T2	2013	0.5	Energy World Corporation	-
Africa	Algeria	Arzew - GL2Z (T1-6)	1981	8.2	Sonatrach	Prico
	Algeria	Arzew - GL1Z (T1-6)	1978	6.6	Sonatrach	C3MR
	Angola	Angola LNG T1	2013	5.2	Chevron, Sonangol, BP, Eni, TOTAL	-
	Egypt	SEGAS T1	2005	5	Gas Natural Fenosa, Eni, EGPC, EGAS	C3MR
	Algeria	Skikda - GL1K Rebuild	2013	4.5	Sonatrach	-
	Nigeria	NLNG T4	2006	4.1	NNPC, Shell, TOTAL, Eni	C3MR

Region	Country	Project Name	Year Operation Started	Capacity (MTPA)	Owner(s)	Process
	Nigeria	NLNG T5	2006	4.1	NNPC, Shell, TOTAL, Eni	C3MR
	Nigeria	NLNG T6	2008	4.1	NNPC, Shell, TOTAL, Eni	C3MR
	Equatorial Guinea	EG LNG T1	2007	3.7	Marathon, Sonagas, Mitsui, Marubeni	Linde
	Egypt	ELNG T1	2005	3.6	BG, PETRONAS, EGAS, EGPC, GDF SUEZ	ConocoPhillips
	Egypt	ELNG T2	2005	3.6	BG, PETRONAS, EGAS, EGPC	C3MR
	Nigeria	NLNG T1	1999	3.3	NNPC, Shell, TOTAL, Eni	C3MR
	Nigeria	NLNG T2	2000	3.3	NNPC, Shell, TOTAL, Eni	C3MR
	Nigeria	NLNG T3	2002	3	NNPC, Shell, TOTAL, Eni	ConocoPhillips
	Algeria	Skikda - GL2K (T5-6)	1981	2.2	Sonatrach	C3MR
	Algeria	Skikda - GL1K (T1-4)	1972	1	Sonatrach Teal (T1-3)	C3MR

Table B-3: Planned liquefaction plants across the globe

Region	Country	Project Name	Year to be Operated	Planned Capacity (MTPA)	Owner(s)
North America	US	Sabine Pass T1	2015	4.5	Cheniere
	US	Sabine Pass T2	2016	4.5	Cheniere
	US	Sabine Pass T3	2016	4.5	Cheniere
	US	Sabine Pass T4	2017	4.5	Cheniere
South America	Colombia	Pacific Rubiales	2014	0.5	Exmar
Asia Pacific	Australia	Gorgon LNG T1	2015	5.2	Chevron, ExxonMobil, Shell, Osaka Gas, Tokyo Gas, Chubu Electric
	Australia	Gorgon LNG T2	2015	5.2	Chevron, ExxonMobil, Shell, Osaka Gas, Tokyo Gas, Chubu Electric
	Australia	Gorgon LNG T3	2016	5.2	Chevron, ExxonMobil, Shell, Osaka Gas, Tokyo Gas, Chubu Electric
	Australia	Australia Pacific LNG T1	2015	4.5	ConocoPhillips, Origin Energy, Sinopec

Region	Country	Project Name	Year to be Operated	Planned Capacity (MTPA)	Owner(s)
	Australia	Australia Pacific LNG T2	2015	4.5	ConocoPhillips, Origin Energy, Sinopec
	Australia	Wheatstone LNG T1	2016	4.5	Chevron, Apache, Pan Pacific Energy, KUFPEC, Shell, Kyushu Electric
	Australia	Wheatstone LNG T2	2017	4.5	Chevron, Apache, Pan Pacific Energy, KUFPEC, Shell, Kyushu Electric
	Australia	Queensland Curtis LNG T1	2014	4.3	BG, CNOOC
	Australia	Queensland Curtis LNG T2	2015	4.3	BG, Tokyo Gas
	Australia	Ichthys LNG T1	2017	4.2	INPEX, TOTAL, Tokyo Gas, Osaka Gas, Chubu Electric, Toho Gas

Region	Country	Project Name	Year to be Operated	Planned Capacity (MTPA)	Owner(s)
	Australia	Ichthys LNG T2	2017	4.2	INPEX, TOTAL, Tokyo Gas, Osaka Gas, Chubu Electric, Toho Gas
	Australia	Gladstone LNG T1	2015	3.9	Santos, PETRONAS, TOTAL, KOGAS
	Australia	Gladstone LNG T2	2016	3.9	Santos, PETRONAS, TOTAL, KOGAS
	Malaysia	PETRONAS LNG 9	2015	3.6	PETRONAS
	Australia	Prelude LNG (Floating)	2017	3.6	Shell, INPEX, KOGAS, CPC
	Papua New Guinea	Guinea PNG LNG T1	2014	3.5	ExxonMobil, Oil Search, Government of Papua New Guinea, Santos, Nippon Oil, PNG Landowners (MRDC), Marubeni, Petromin PNG

Region	Country	Project Name	Year to be Operated	Planned Capacity (MTPA)	Owner(s)
	Papua New Guinea	Guinea PNG LNG T2	2014	3.5	ExxonMobil, Oil Search, Government of Papua New Guinea, Santos, JX Nippon Oil & Energy, MRDC, Marubeni, Petromin PNG
	Indonesia	Donggi-Senoro LNG	2014	2	Mitsubishi, Pertamina, KOGAS, Medco,
	Malaysia	PETRONAS FLNG	2015	1.2	PETRONAS
	Malaysia	MLNG Mini-Expansion	2014	0.67	PETRONAS
Africa	Algeria	Arzew - GL3Z (Gassi Touil)	2014	4.7	Sonatrach

Appendix C: Cost analysis

Although cyclone separators are less efficient than other types of filters such as bag filters, they are commonly used to remove the bulk of the solid particles in the upstream of the NG plants due to their low maintenance cost as compared to bag filters [29, 39, 41]. For example, cartridge filters (bag filters) cause an increase in the pressure drop over time due to the blockage of the filter element [29, 39, 41]. This blockage requires an additional annual maintenance cost as well as the installation of a second cartridge in parallel to the main one to avoid shutdown of the pipeline [29]. On the other hand, cyclone separators have a fixed pressure drop over time, and hence, can provide a reliable filtration mechanism in the upstream of the flow [29, 39, 41]. In this section, the additional costs associated with the modifications (active and passive) proposed in this thesis are presented.

C.1. Electro-coating

There are many factors which determine the total cost required for the electro-coating process [87]. Two major items contributing to the total cost are the electric power consumption and the electro-coat material. In this study, 30 kV is applied across the paint which would require 3 A if electric paint is used as a resistance medium (i.e., the material with 1000 Ohm resistance value) [88]. In addition to the cost associated with the electro-coating process, the total cost accompanying the generation of the electric field should also be considered. of the high-energy expenditure.

Table C-1 shows the relative running costs of using the electro-coating process [88]. A compressor station has a maximum rated capacity of 1680 kWh per day [89]. The additional electro-coating process cost compared to the conventional separation process would be 44.52% for the electrostatic-based enhancement. As noticed, the high efficiency enhancement using the electric field would come on the expense of the high-energy expenditure.

Table C-1: Cost for the required for the addition of the electrostatic-based enhancement

Enhancement Process	Field Requirements	Current Required	Running Cost / Day [88]
Electric Field	0.05 N/C	10.6A (assuming 3×10^5 mho/m conductivity and 1.5 cm wire radius)	\$62.58 USD

C.2. Ferrous powder

Two major items contributing to the total cost of the ferrous powder coating process are: 1) the ferrous powder injection process (\$3 USD per 0.5 liter), and 2) the permanent magnets used (\$30 USD per 50 pieces of permanent magnets with a 20-mm diameter). The amount of the ferrous powder required in any cyclone process depends on the amount of the solid particles contained in the gas stream. In this study, the amount of the ferrous powder injected is about 3 times of the amount of the sand particles injected in the gas stream.

C.3. Additional chamber

Although the addition of the tangential chamber adds to the cyclone manufacturing cost, which depends on the dimensions of the chamber (e.g., the average chamber would cost between 50-100 USD for a width of 1 cm and length of 40 cm), it reduces the number of 4- μ particles in the flow by 26% which translates to the reduction of the maintenance costs of the highly expensive downstream equipment such as compressors.